AD-A173 992 COMPUTATIONAL ANALYSIS OF THE EFFECTS OF SURFACE FILMS ON THE SCATTERING.. (U) WASHINGTON STATE UNIV PULLMAN DEPT OF PHYSICS S C BILLETTE ET AL. 01 OCT 86 1/2

UNCLASSIFIED N00014-86-K-0242 F/G 20/6 NL

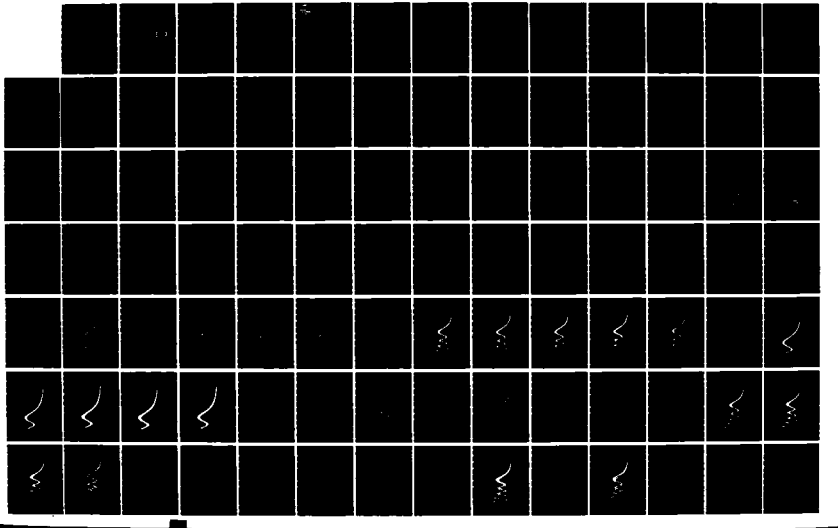

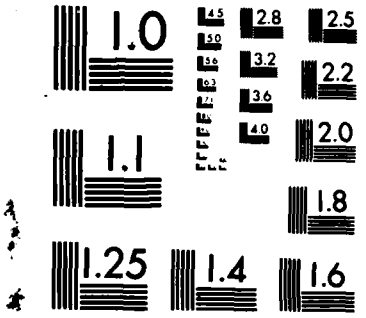

(12)

COMPUTATIONAL ANALYSIS OF THE EFFECTS OF SURFACE FILMS ON THE OPTICAL SCATTERING PROPERTIES OF BUBBLES IN WATER

By

STUART C. BILLETTE

A thesis submitted in partial fulfillment of
the requirements for the degree of

MASTER OF SCIENCE IN PHYSICS

WASHINGTON STATE UNIVERSITY
DEPARTMENT OF PHYSICS

~~August~~ 1986
1 OCTOBER

With a Supplement by Professor P. L. Marston on pages 151-156.

To the Faculty of Washington State University:

The members of the Committee appointed to examine the thesis of **STUART C. BILLETTE** find it satisfactory and recommend that it be accepted.

Chair

DISCLAIMER NOTICE

THIS DOCUMENT IS BEST QUALITY PRACTICABLE. THE COPY FURNISHED TO DTIC CONTAINED A SIGNIFICANT NUMBER OF PAGES WHICH DO NOT REPRODUCE LEGIBLY.

UNCLASSIFIED

SECURITY CLASSIFICATION OF THIS PAGE

AD-A173992

REPORT DOCUMENTATION PAGE

1a. REPORT SECURITY CLASSIFICATION UNCLASSIFIED	1b. RESTRICTIVE MARKINGS
2a. SECURITY CLASSIFICATION AUTHORITY N/A since Unclassified	3. DISTRIBUTION/AVAILABILITY OF REPORT Approved for public release; distribution is unlimited.
2b. DECLASSIFICATION/DOWNGRADING SCHEDULE N/A since Unclassified	
4. PERFORMING ORGANIZATION REPORT NUMBER(S) N00014-86-K-0242-TR6	5. MONITORING ORGANIZATION REPORT NUMBER(S)
6a. NAME OF PERFORMING ORGANIZATION Washington State University Department of Physics 6b. OFFICE SYMBOL (If applicable)	7a. NAME OF MONITORING ORGANIZATION Office of Naval Research Resident Representative, University of Washington
6c. ADDRESS (City, State, and ZIP Code) Pullman, WA 99164-2814	7b. ADDRESS (City, State, and ZIP Code) 1107 N.E. 45th Street Seattle, WA 98105-4631
8a. NAME OF FUNDING/SPONSORING ORGANIZATION Office of Naval Research 8b. OFFICE SYMBOL (If applicable) ONR	9. PROCUREMENT INSTRUMENT IDENTIFICATION NUMBER N00014-86-K-0242 and N00014-85-C-0141
8c. ADDRESS (City, State, and ZIP Code) 800 N Quincy Street Arlington, VA 22217-5000	10. SOURCE OF FUNDING NUMBERS PROGRAM ELEMENT NO.: 61153N / 61153N 11 PROJECT NO.: 03105 / --- TASK NO.: 330 / --- WORK UNIT ACCESSION NO.: 133160 / 4126934

11. TITLE (Include Security Classification)
COMPUTATIONAL ANALYSIS OF THE EFFECTS OF SURFACE FILMS ON THE OPTICAL SCATTERING PROPERTIES OF BUBBLES IN WATER

12. PERSONAL AUTHOR(S)
Stuart C. Billette and Philip L. Marston

13a. TYPE OF REPORT	13b. TIME COVERED	14. DATE OF REPORT (Year, Month, Day)	15. PAGE COUNT
Technical	FROM 850815 TO 860930	86 10 01	156 + x = 166

16. SUPPLEMENTARY NOTATION Contains a Master of Science thesis of S. C. Billette and a supplement by P. L. Marston. The telephone number for the Principal Investigator for the contracts (P.L. Marston) is 509-335-5343.

17. COSATI CODES		
FIELD	GROUP	SUB-GROUP

18. SUBJECT TERMS (Continue on reverse if necessary and identify by block number)
Microbubbles, Bubbles, Bubble Detection, Cavitation, Light Scattering, Mie theory

19. ABSTRACT (Continue on reverse if necessary and identify by block number)

A scattering algorithm for coated spheres was developed using the partial wave series of Aden and Kerker to theoretically determine if surface films on air bubbles in water have a significant effect on optical scattering patterns. The air bubbles were modeled as spheres (of radius a) coated by a film of uniform thickness h and complex refractive index n_c surrounded by water of refractive index n_w equal to 4/3. Size parameters of ka (where $2\pi/k$ equals the optical wavelength in water) equal to 100, 500, 1000, and 2500 (corresponding to radii a ≈ 7.5 μm to 189 μm for a wavelength in air = 632.8 nm) were modeled for values of h ranging from 0 to 3 μm. Irradiance results are plotted as a function of scattering angle θ with emphasis on the critical scattering region. Comparison is made with known results from Mie theory for noncoated spheres as well as a physical-optics approximation developed by Marston and Kingsbury. Some modeling is done in terms of geometric ray optics, in order to explain observed effects. Finally, observations regarding the

20. DISTRIBUTION/AVAILABILITY OF ABSTRACT	21. ABSTRACT SECURITY CLASSIFICATION	
☒ UNCLASSIFIED/UNLIMITED ☐ SAME AS RPT. ☐ DTIC USERS	UNCLASSIFIED	
22a. NAME OF RESPONSIBLE INDIVIDUAL Ming-Yang Su	22b. TELEPHONE (Include Area Code) 601-688-5241	22c. OFFICE SYMBOL NORDA Code 331

DD FORM 1473, 84 MAR 83 APR edition may be used until exhausted. All other editions are obsolete.

SECURITY CLASSIFICATION OF THIS PAGE

UNCLASSIFIED

19. ABSTRACT (continued)

use of noncoated versus coated bubble results for the sizing and detection of microbubbles in various experimental applications is discussed.

ACKNOWLEDGMENTS

I would like to express my gratitude to Professor Philip Marston, my thesis advisor, for his help, advice, and patience during the past year. His enthusiasm and willingness to discuss anything and everything made working for him a pleasure. I wish him and his family all the best in the years to come.

Others I wish to express my gratitude to include Mickey Daniels for her time and patience in preparing this work, Dr. Michael Miller for answering my many programming questions, and Pat, Tom, and the rest of my classmates for their late night discussions and escapades. I also wish to thank my wife, Cheryl, for her help and just believing.

I am grateful to the Naval Ocean Research and Development Activitiy (NORDA) and to the Office of Naval Research (Physics Division) for providing the funding which permitted this work to be done. Finally, I am also indebted to the Hughes Aircraft Company Fellowship and Rotation Program for their aid in making my graduate education possible.

COMPUTATIONAL ANALYSIS OF THE EFFECTS OF SURFACE FILMS ON THE OPTICAL SCATTERING PROPERTIES OF BUBBLES IN WATER

Abstract

by Stuart C. Billette, M.S.
Washington State University
August 1986

Chair: Philip L. Marston

A scattering algorithm for coated spheres was developed using the partial wave series of Aden and Kerker to theoretically determine if surface films on air bubbles in water have a significant effect on optical scattering patterns. The air bubbles were modeled as spheres (of radius a) coated by a film of uniform thickness h and complex refractive index n_c surrounded by water of refractive index n_w equal to 4/3. Size parameters of ka (where $2\pi/k$ equals the optical wavelength in water) equal to 100, 500, 1000, and 2500 (corresponding to radii a = 7.5 μm to 189 μm for $\lambda_{in\ air}$ = 632.8 nm) were modeled for values of h ranging from 0 to 3 μm. Irradiance results are plotted as a function of scattering angle θ with emphasis on the critical scattering region. Comparison is made with known results from Mie theory for noncoated spheres as well as a physical-optics approximation developed by Marston and Kingsbury. Some modeling is done in terms of geometric ray optics, in order to explain observed effects. Finally, observations regarding the use of noncoated versus coated bubble results for the sizing and detection of microbubbles in various experimental applications is discussed.

TABLE OF CONTENTS

LIST OF TABLES

LIST OF FIGURES

To the memory of my father;

Richard Joseph Billette

CHAPTER 1

INTRODUCTION

1.1. Overview

In recent years a great deal of experimental laboratory research and computational modeling has been done regarding the behavior of light scattered by air bubbles in water.[1-8] In these investigations the bubbles have generally been modeled as a non-absorbing uncoated sphere of given radius a and relative refractive index m less than 1. Recent oceanographic *in situ* experiments, however, have suggested that bubbles found outside the laboratory may possess coatings estimated to range from 10 nm to 1 μm in thickness.[9-13] If this is indeed the case, it becomes important to understand and model the effects of these surface films in order to establish the range of validity of the uncoated laboratory bubble results. In addition, if coated bubble results were found to vary significantly, the modeling done here could be useful in determining the size and nature of the coating found on the bubble which, at present, is still unresolved.

The approach taken in this study may be broken down as follows; first, an outline of the partial wave solution used for the case of a coated sphere is presented. This mathematical development gives some insight into the complexities involved in the calculation of scattering coefficients and also serves as a precursor for the actual computational results which follow in Chapter 2. In Chapter 2, the computational considerations involved in writing and testing the coated sphere algorithm are discussed. The results for the range of parameters tested are then presented along with a discussion of noted effects. A comparison is also made with Mie results for a noncoated sphere as well as a physical-optics approximation developed by Marston and Kingsbury.[2] Using this

technique it was possible to determine the range of validity for the noncoated bubble results. An effort has been made to isolate each parameter and analyze it individually following the relevant computations as a greater sense of continuity is thereby maintained. Finally, a discussion of the experimental application of the overall results is presented.

1.2. Coated Sphere Scattering

The exact solution to the problem of the scattering of electromagnetic waves from concentric spheres was first presented in a paper by Aden and Kerker in 1951.[14] It was based on a development presented in 1908 by Gustave Mie regarding the field scattered by any spherically symmetric particle of arbitrary radius and refractive index (commonly referred to as Mie theory). Although the solution to the problem of scattering by coated and noncoated spheres has been available for many years, it is only since the advent of large digital computers that it has become practical to use in scattering calculations. The reason for this will become apparent in the following development for an electromagnetic wave incident on a coated sphere.

Consider an electromagnetic plane wave which is incident upon a coated sphere of radius a and outer radius b as is shown in Fig. 1.1. The relative refractive index of the core is $m_1 = n_i/n_0$ while that of the coat is $m_2 = n_c/n_0$ where n_0, n_c and n_i are the refractive indices of the outer medium, coating and inner medium respectively. For our particular application of a coated air bubble in water $n_0 = n_w$, the refractive index of water and $n_i = n_{air}$. In order to determine the fields in the given regions; $0 \le r \le a$, $a \le r \le b$ $(a \neq 0)$ and $r \ge b$ it is necessary to solve the pertinent vector wave equations given by Maxwell's relations using spherical geometry and the appropriate boundary conditions. The mathematics required to do this is straightforward but extremely tedious and therefore steps have been omitted and emphasis placed on the solutions. The reader is referred to

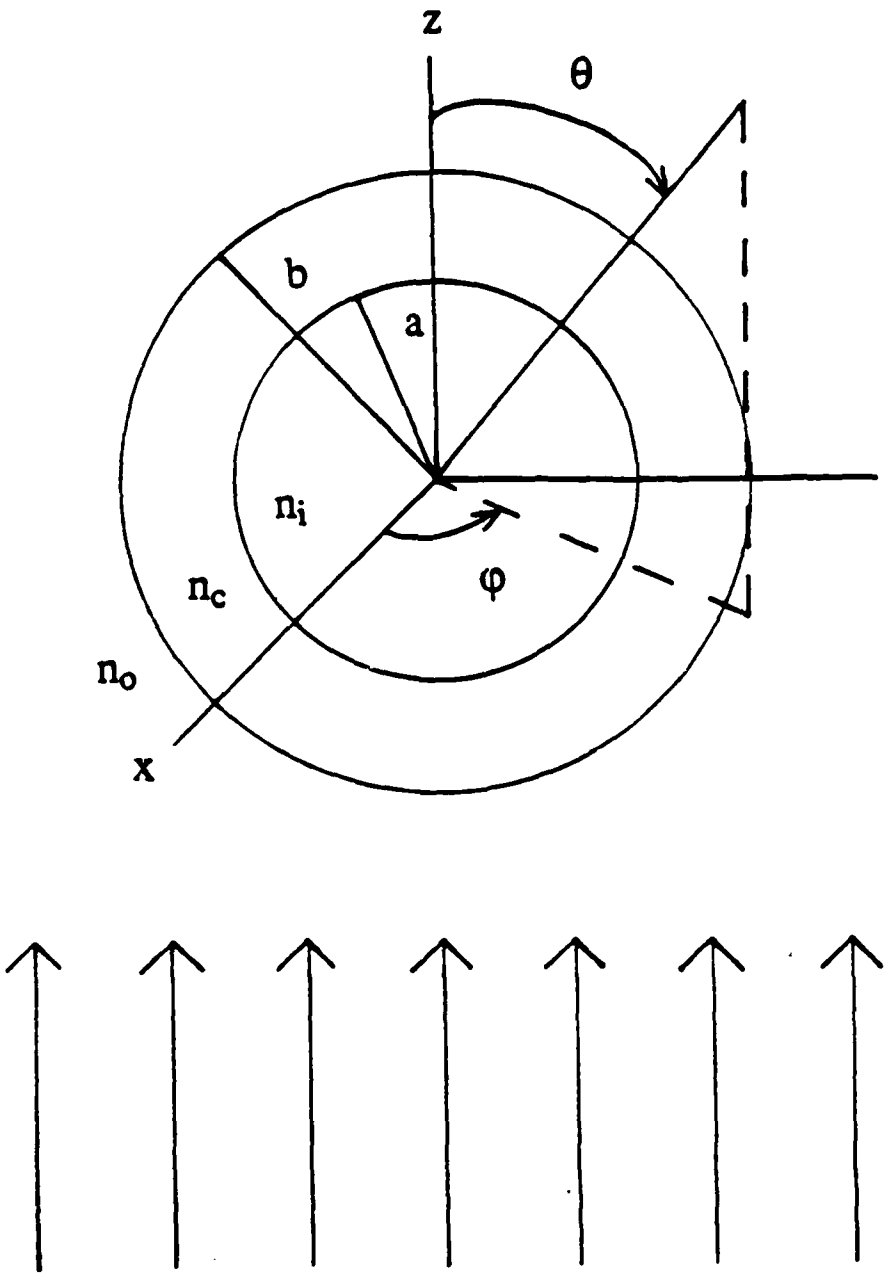

Fig. 1.1.--Electromagnetic wave incident upon a coated sphere.

texts by van de Hulst[15] and Bohren and Huffman[16] for a more thorough description. The following outline was taken from Chapter 8 of the Bohren and Huffman text.

Considering again the situation shown in Fig. 1.1, the solution of the scalar wave equations in spherical polar coordinates yields:

$$\psi_{emn} = \cos m\phi \, P_n^m(\cos\theta) z_n(kr), \tag{1}$$

$$\psi_{omn} = \sin m\phi \, P_n^m(\cos\theta) z_n(kr), \tag{2}$$

where $P_n^m(\cos\theta)$ are the associated Legendre functions and z_n is any of the four spherical Bessel functions j_n, y_n, $h_n^{(1)}$, or $h_n^{(2)}$ depending on the region of interest. The subscripts e and o denote even and odd. Due to the completeness of the functions $\cos m\phi$, $\sin m\phi$, $P_n^m(\cos\theta)$ and $z_n(kr)$, any function that satisfies the scalar wave equation in spherical polar coordinates may be expanded as an infinite series in the functions (1) and (2). The vector spherical harmonics generated by ψ_{emn} and ψ_{omn} are

$$\mathbf{M}_{emn} = \nabla \times (\mathbf{r}\,\psi_{emn}), \qquad \mathbf{M}_{omn} = \nabla \times (\mathbf{r}\,\psi_{omn}),$$

$$\mathbf{N}_{emn} = (\nabla \times \mathbf{M}_{emn})/k, \qquad \mathbf{N}_{omn} = (\nabla \times \mathbf{M}_{omn})/k,$$

which are written out in component form in Bohren and Huffman.[17] Finally, the incident wave is taken to be of the form $\mathbf{E}_i = E_0 e^{i(k\cdot r - \omega t)}\hat{e}_x$ where $\hat{e}_x$ indicates the x unit vector in spherical coordinates. In the following description we omit the $\exp(-i\omega t)$ time dependence for all fields.

With this information it is now possible to write out the fields for the various regions of the coated sphere. The electromagnetic field $(\mathbf{E}_1, \mathbf{H}_1)$ in the region from $0 \le r \le a$ is given by

$$\mathbf{E}_1 = \sum_{n=1}^{\infty} E_n[c_n \mathbf{M}_{o1n}^{(1)} - i d_n \mathbf{N}_{e1n}^{(1)}], \tag{3a}$$

$$\mathbf{H}_1 = -k_1/\omega\mu_1 \sum_{n=1}^{\infty} E_n[d_n \mathbf{M}_{e1n}^{(1)} + i c_n \mathbf{N}_{o1n}^{(1)}], \tag{3b}$$

where $E_n = i^n E_o(2n+1)/n(n+1)$, μ_1 is the permeability of region 1, k_1 is the wave number of the wave with frequency ω in that region and c_n, d_n are coefficients determined by the boundary conditions. The scattered field $(\mathbf{E}_s, \mathbf{H}_s)$ is given by

$$\mathbf{E}_s = \sum_{n=1}^{\infty} E_n[i a_n \mathbf{N}_{e1n}^{(3)} - b_n \mathbf{M}_{o1n}^{(3)}], \tag{4a}$$

$$\mathbf{H}_s = k/\omega\mu \sum_{n=1}^{\infty} E_n[i b_n \mathbf{N}_{o1n}^{(3)} + a_n \mathbf{M}_{e1n}^{(3)}], \tag{4b}$$

where again a_n and b_n are coefficients which will be determined by the appropriate boundary conditions. The (3) superscript indicates that the outgoing wave solutions in Eqs. (1) and (2) with $z_n(kr) = h_n^{(1)}(k_1 r)$ are to be used. Due to the requirement of finiteness at the origin, the radial part of the functions in Eqs. (1) and (2) which generate the vector harmonics in the expansion of $(\mathbf{E}_1, \mathbf{H}_1)$ is constrained to be j_n [indicated by (1) superscript]. However, in the region $a \le r \le b$ $(a \neq 0)$, both the spherical Bessel functions j_n and y_n are finite; as a consequence the field in region 2 $(\mathbf{E}_2, \mathbf{H}_2)$ is written as

$$\mathbf{E}_2 = \sum_{n=1}^{\infty} E_n[f_n \mathbf{M}_{o1n}^{(1)} - i g_n \mathbf{N}_{e1n}^{(1)} + v_n \mathbf{M}_{o1n}^{(2)} - i w_n \mathbf{N}_{e1n}^{(2)}], \tag{5a}$$

$$\mathbf{H}_2 = -k_2/\omega\mu_2 \sum_{n=1}^{\infty} E_n[g_n \mathbf{M}_{e1n}^{(1)} + i f_n \mathbf{N}_{o1n}^{(1)} + w_n \mathbf{M}_{e1n}^{(2)} + i v_n \mathbf{N}_{o1n}^{(2)}], \tag{5b}$$

where the vector harmonics $M_{e1n}^{(2)}$ and so on, are generated by functions of the form of Eqs. (1) and (2) with radial dependence $y_n(k_2r)$. The boundary conditions

$$(\mathbf{E}_2 - \mathbf{E}_1) \times \hat{\mathbf{e}}_r = 0, \qquad (\mathbf{H}_2 - \mathbf{H}_1) \times \hat{\mathbf{e}}_r = 0, \qquad r = a$$

$$(\mathbf{E}_s + \mathbf{E}_i - \mathbf{E}_2) \times \hat{\mathbf{e}}_r = 0, \qquad (\mathbf{H}_s + \mathbf{H}_i - \mathbf{H}_2) \times \hat{\mathbf{e}}_r = 0, \qquad r = b$$

yield eight equations in the coefficients a_n, b_n, c_n, d_n, f_n, g_n, v_n, w_n:

$$f_n m_1 \psi_n(m_2x) - v_n m_1 \chi_n(m_2x) - c_n m_2 \psi_n(m_1x) = 0, \tag{6a}$$

$$w_n m_1 \chi'_n(m_2x) - g_n m_1 \psi'_n(m_2x) + d_n m_2 \psi'_n(m_1x) = 0, \tag{6b}$$

$$v_n \mu_1 \chi'_n(m_2x) - f_n \mu_1 \psi'_n(m_2x) + c_n \mu_2 \psi'_n(m_1x) = 0, \tag{6c}$$

$$g_n \mu_1 \psi_n(m_2x) - w_n \mu_1 \chi_n(m_2x) + d_n \mu_2 \psi_n(m_1x) = 0, \tag{6d}$$

$$m_2 \psi'_n(y) - a_n m_2 \xi'_n(y) - g_n \psi'_n(m_2y) + w_n \chi'_n(m_2y) = 0, \tag{6e}$$

$$m_2 b_n \xi_n(y) - m_2 \psi_n(y) + f_n \psi_n(m_2y) - v_n \chi_n(m_2y) = 0, \tag{6f}$$

$$\mu_2 \psi_n(y) - a_n \mu_2 \xi_n(y) - g_n \mu \psi_n(m_2y) + w_n \mu \chi_n(m_2y) = 0, \tag{6g}$$

$$b_n \mu_2 \xi'_n(y) - \mu_2 \psi'_n(y) + f_n \mu \psi'_n(m_2y) - v_n \mu \chi'_n(m_2y) = 0, \tag{6h}$$

where m_1 and m_2 are the refractive indices of the core and coating relative to the surrounding medium; μ, μ_1, μ_2 are the permeabilities of the surrounding medium, core, and coating; and $x = ka$, $y = kb$. The prime indicates differentiation with respect to x or y in the argument. The Riccati-Bessel function $\chi_n(z)$ is $-zy_n(z)$. Let us assume for simplicity that $\mu = \mu_1 = \mu_2$ and solve the set of above equations for the scattering coefficients a_n and b_n:[18]

$$a_n = \frac{\psi_n(y)[\psi'_n(m_2y) - A_n\chi'_n(m_2y)] - m_2\psi'_n(y)[\psi_n(m_2y) - A_n\chi_n(m_2y)]}{\xi_n(y)[\psi'_n(m_2y) - A_n\chi'_n(m_2y)] - m_2\xi'_n(y)[\psi_n(m_2y) - A_n\chi_n(m_2y)]}, \quad (7a)$$

$$b_n = \frac{m_2\psi_n(y)[\psi'_n(m_2y) - B_n\chi'_n(m_2y)] - \psi'_n(y)[\psi_n(m_2y) - B_n\chi_n(m_2y)]}{m_2\xi_n(y)[\psi'_n(m_2y) - B_n\chi'_n(m_2y)] - \xi'_n(y)[\psi_n(m_2y) - B_n\chi_n(m_2y)]}, \quad (7b)$$

$$A_n = \frac{m_2\psi_n(m_2x)\psi'_n(m_1x) - m_1\psi'_n(m_2x)\psi_n(m_1x)}{m_2\chi_n(m_2x)\psi'_n(m_1x) - m_1\chi'_n(m_2x)\psi_n(m_1x)}, \quad (7c)$$

$$B_n = \frac{m_2\psi_n(m_1x)\psi'_n(m_2x) - m_1\psi'_n(m_2x)\psi'_n(m_1x)}{m_2\chi'_n(m_2x)\psi_n(m_1x) - m_1\psi'_n(m_1x)\chi_n(m_2x)}. \quad (7d)$$

Thus we find that the determination of scattering coefficients a_n and b_n becomes an impressive task. However, with the aid of a computer the computation can be accomplished as will be shown in Chapter 2.

For future reference it is desirable to define the following complex scattering amplitudes which are descriptive of the scattered fields:[19]

$$S_1(\cos\theta) = \sum_{n=1}^{N} \frac{2n+1}{n(n+1)} [a_n\pi_n(\cos\theta) + b_n\tau_n(\cos\theta)], \quad (8a)$$

$$S_2(\cos\theta) = \sum_{n=1}^{N} \frac{2n+1}{n(n+1)} [a_n\tau_n(\cos\theta) + b_n\pi_n(\cos\theta)]. \quad (8b)$$

The angular functions τ_n and π_n are defined by the relations

$$\pi_n(\cos\theta) = \frac{1}{\sin\theta} P_n^1(\cos\theta),$$

$$\tau_n(\cos\theta) = \frac{d}{d\theta} P_n^1(\cos\theta),$$

where θ is the scattering angle. The scattered irradiances proportional to $|S_1|^2$ and $|S_2|^2$. The subscripts $j = 1$ and $j = 2$ on S_j refer to the two orthogonal directions of incident polarization which are defined in Chapter 2.

REFERENCES TO CHAPTER 1

1. Dean S. Langley and Philip L. Marston, "Critical-angle scattering of laser light from bubbles in water: measurements, models, and application to sizing of bubbles," App. Opt. 23, 1044-1054 (1984).
2. Philip L. Marston and Dwight L. Kingsbury, "Scattering by a bubble in water near the critical angle: interference effects," J. Opt. Soc. Am. 71, 192-196 (1981); 71, 917(E) (1981).
3. Dwight L. Kingsbury and Philip L. Marston, "Mie scattering near the critical angle of bubbles in water," J. Opt. Soc. Am. 71, 358-361 (1981).
4. George E. Davis, "Scattering of light by an air bubble in water," J. Opt. Soc. Am. 45, 572-581 (1955).
5. P. L. Marston, D. S. Langley, and D. L. Kingsbury, "Light scattering by bubbles in liquids: Mie theory, physical-optics approximations, and experiments," App. Sci. Res. 38, 373-383 (1982).
6. D. S. Langley and P. L. Marston, "Glory in optical backscattering from air bubbles," Phys. Rev. Lett. 47, 913-916 (1981).
7. G. M. Hansen, "Mie scattering as a technique for the sizing of air bubbles," App. Opt. 24, 3214-3220 (1985).
8. Philip L. Marston, "Critical angle scattering by a bubble: physical-optics approximation and observations," J. Opt. Soc. Am. 69, 1205-1211 (1979); 70, 353(E) (1980).
9. Bruce D. Johnson and Robert C. Cooke, "Generation of stabilized microbubbles in sea water," Science 213, 209-211 (1981).
10. B. D. Johnson and R. C. Cooke, "Bubble populations and spectra in coastal waters: A photographic approach," J. Geo. Phys. Res. 84, 3761-3766 (1979).

11. V. K. Goncharov, S. N. Kuznetsova, G. G. Neuimin, and N. A. Sorokina, "Determination of the diffusion constant of a gas in sea water from the solution of air bubbles in the medium," Sov. Phys. Acoust. 30, 273-275 (1984).

12. R. E. Glazman, "Effects of adsorbed films on gas bubble radial oscillations," J. Acoust. Soc. Am. 74, 980-986 (1983).

13. R. E. Glazman, "Damping of bubble oscillations induced by transport surfactants between the adsorbed film and the bulk solution," J. Acoust. Soc. Am. 76, 890-896 (1984).

14. Arthur L. Aden and Milton Kerker, "Scattering of electromagnetic waves from two concentric spheres," J. Appl. Phys. 22, 1242-1246 (1951).

15. H. C. van de Hulst, Light Scattering by Small Particles (Dover, N.Y. 1981).

16. C. F. Bohren and D. R. Huffman, Absorption and Scattering of Light by Small Particles (Wiley, N.Y., 1983).

17. Ref. 16, p. 89.

18. Ref. 16, p. 183. Note also that ψ_n and ξ_n are Riccati-Bessel functions of the kind which commonly appear in the Mie solution with an $\exp(-i\omega t)$ time dependence: $\psi_n(\rho) = \rho j_n(\rho)$ and $\xi_n(\rho) = \rho h_n^{(1)}(\rho)$. See, e.g., Ref. 16, p. 101..

19. Ref. 16, p. 112.

CHAPTER 2

COATED BUBBLE SCATTERING COMPUTATIONS

2.1. Computational Considerations

A computational scheme is presented in this section for the calculations of the scattered irradiances I_j, where $j = 1$ indicates polarization of the incident electric field vector perpendicular to the scattering plane and $j = 2$ indicates the parallel case. It is based on similar schemes developed by Wiscombe[1,2] and Bohren and Huffman[3] but differs in that it computes the coated sphere scattering irradiance as a function of scattering angle rather than just the efficiency factors. Another difference is that it also uses down recursion for all logarithmic derivative calculations.

Adopting the notation of Bohren and Huffman, we may calculate irradiances (I_j) by way of Eqs. (8a) and (8b) using the values of the coefficients a_n and b_n determined in Eqs. (7a) and (7b). The logarithmic derivatives of the Ricatti-Bessel functions found in Eqs. (7c) and (7d) were calculated by the down recursion technique for Mie scattering developed by Wiscombe, which is known to be stable. This technique consists of specifying *a priori* the last term in the partial wave series denoted by N and then using recursion relations to calculate down to the $n = 0$ term. By doing this the computational error is decreased in each step. The problem with the method, however, lies in selection of the N^{th} term. Wiscombe, through extensive testing, has determined $N = kb + 4.05 (kb)^{1/3} + 2$ (where here b is the radius of the outer sphere shown in Fig. 1.1) is the appropriate relation to determine N and hence this was the expression used in our computations. Another necessary consideration was the preliminary determination of angle step size N_{ang}, which increases in proportion to ka. In order to resolve the fine

structure shown in Mie results, the value of $N_{ang} < \lambda/7a$ rad (where a is the inner sphere radius shown in Fig. 1.1) was taken from previously published bubble results.[4]

The partial wave scattering coefficients a_n and b_n were computed using the IBM FORTRAN VS program which is given in Appendix A. All computations were performed on an IBM 3090-200 computer. The program was written using IBM quadruple precision (32 significant digits) as this insured that the effects of the coating would not cause numerical instabilities. The complex arithmetic was done using IBM FORTRAN VS subroutines again using quadruple precision which allowed both the real and imaginary components in all calculations to have 32 significant digit precision.

The program was tested in a wide variety of ways. Limiting cases were taken in which the coating was allowed to go to zero thickness which gave the expected noncoated bubble Mie results previously published.[5] The coating was also given the same index of refraction as the surrounding medium (water) which again yielded the correct Mie results. Next, results were checked against other coated sphere calculations done by Cooper et al.[6] and Brunsting.[7] We were able to duplicate Cooper's results exactly for all cases and Brunsting's for scattering angles ranging from approximately $\theta = 0°$ to 90°. Scattering coefficients and efficiency factors calculated by our program were checked against results from the subroutine written by Bohren and Huffman[8] and were also in perfect agreement.

Due to the use of quadruple precision and the need to calculate three logarithmic derivatives by down recursion the program is rather slow. Typical times ranged from approximately 10 c.p.u. seconds for ka = 100 with a 1 μm coating to roughly 150 c.p.u. seconds for ka = 2500 with a coating of 1 μm. Angle step size was typically on the order of $(\lambda/14\ a)$ rad to avoid sampling errors for any size coating calculatic ntrast this the physical-optics approximation program (given in Appendix A), whic. e to predict

the coarse structure, executes in a few seconds regardless of the size of ka. The equations used to develop this program are listed at the end of Section II of Ref. 9. Comparison of coated bubble cases will be made with the physical-optics approximation for forward scattering ($\theta = 0°$ to 90°) to determine its usefulness in coarse structure calculations for coated bubbles.

2.2. Results

A. Effect of Increasing Coating Thickness

A typical set of calculations for a coated air bubble in water with $ka = 100$ ($a \approx 7.5$ μm for $\lambda_w = 474.6$ nm) over the $\theta = 0°$ to 180° range are shown in Figs. 2.1 and 2.2. The parameters used were the following: the index of refraction of the coat n_c was real (nonabsorbing coat) and equal to 1.5, the index of refraction of the water n_w was also real and equal to 4/3. The thickness of the coatings h were 0.26 μm and 1.14 μm respectively. The values of the coating were determined by taking the ratio of the inner sphere radius a and the outer sphere b (described by expression AOB in the COATSPHR program in Appendix A). The coating thickness h was then determined by the relation $h = b - a = b(1 - AOB)$. The range of bubble sizes can be illustrated by considering HeNe laser illumination with a wavelength in air λ_{air} equal to 632.8 nm. The wavelength in water is then given by $\lambda_w = \lambda_{air}/n_w = 474.6$ nm. Using λ_w to determine a for $ka = 100$ gives $a \approx 7.5$ μm. A list of bubble sizes in terms of h and the actual AOB values used in the calculations for $\lambda_w = 474.6$ nm are given in Table 2.1. Some concern may be raised about using the approximate value of $n_w = 4/3$; however, computational testing over a range of n_w from to 1.332 (water at 30°C for $\lambda_{air} = 589.2$ nm) to 1.338 (high salinity) showed the 4/3 value to be a very good approximation. Representative results of this evaluation are given in Appendix C. Normalization in the figures was chosen so that $I_j(\theta) = 1$ represents perfect reflection from an uncoated sphere of radius a

Table 2.1

Coating Thickness Values for λ_w = 474.6 nm (λ_{air} = 632.8 nm)

This table may be used to find the actual value of AOB used in the computations except in certain cases where the value of AOB is noted in the figure caption.

ka	radius = a(μm)	h(μm)	kb	radius = b(μm)	AOB
100	7.5	0.25	103.3	7.75	.9677
		0.26	103.4	7.76	.9670
		0.50	106.7	8.00	.9375
		0.53	107.1	8.03	.9340
		1.00	113.3	8.50	.8824
		1.14	115.2	8.64	.8680
		2.00	126.7	9.50	.7895
		3.00	140.0	10.50	.7143
500	37.8	0.25	503.3	38.05	.9934
		0.27	503.5	38.07	.9930
		0.50	506.6	38.30	.9870
		1.01	513.2	38.81	.9742
		2.00	526.5	39.80	.9497
		3.00	539.7	40.80	.9264
1000	75.5	0.23	1003.0	75.73	.9970
		0.25	1003.3	75.75	.9967
		0.53	1007.0	76.03	.9930
		0.99	1013.2	76.49	.9870
		2.01	1026.7	77.51	.9740
		3.00	1039.7	78.50	.9618
		3.14	1041.7	78.64	.9600
		5.00	1066.2	80.50	.9379
2500	189	0.25	2503.3	189.25	.9987
		0.49	2506.6	189.50	.9974
		1.01	2513.2	190.01	.9947
		2.02	2526.5	191.02	.9894
		3.05	2539.7	192.05	.9841

Figure 2.1. Calculated normalized scattering irradiances for ka = 100, $n_w = 4/3$, $n_c = 1.5$, $\theta = 0°$ to 180° for the log of the perpendicular polarization I_1. The solid curve is from Mie theory. The thin-dashed curve is the calculated coated sphere result for (a) h = 0.26 μm, (b) h = 1.14 μm. All values of h are for HeNe laser light in water with $\lambda_{air} = 632.8$ nm. The inner radius a = 7.5 μm.

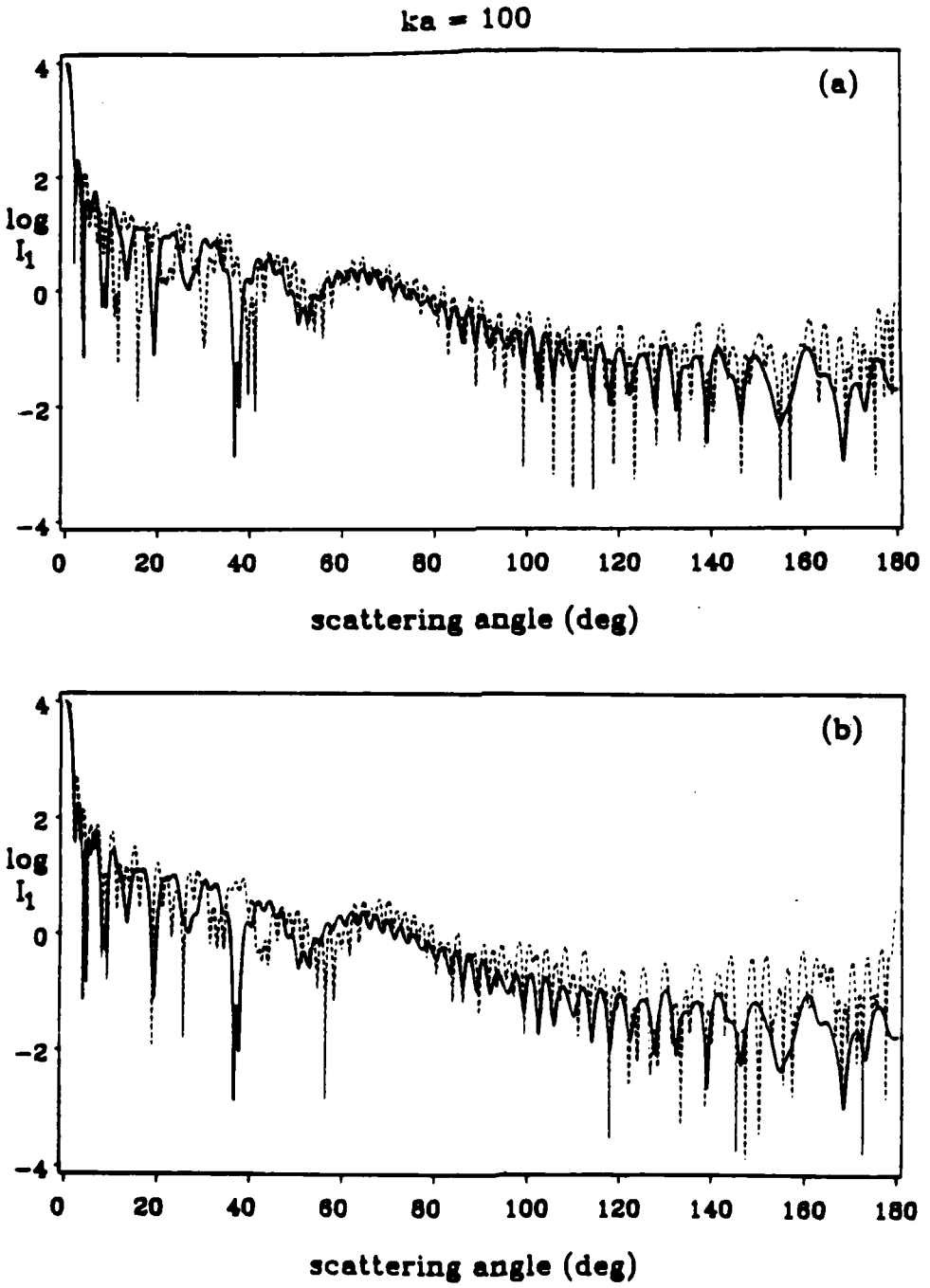
ka = 100
(a)
log I_1
4
2
0
-2
-4
0
20
40
60
80
100
120
140
160
180
scattering angle (deg)
(b)
log I_1
4
2
0
-2
-4
0
20
40
60
80
100
120
140
160
180
scattering angle (deg)

Fig. 2.1 (a) and (b)

Figure 2.2 Like Figure 2.1 but for the parallel polarization case, I_2.

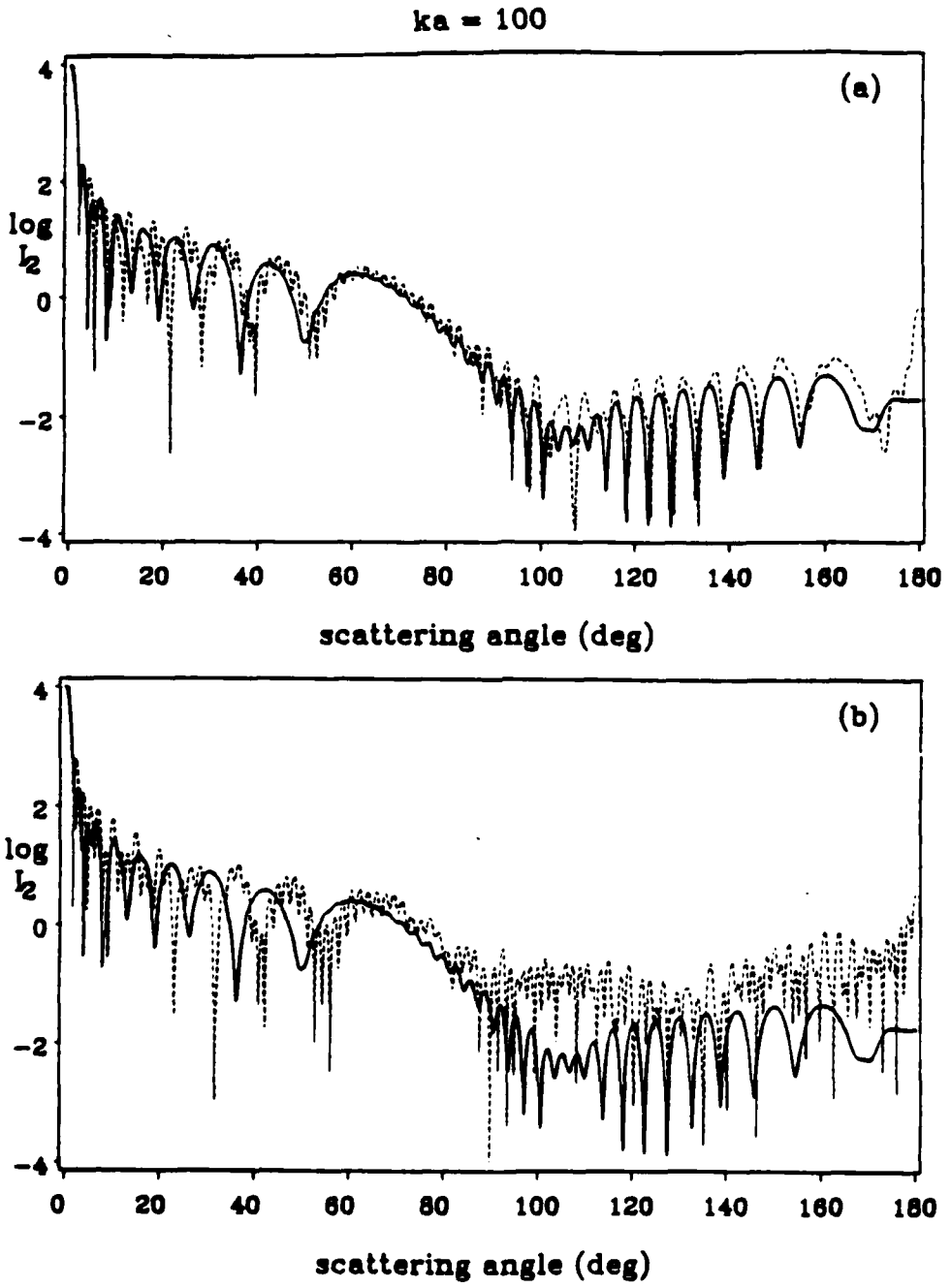
ka = 100
(a)
log I2
4
2
0
-2
-4
0
20
40
60
80
100
120
140
160
180
scattering angle (deg)
(b)
log I2
4
2
0
-2
-4
0
20
40
60
80
100
120
140
160
180
scattering angle (deg)

Fig. 2.2 (a) and (b)

according to geometric optics.[10] At a distance $R >> ka^2$ from the center of the bubble, the actual j-polarization irradiance is incident j-polarized irradiance multiplied by $I_j[(a/R)^2/4]$ where $I_j = 4|S_j|^2 (ka)^{-2}$ with j again denoting the previously mentioned polarization cases.[11]

Analysis of Mie results (indicated by solid curve in Figs. 2.1 and 2.2) has shown[12] two distinct regions of interest for detecting and sizing of noncoated bubbles in water. The first of these regions known as the Brewster scattering angle region, is the region around the Brewster angle determined by the condition $\theta_B = \pi - 2\tan^{-1}(m_1)$ ($\theta_B \approx 106.3°$ for a noncoated air bubble in water) where $m_1 = n_{air}/n_w$. The second region is that near the critical angle given by $\theta_c = \pi - 2\sin^{-1}(m_1)$ ($\theta_c \approx 82.8°$ for noncoated air bubbles in water). The critical angle region irradiance is generally used for size determination while the ratio of the two regions may be used to determine if the scattered irradiance is indeed from a bubble. Furthermore, data[13] and inspection of Mie results for uncoated bubbles, suggests that the normalized irradiance for the $j = 2$ case is closer to the universal value of $I_j = 1/4$ predicted at θ_c by the physical-optics approximation.[9] For this reason and the fact that parallel polarization has a simpler fine structure the $j = 2$ case is preferred for sizing and detecting microbubbles in water. Therefore in further illustrations we shall use the $j = 2$ case while the supplementary $j = 1$ cases are given in Appendix B.

Figures 2.1 and 2.2 show that even with the coating, the coarse and fine structure oscillations described by Langley and Marston[13] still exist. However, with increasing coating thickness some structural changes become apparent. An example of these changes in the Brewster angle region is shown in Figs. 2.3(a)-(c) and 2.4(a)-(c) (thin-dashed curve). Through inspection of Figs. 2.3 and 2.4 one finds, in general, that the effect of the coating is to raise the baseline irradiance near θ_B and to increase the magnitude of the

Figure 2.3. Calculated normalized irradiances for ka = 100 in the Brewster angle scattering region for I_2. The solid curve is from Mie theory and the thin-dashed curve is the calculated coated sphere result. With λ_{air} = 632.8 nm the coating thickness values are (a) h = 0.26 μm, (b) h = 0.53 μm, and (c) h = 1.14 μm.

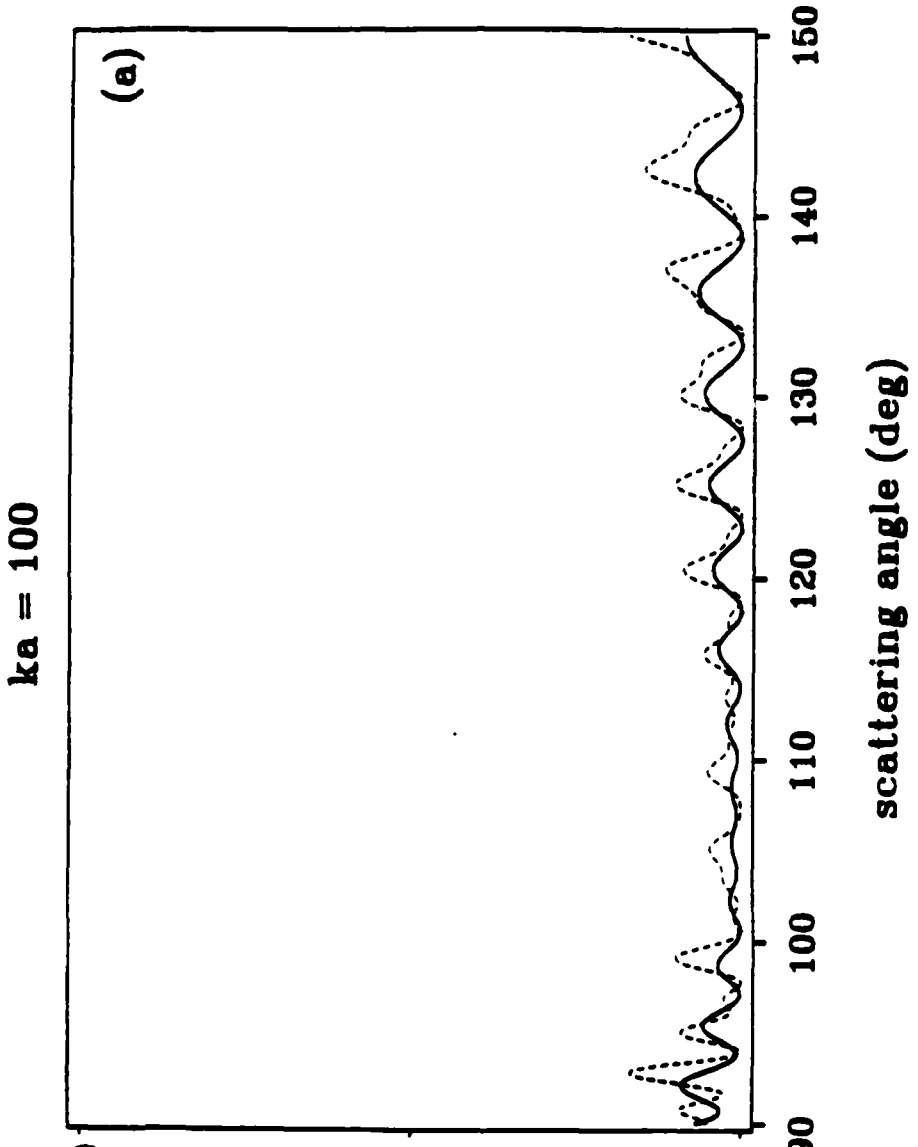
(a)
ka = 100
0.50
0.25
0.00
I_2
90
100
110
120
130
140
150
scattering angle (deg)

Fig. 2.3 (a)

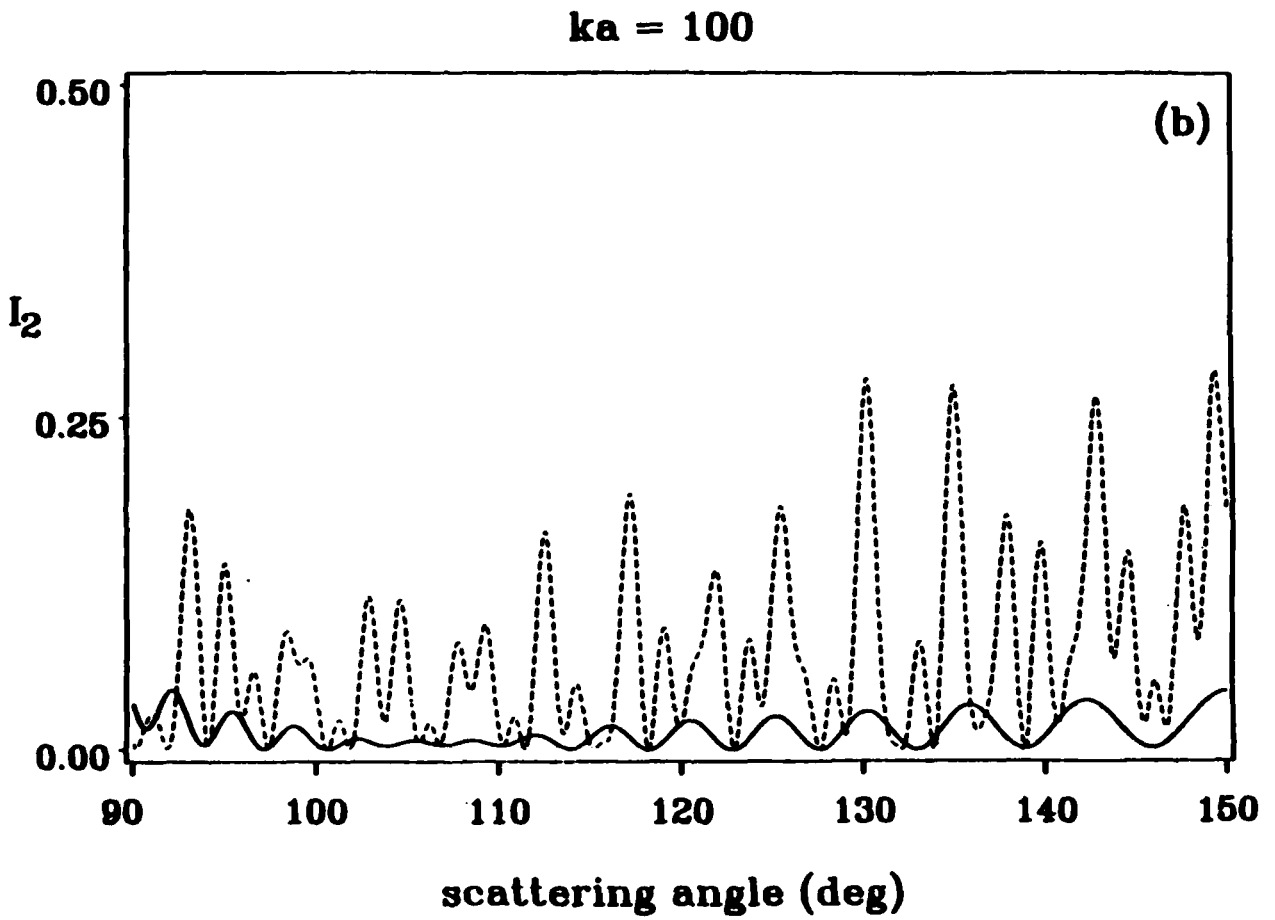
ka = 100
(b)
0.50
0.25
0.00
I_2
90
100
110
120
130
140
150
scattering angle (deg)

Fig. 2.3 (b)

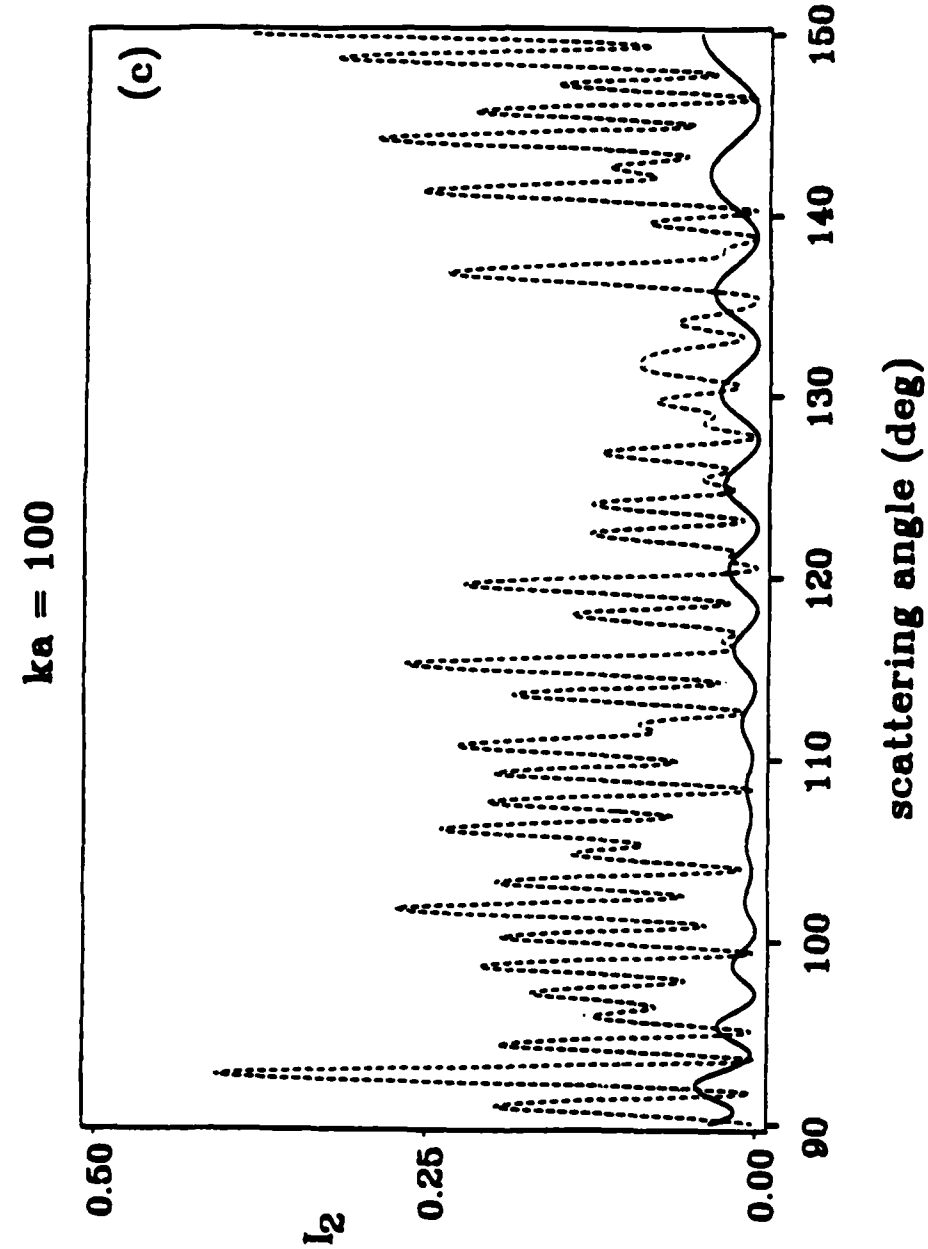
(c)
ka = 100
0.60
0.25
0.00
I_2
90
100
110
120
130
140
150
scattering angle (deg)

Fig. 2.3 (c)

Figure 2.4. Like Figure 2.3 but for ka = 1000 (a = 75.5 μm) and (a) h = 0.23 μm, (b) h = 0.53 μm, (c) h = 0.99 μm.

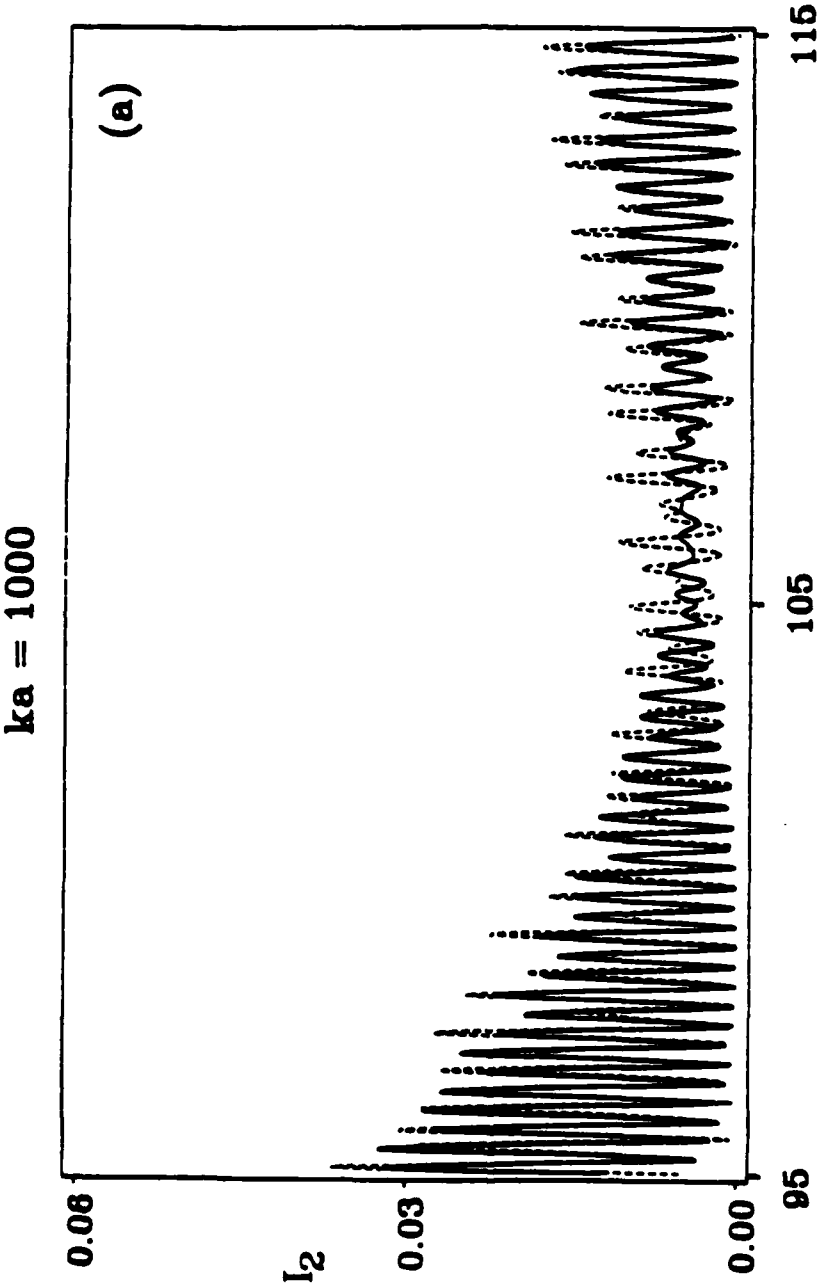

Fig. 2.4 (a)

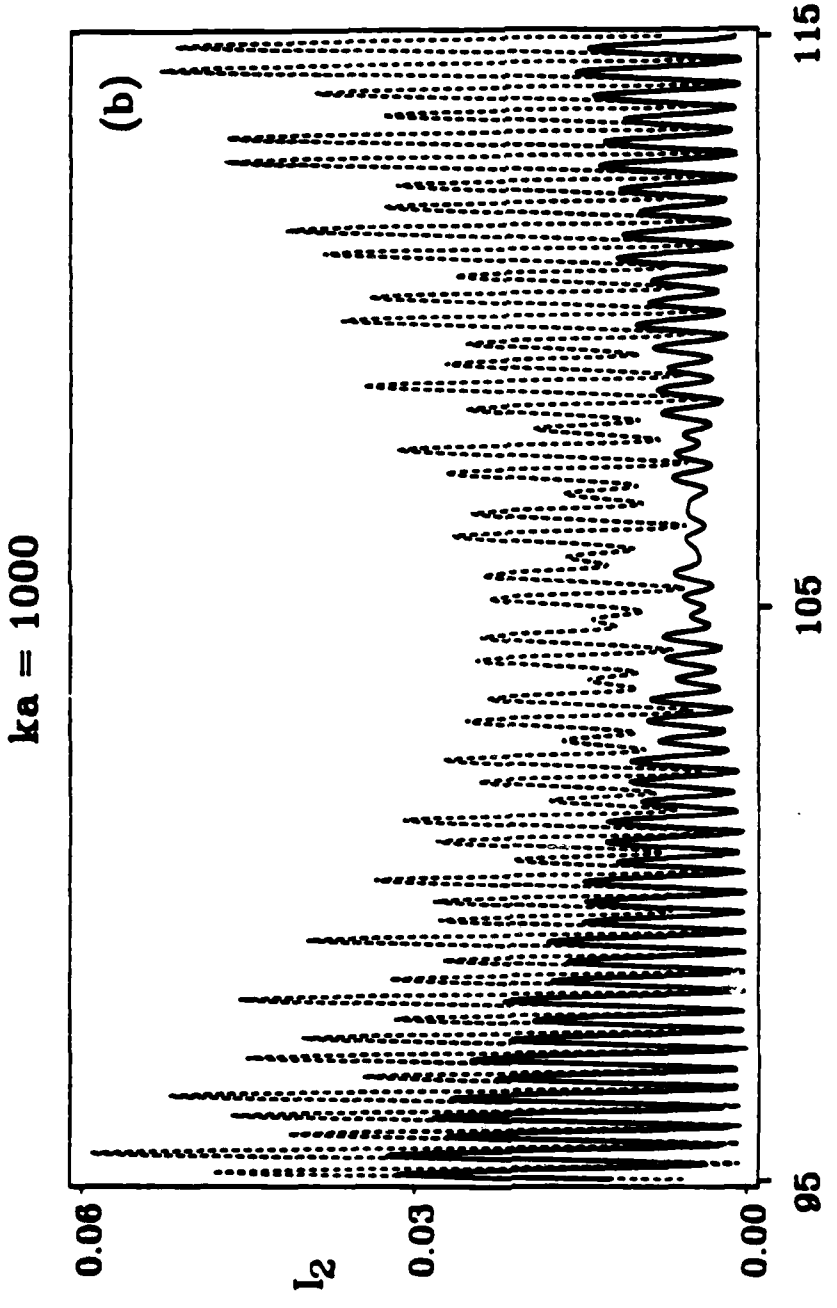

Fig. 2.4 (b)

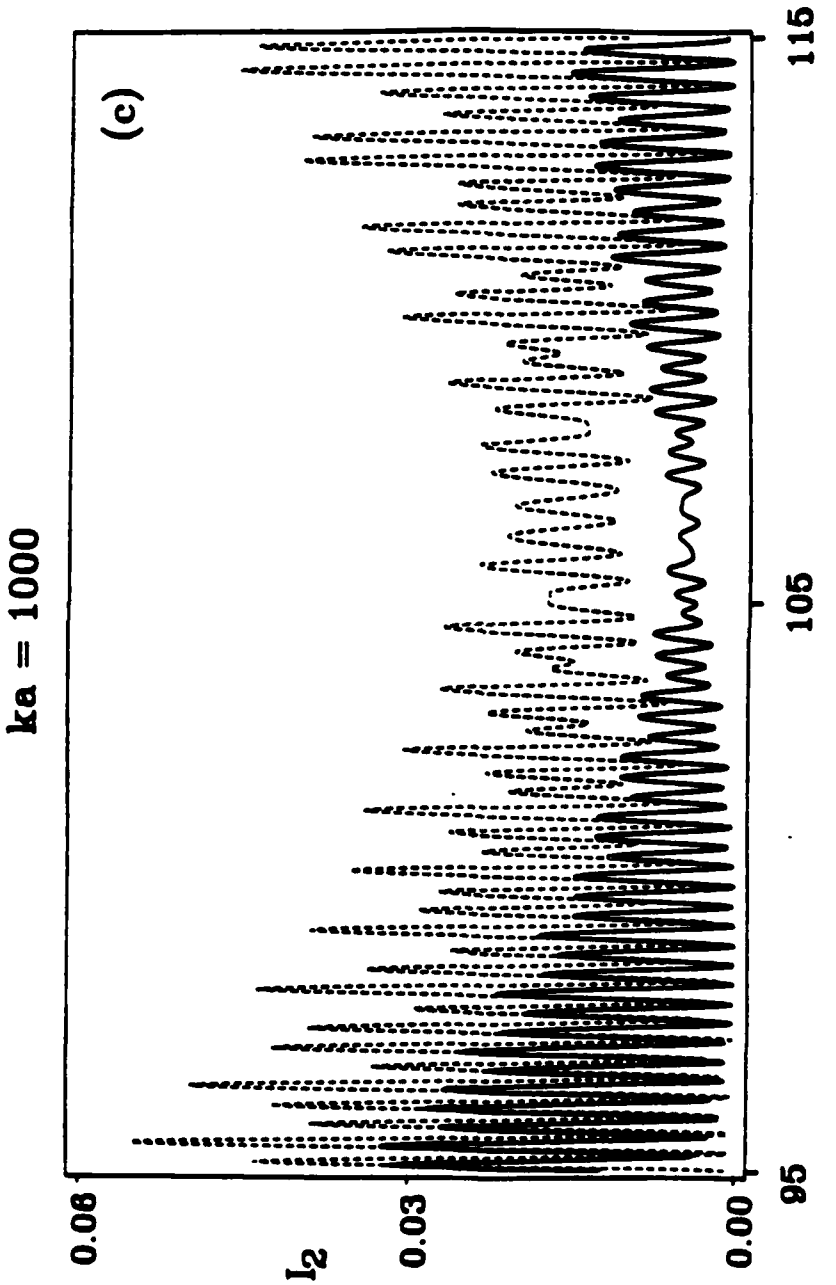

Fig. 2.4 (c)

fine structure oscillations (especially prominent in Fig. 2.4(c)). This behavior may affect the use of the Brewster angle region as a method of discriminating bubbles from particles in water since the ratio of the irradiances between it and the critical region vary non-uniquely for different coating values. The critical angle region also shows this behavior but due to the fact that irradiance values are generally several orders of magnitude higher the effects are of greater interest for the sizing of coated bubbles and hence further analysis shall be concentrated on this region.

It has been demonstrated by Marston and Langley[14] that noncoated bubbles exhibit coarse irradiance oscillations as the scattering angle θ decreases below a critical value for total reflection $\theta_c = 82.82°$ in water. With the introduction of a coating under the condition $n_c > n_w$, we find that this coarse structure begins to shift towards this noncoated critical angle with the degree of the angle shift dependent on the coating thickness h and the coating index of refraction n_c. In addition to this coarse structure angle shift the magnitude of both I_1 and I_2 can generally increase. Examples of this angular shift and magnitude amplification for $ka = 100$ with thickness values ranging from 0.25 μm to 3.0 μm are shown in Fig. 2.5(a)-(e). (Note that in these figures coarse structure comparison is also made with the physical-optics approximation.) The fact that the shifting of coarse structure is small near θ_c is noteworthy since noncoated results may be used to estimate the magnitude of the scattering from coated bubbles in many cases of interest. Note also that the physical-optics approximation does very well for coated bubbles in the critical angle region for thickness values less than 1 μm. The next structural change examined is the change in magnitude and period of the superposed fine structure.

Figure 2.6 illustrates the evolution of the fine structure in I_2 from 30° to 90° as a function of coating thickness. In this figure the effects of the coating can be seen as early as $h = 0.08$ μm (Fig. 2.6(a)). As the thickness increases, both the first and second peaks

Figure 2.5. Calculated normalized irradiances for ka = 100 in the critical angle scattering region for I_2. The solid curve is from Mie theory, the thin-dashed curve is the calculated coated sphere result, and the thick-dashed curve is from the Marston-Kingsbury physical-optics approximation. The coating thickness values for λ_{air} = 632.8 nm are (a) h = 0.25 μm, (b) h = 0.5 μm, (c) h = 1.0 μm, (d) h = 2.0 μm, and (e) h = 3.0 μm.

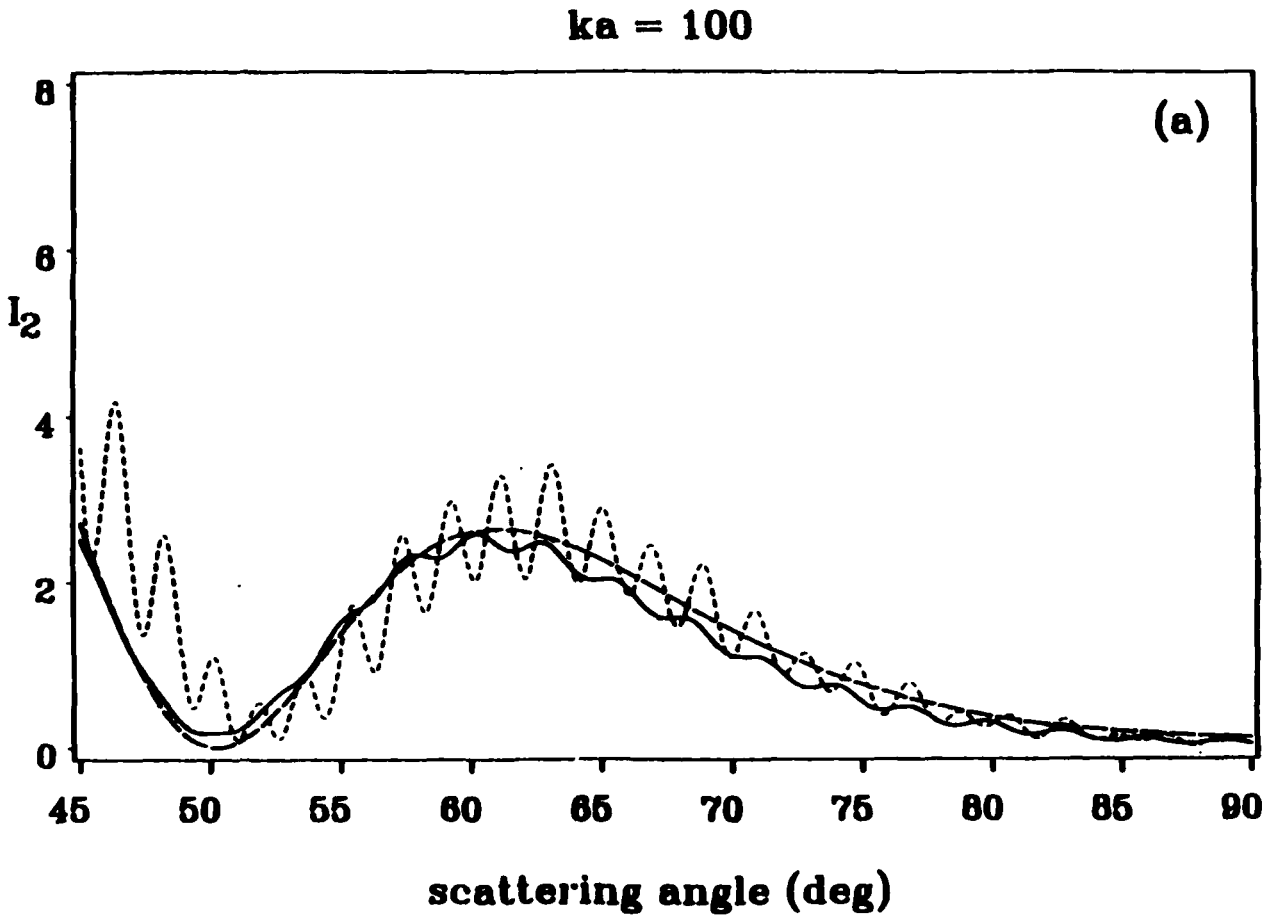
ka = 100
(a)
8
6
4
2
0
I_2
45
50
55
60
65
70
75
80
85
90
scattering angle (deg)

Fig. 2.5 (a)

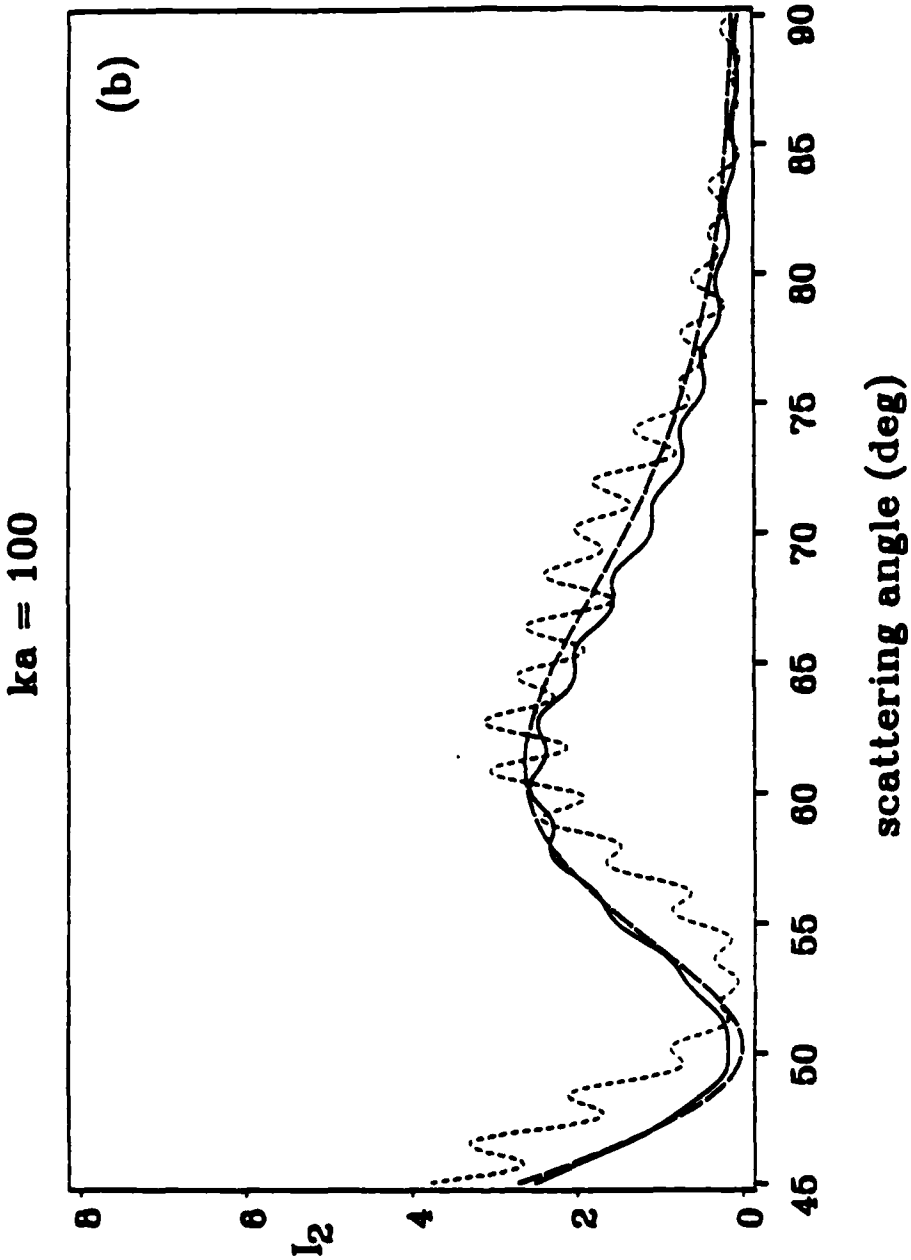
(b)
ka = 100
I_2
0
2
4
6
8
45
50
55
60
65
70
75
80
85
90
scattering angle (deg)

Fig. 2.5 (b)

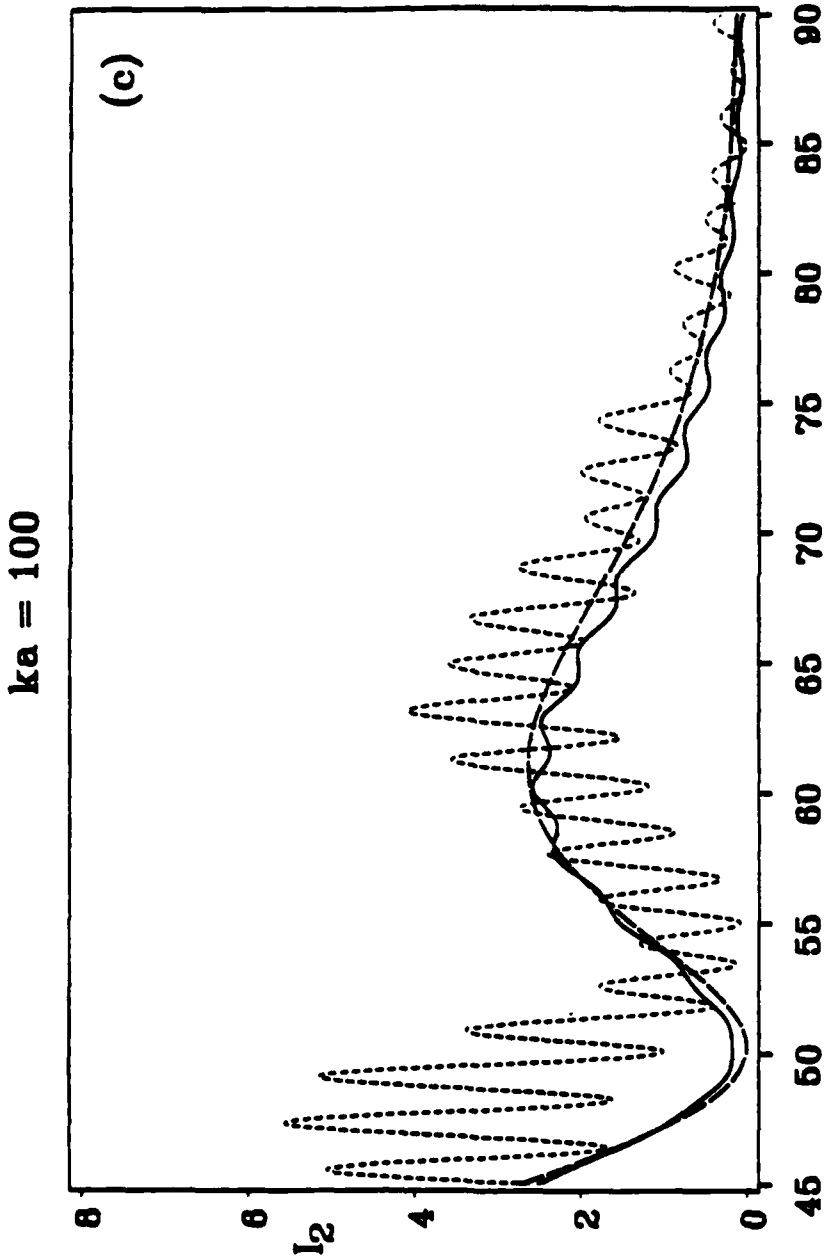
(c)
ka = 100
I_2
0
2
4
6
8
45
50
55
60
65
70
75
80
85
90
scattering angle (deg)

Fig. 2.5 (c)

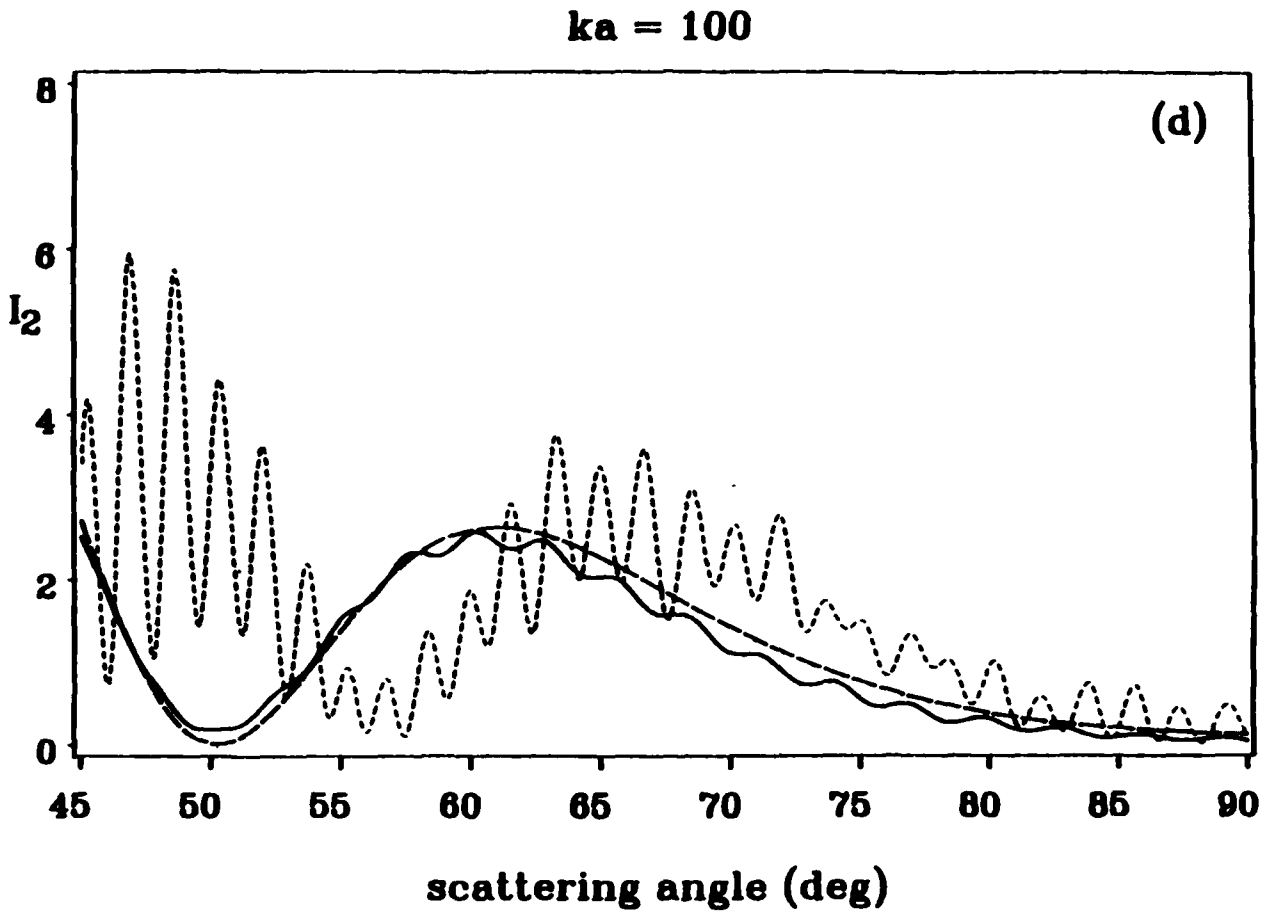
ka = 100
(d)
I_2
0
2
4
6
8
45
50
55
60
65
70
75
80
85
90
scattering angle (deg)

Fig. 2.5 (d)

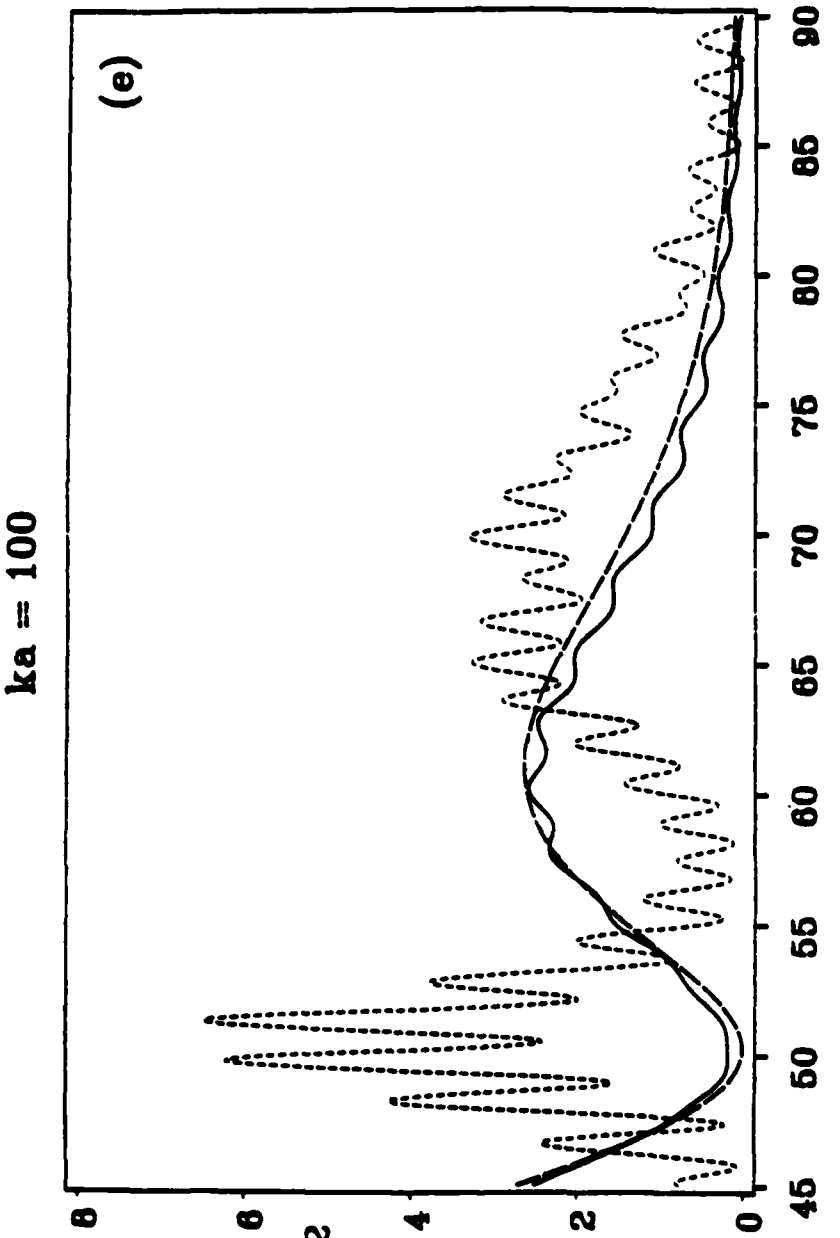
(e)
ka = 100
I_2
0
2
4
6
8
45
50
55
60
65
70
75
80
85
90
scattering angle (deg)

Fig. 2.5 (e)

Figure 2.6. Evolution of the fine structure as a function of coating thickness for parallel polarized irradiance for ka = 100. Coating thickness values for λ_{air} = 632.8 nm are (a) 0 μm, (b) 0.08 μm, (c) 0.15 μm, (d) 0.19 μm, (e) 0.23 μm, (f) 0.48 μm, (g) 0.66 μm, (h) 0.93 μm, and (i) 1.13 μm. The corresponding values of AOB specified in the computation were: (a) 1.0, (b) 0.990, (c) 0.980, (d) 0.975, (e) 0.970, (f) 0.940, (g) 0.920, (h) 0.890, (i) 0.870.

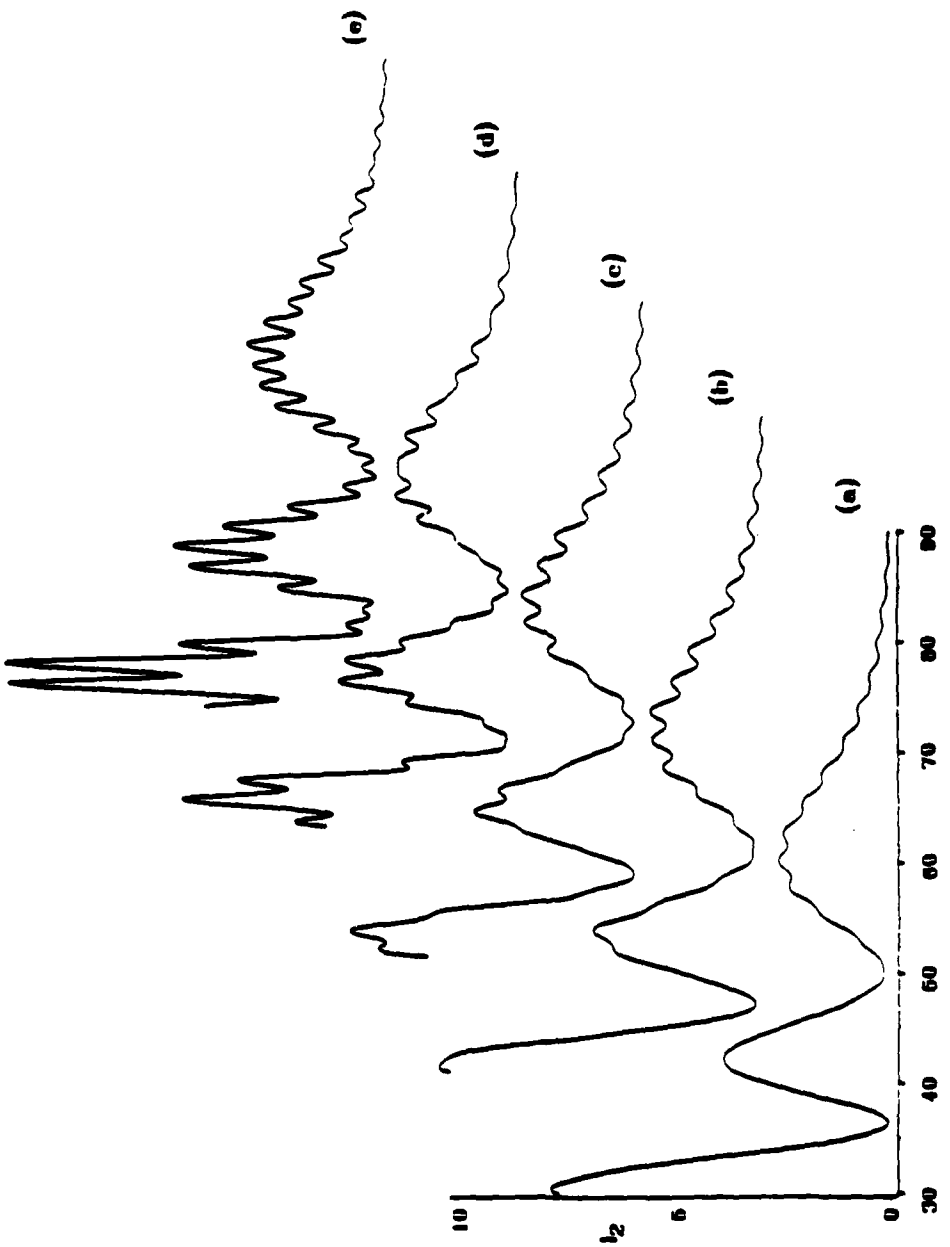

Fig. 2.6.

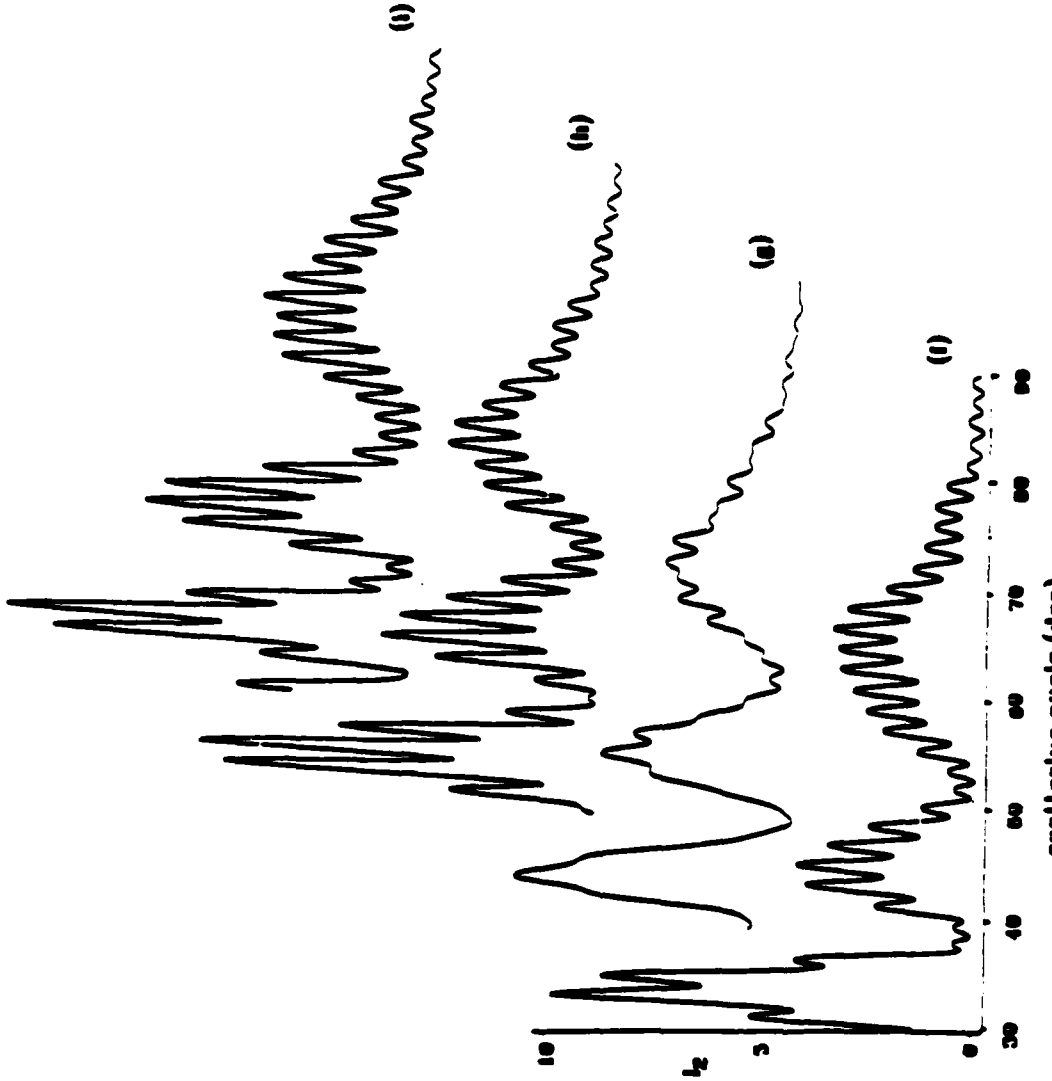

Fig. 2.6 (cont.).

from the left begin to decay into finer structure while the large number of smaller peaks increase in amplitude and move closer together. At $h = 0.23\ \mu m$ (Fig. 2.6(e)) the fine structure becomes quite prominent. An interesting effect was also noted certain values like $h = 0.66\ \mu m$ (Fig. 2.6(g)). At these particular values the fine structure amplitude is diminished as is shown. Possible reasons for this will be discussed in the next section.

B. Geometric Modeling

Interpretation of the results found in Section A may be done using Fig. 2.7. Adopting the notation of Langley we define rays using the notation (p,l), where p is the number of chords within the bubble and l equals the number of crossings of the optic axis. Note that a subscript b will be used to indicate rays that pertain to the outer sphere only. Examining the two rays used in the physical-optics approximation, namely the (0,0) and (1,0) rays, and the (2,1) ray the figure shows that the coating shifts the scattered ray towards higher values of θ as well as increasing the distance between the (0,0) and (2,1) ray. The first mentioned effect partially accounts for the observed coarse structure angle shift while the second partially accounts for the change in the fine structure.

It has been shown[14] that interference between the (0,0) and (2,1) rays is partially responsible for the fine structure oscillations. The quasi-period $\Delta\theta_{fs}$ of this structure near the critical angle has been calculated in a first term approximation to be roughly equal to λ_w/B_2, where B_2 is the distance between the (0,0) and the (2,1) ray. Thus, by increasing B_2 with the addition of the coating, the fine structure will have a smaller period which is clearly the case. The damped fine structure seen in Fig. 2.6(g) is most likely due to effect of the coating on reflection and transmission coefficients. The purpose of the geometric modeling is to give the reader some physical insight in the interpretation of the computational results presented. It is by no means meant to be a complete

Figure 2.7. Coated sphere geometric model. Rays are specified by (p,l) where p = the number of chords within the bubble, and l = the number of crossings of the optic axis. Dashed lines indicate the uncoated sphere ray paths while solid lines represent coated sphere ray paths. Note that bending of the rays is exaggerated for effect. The subscript b indicates rays which pertain to the outer sphere only.

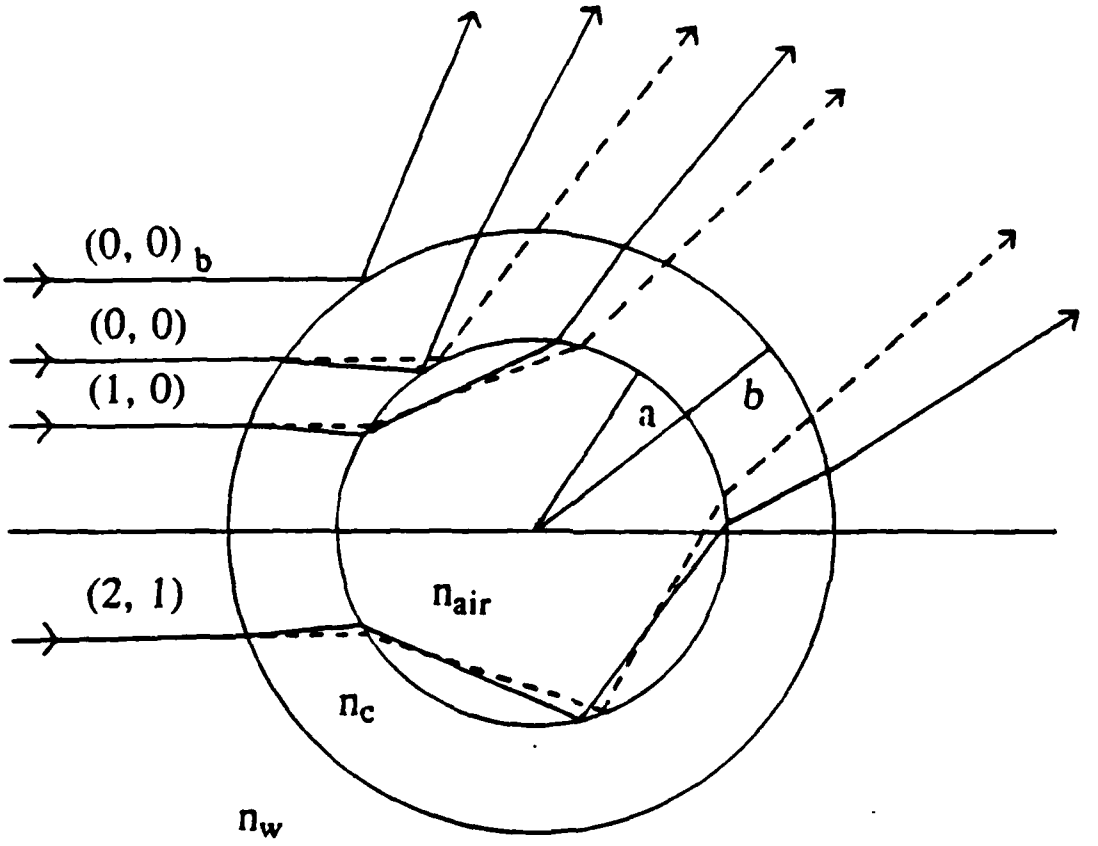

Fig. 2.7.--Coated sphere geometric model.

description of the rather complex phenomena of scattering of radiation by coated bubbles. Note also that the bending of rays is exaggerated for illustration of the effect of the coating.

C. Coating Effects on Larger Bubbles

The calculated $j = 2$ critical angle region results for a range of coating thicknesses for ka equal to 500, 1000, and 2500 ($a \approx 37.8$ μm to 189 μm for $\lambda_w = 474.6$ nm) respectively are shown in Figs. 2.8 to 2.10. The parameters used were similar to those used for Fig. 2.5. The effects of the coating on increasing bubble size indicate that as ka becomes larger with h fixed the angular phase shift in the coarse structure is diminished. Marston has calculated this shift in the thin film limit for the critical angle region to be proportional to h/a which agrees with the shown results. Another effect noted with increasing bubble size is that the changes in the fine-structure are less drastic for a given value of h as bubble size increases. As an example, comparison between Figs. 2.5(e) and 2.9(e) (the 3 μm thickness cases for $ka = 100$ and $ka = 1000$) shows that in the smaller bubble case a 3 μm thickness (thin-dashed line) has drastically changed the intensity structure from the original noncoated case (solid line) while for the large bubble results, a lesser shift in the coarse oscillations and a slight increase in fine-structure amplitude has occurred. The original noncoated structure, however, has remained. Another feature overlayed on these graphs is the physical-optics approximation. The approximation does well predicting the coarse structure for larger values of ka for thin coatings (less than 0.5 μm) over most of the graphed regions and is capable of accounting for coarse structure at most coating thickness values in the critical angle region (approximately 80° to 85°) due to the stationary behavior of the angular shift near θ_c.

Figure 2.8. Calculated normalized irradiances for ka = 500 (a = 37.8 μm) in the critical scattering region for I_2. The solid curve is from Mie theory, the thin-dashed curve is the calculated coated sphere result, and the thick-dashed curve is from the phyiscal-optics approximation. The coating thickness values for λ_{air} = 632.8 nm are (a) h = 0.25 μm, (b) h = 0.5 μm, (c) 1.0 μm, (d) h = 2.0 μm, and (e) h = 3.0 μm.

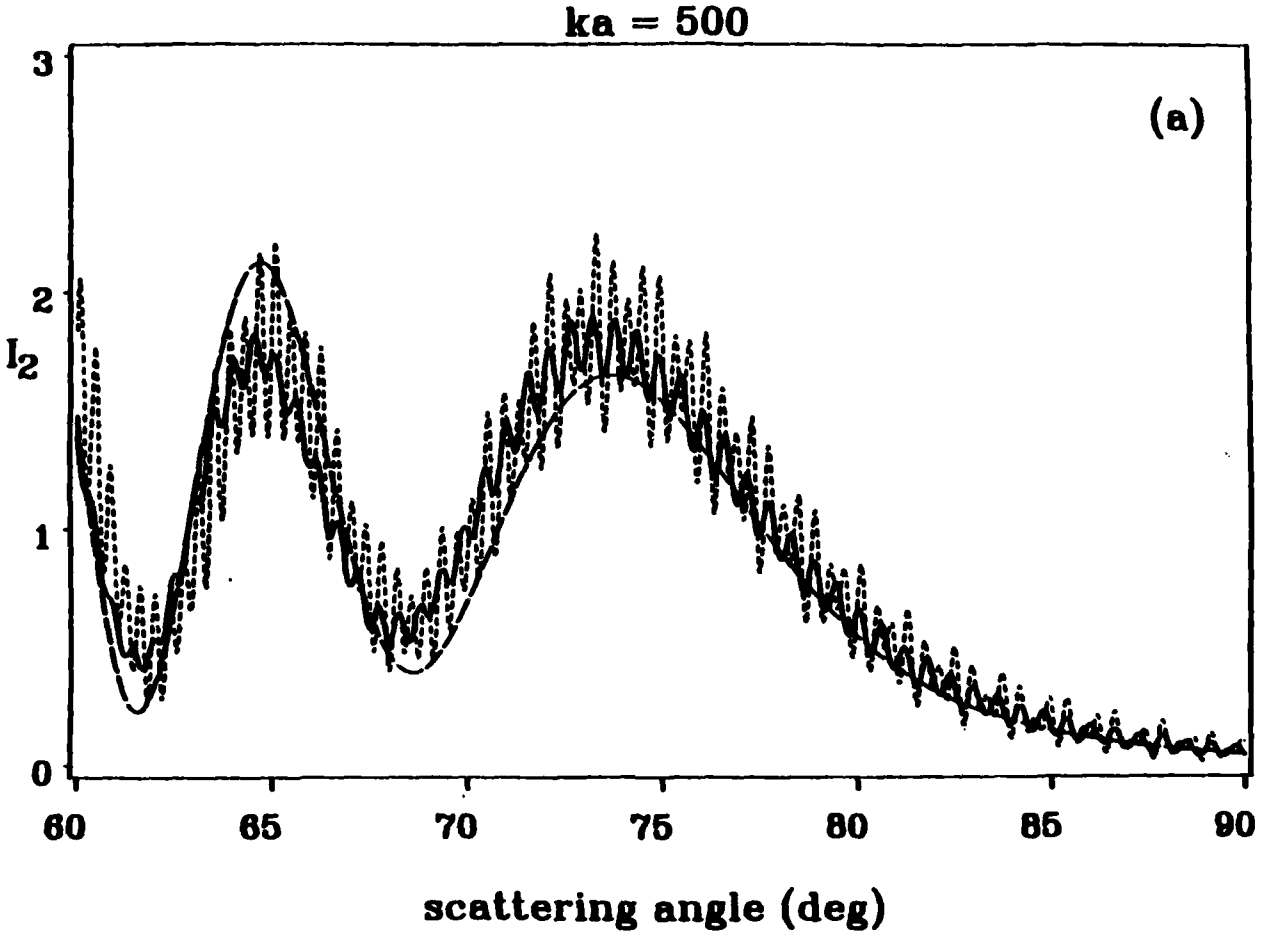

Fig. 2.8 (a)

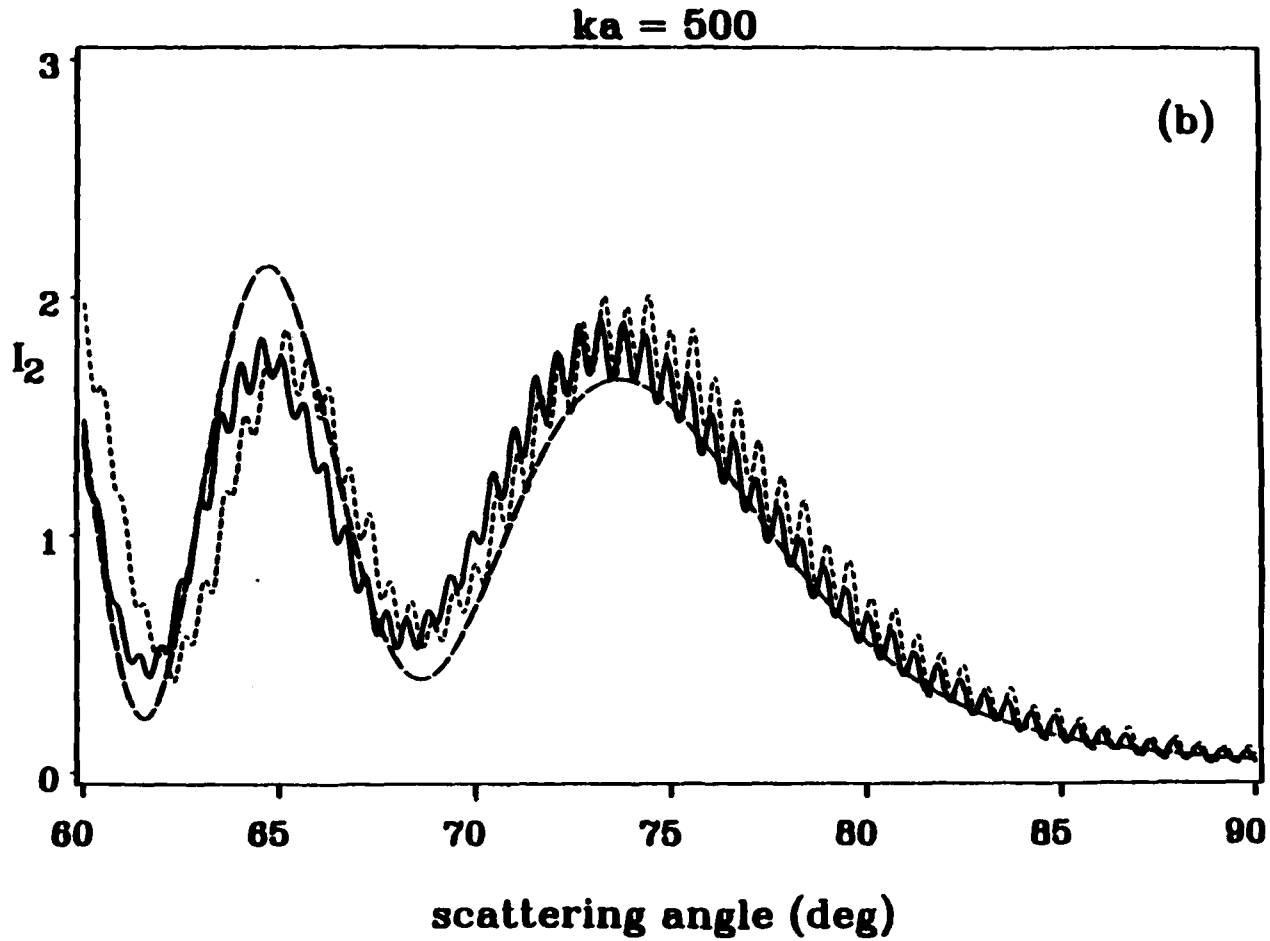

Fig. 2.8 (b)

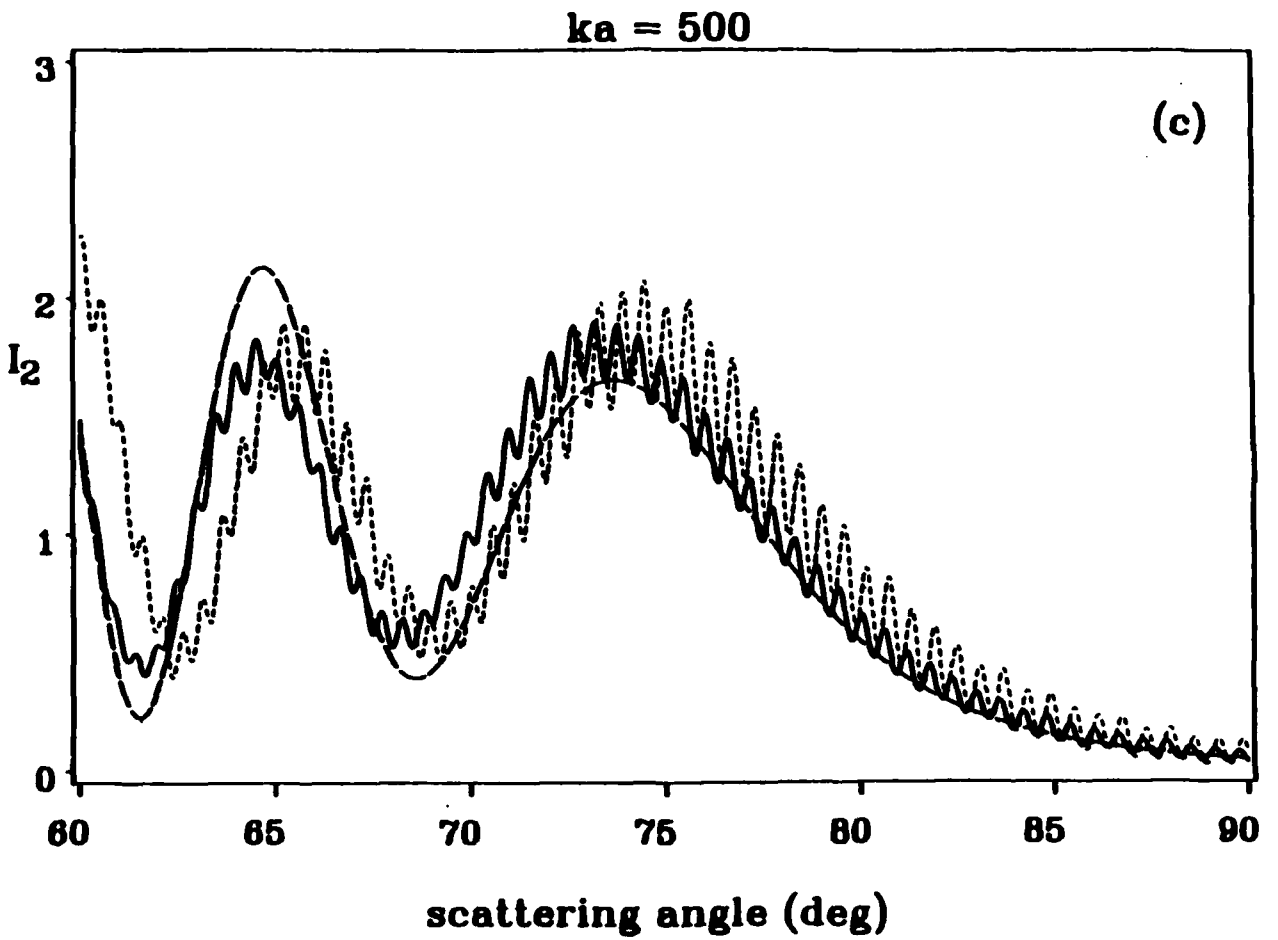

Fig. 2.8 (c)

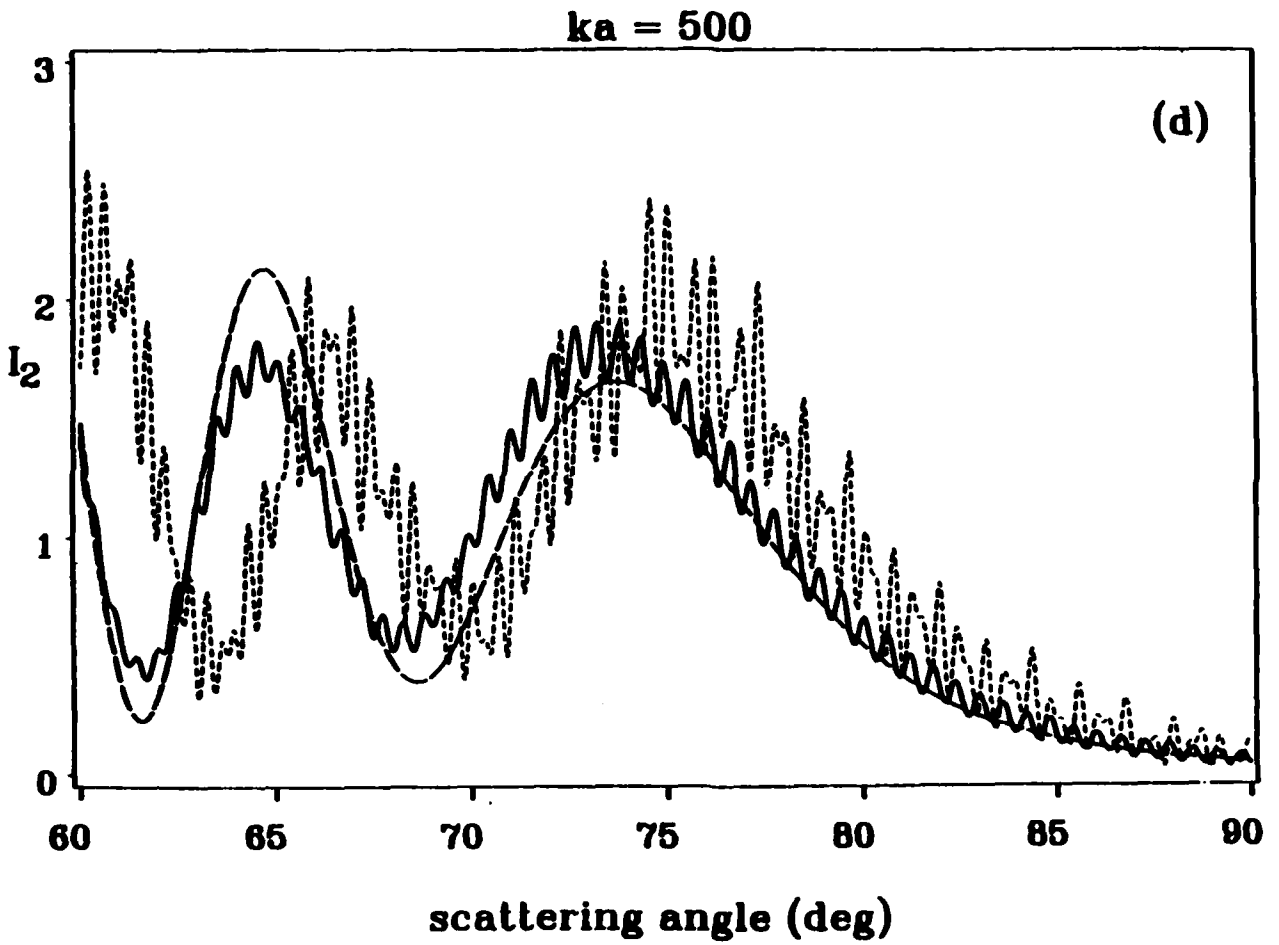

Fig. 2.8 (d)

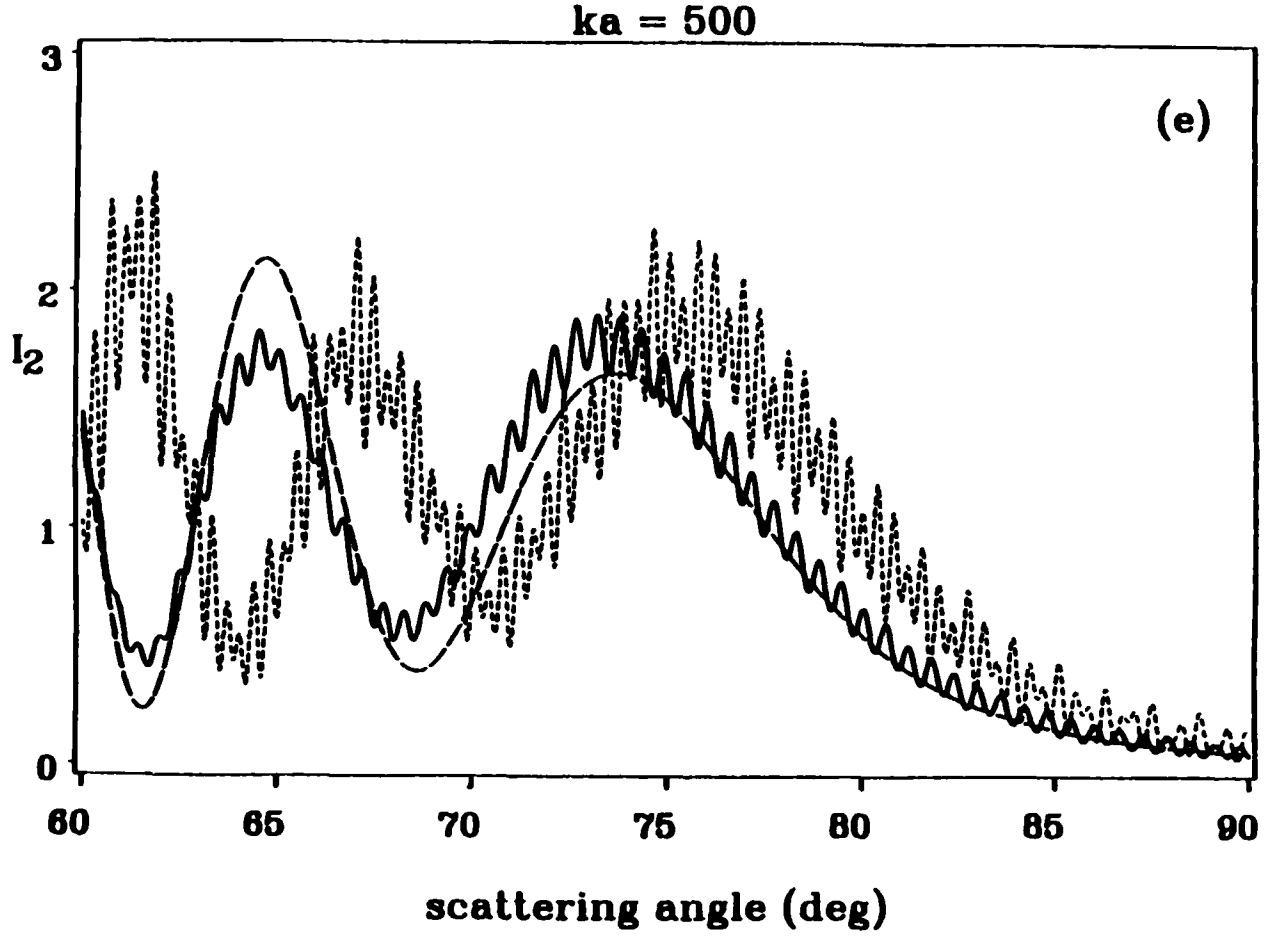

Fig. 2.8 (e)

Figure 2.9. Like Figure 2.8 but for ka = 1000 with (a) h = 0.25 μm, (b) h = 0.53 μm, (c) h = 0.99 μm, (d) h = 2.01 μm, and (e) h = 3.00 μm.

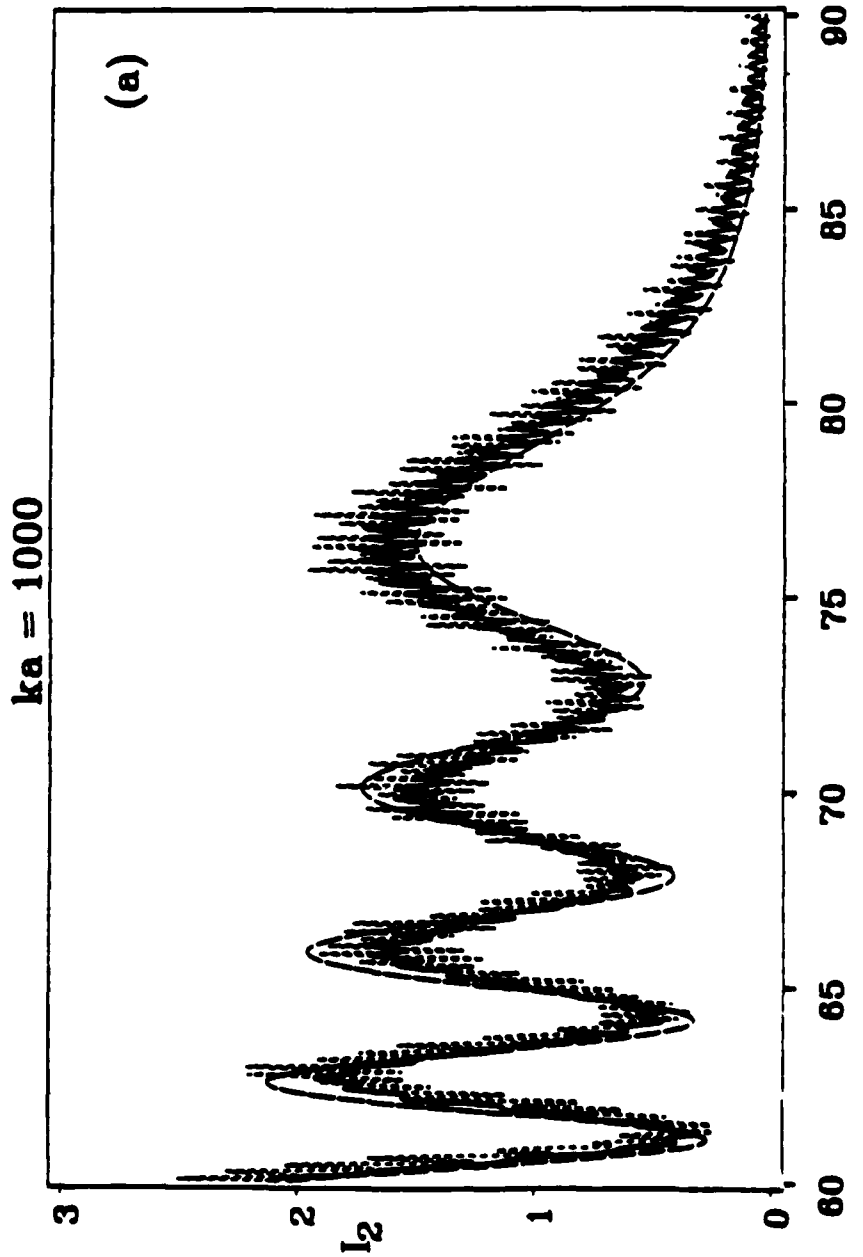

Fig. 2.9 (a)

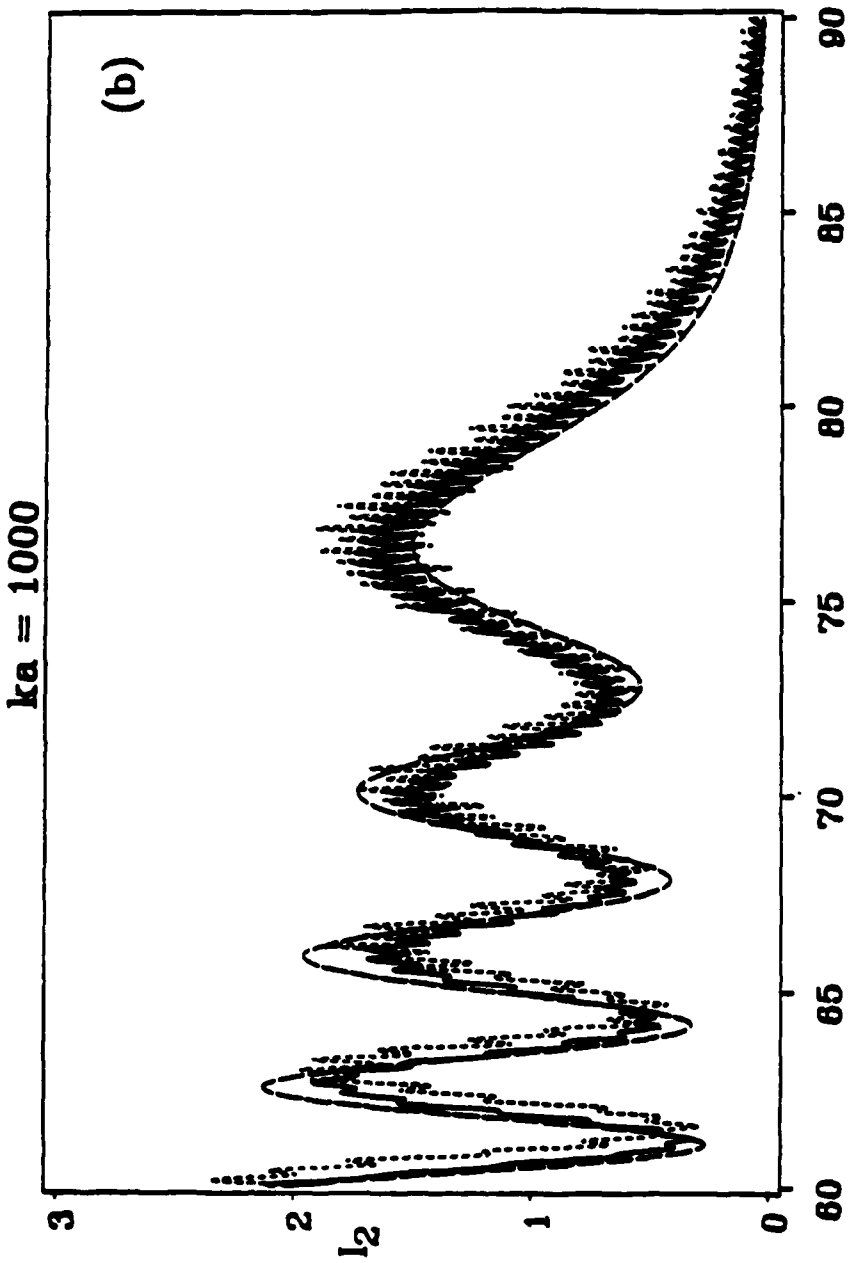

Fig. 2.9 (b)

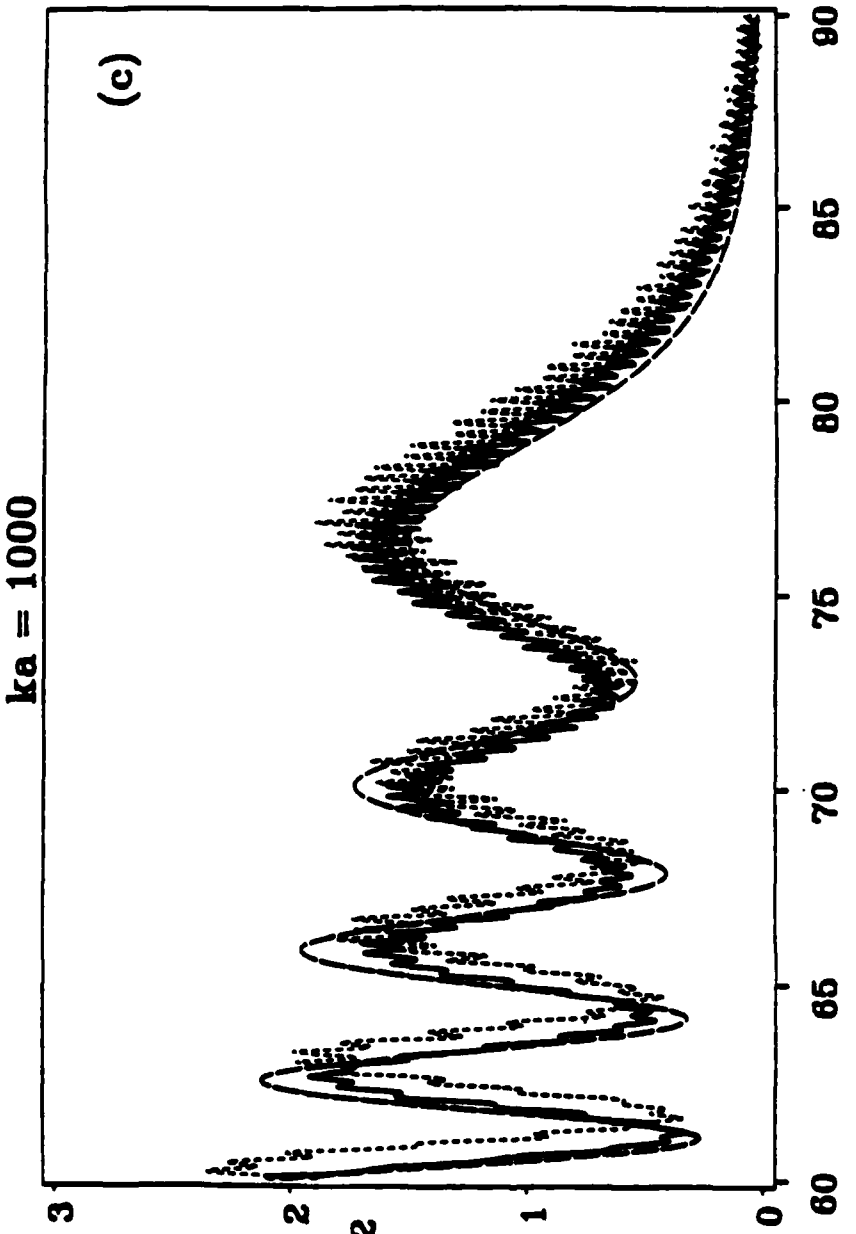

Fig. 2.9 (c)

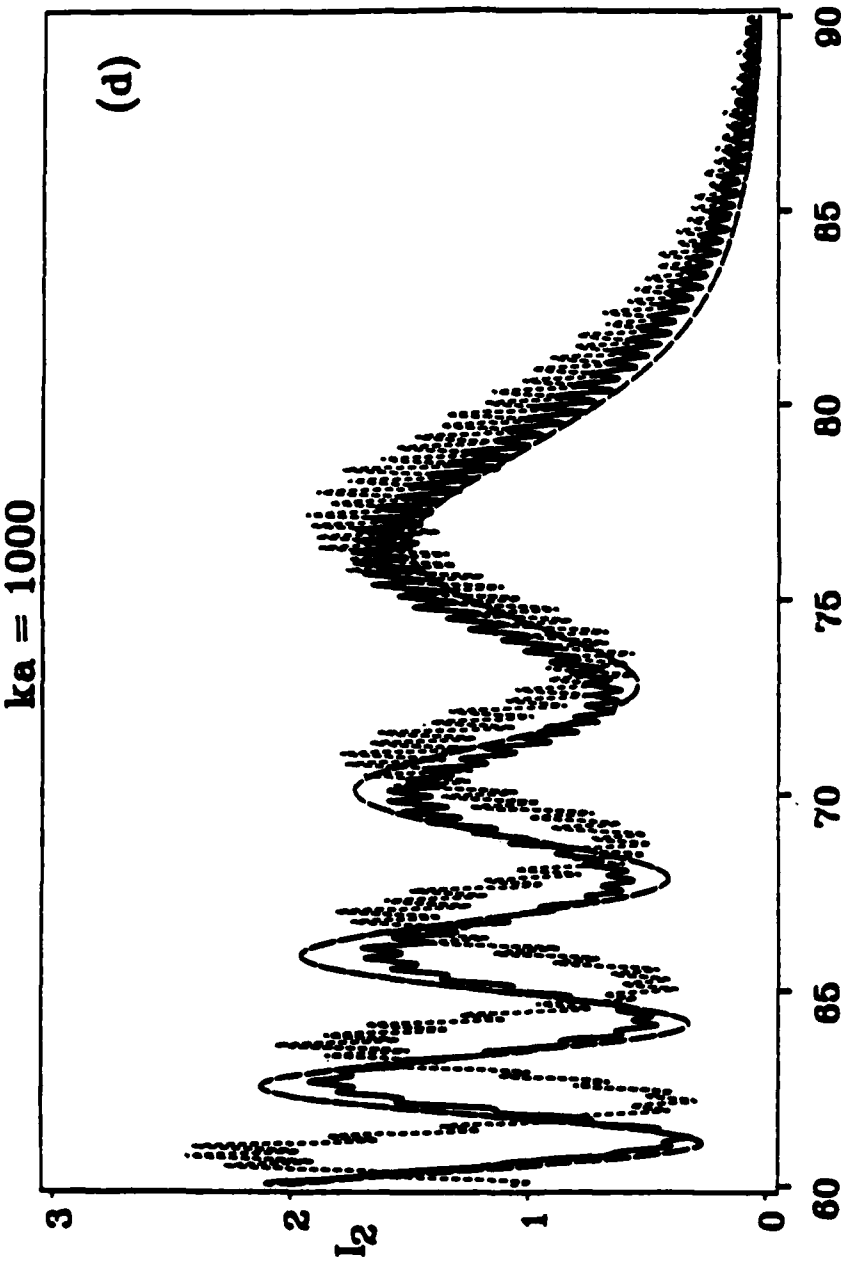

Fig. 2.9 (d)

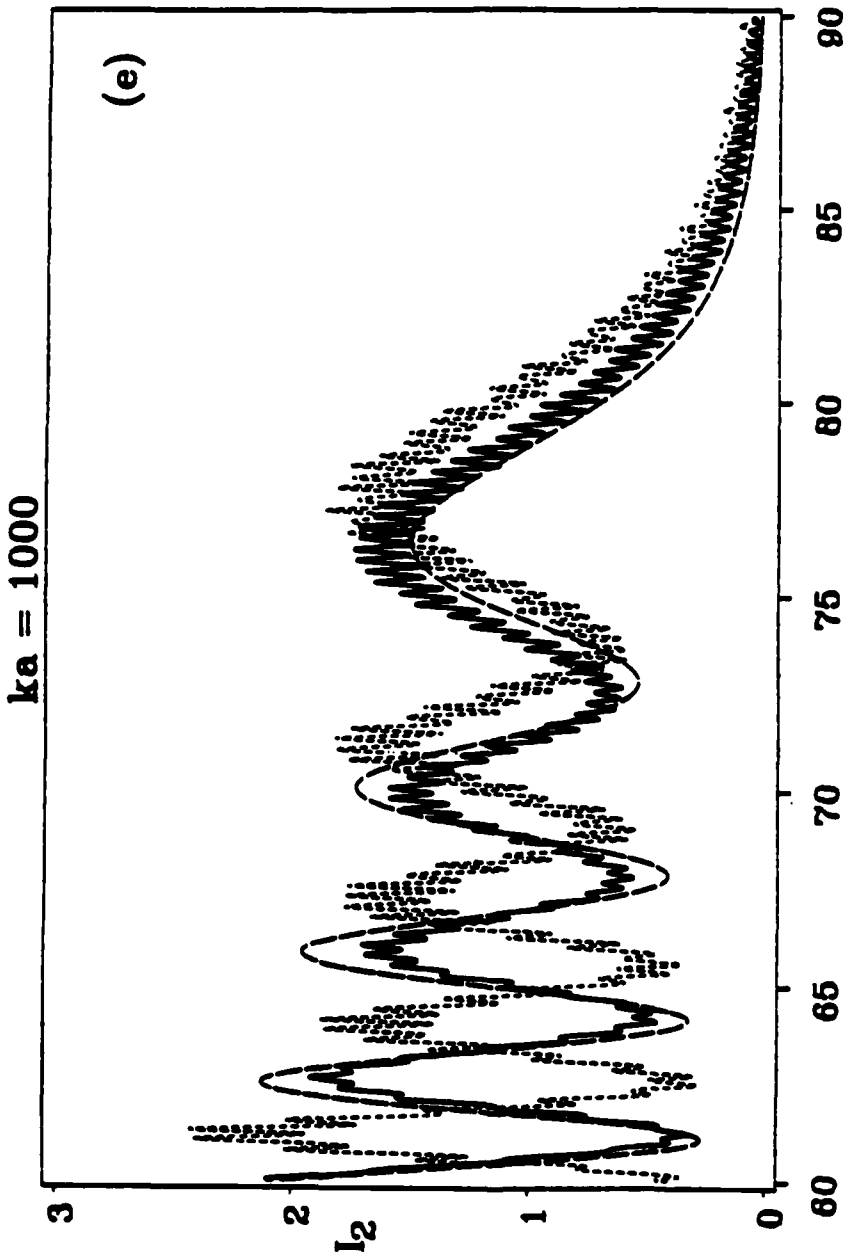

Fig. 2.9 (e)

Figure 2.10. Thickness values approximately equal to those in Figure 2.8 but for ka = 2500. See Table 2.1.

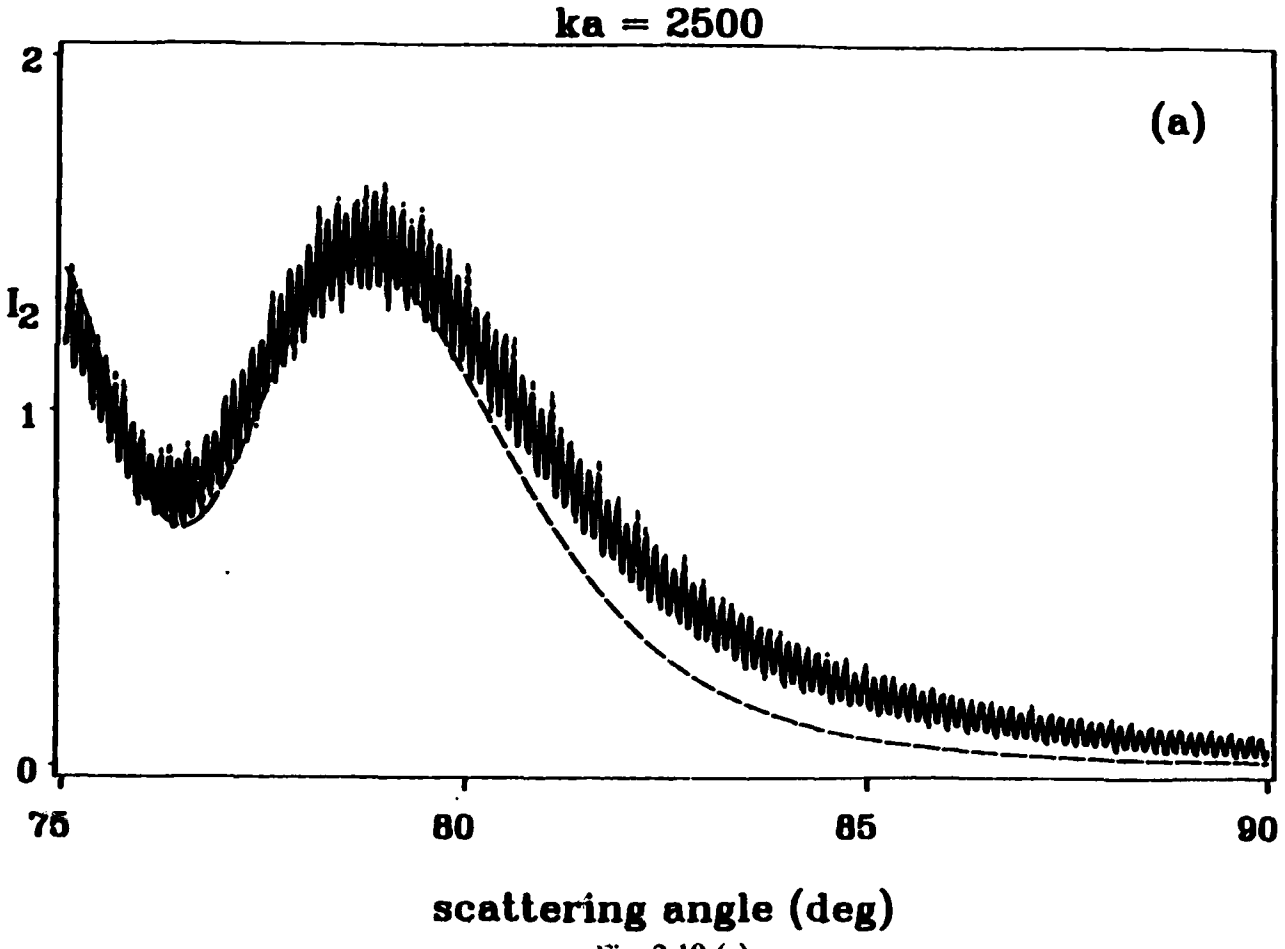

Fig. 2.10 (a)

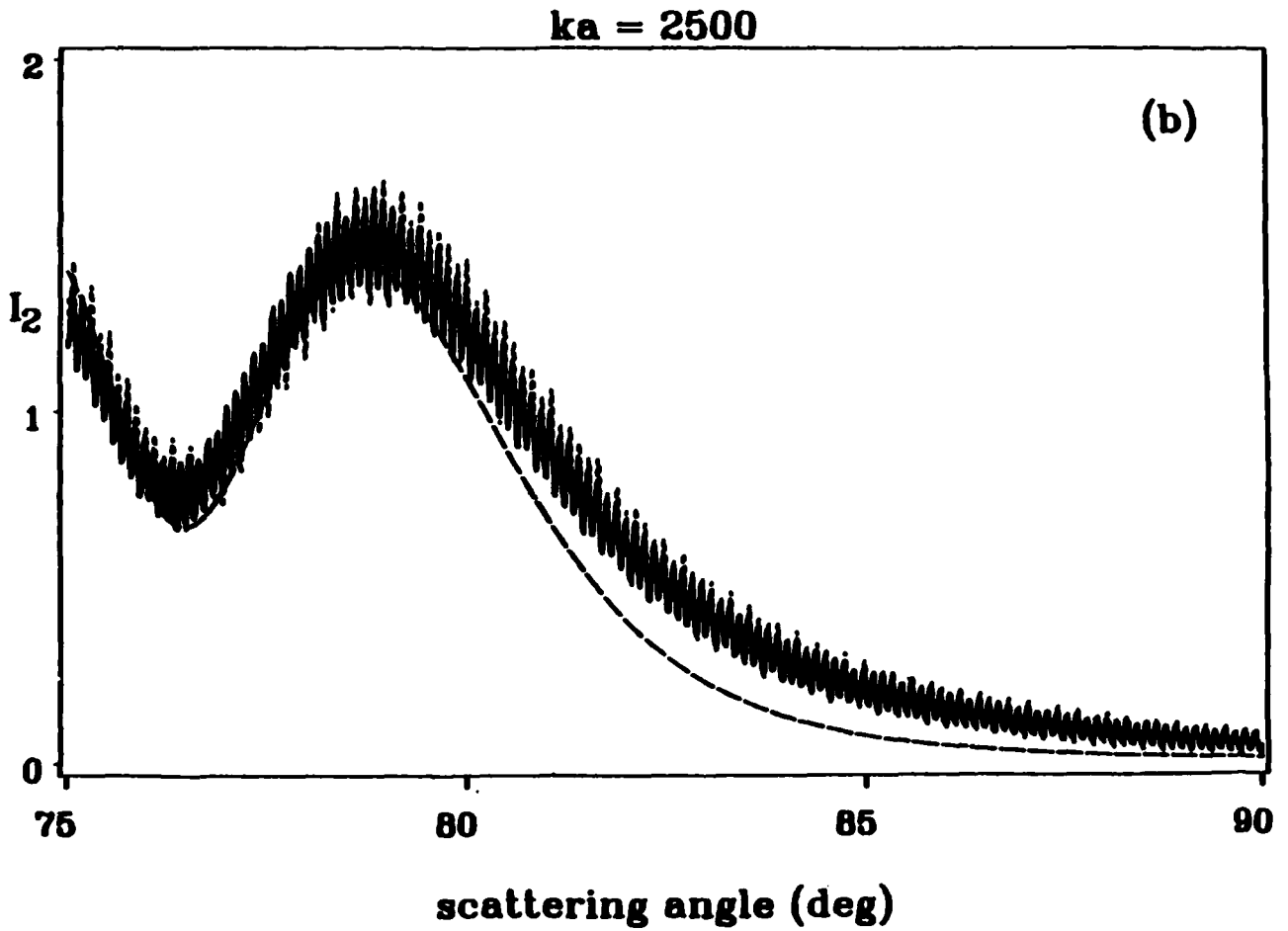

Fig. 2.10 (b)

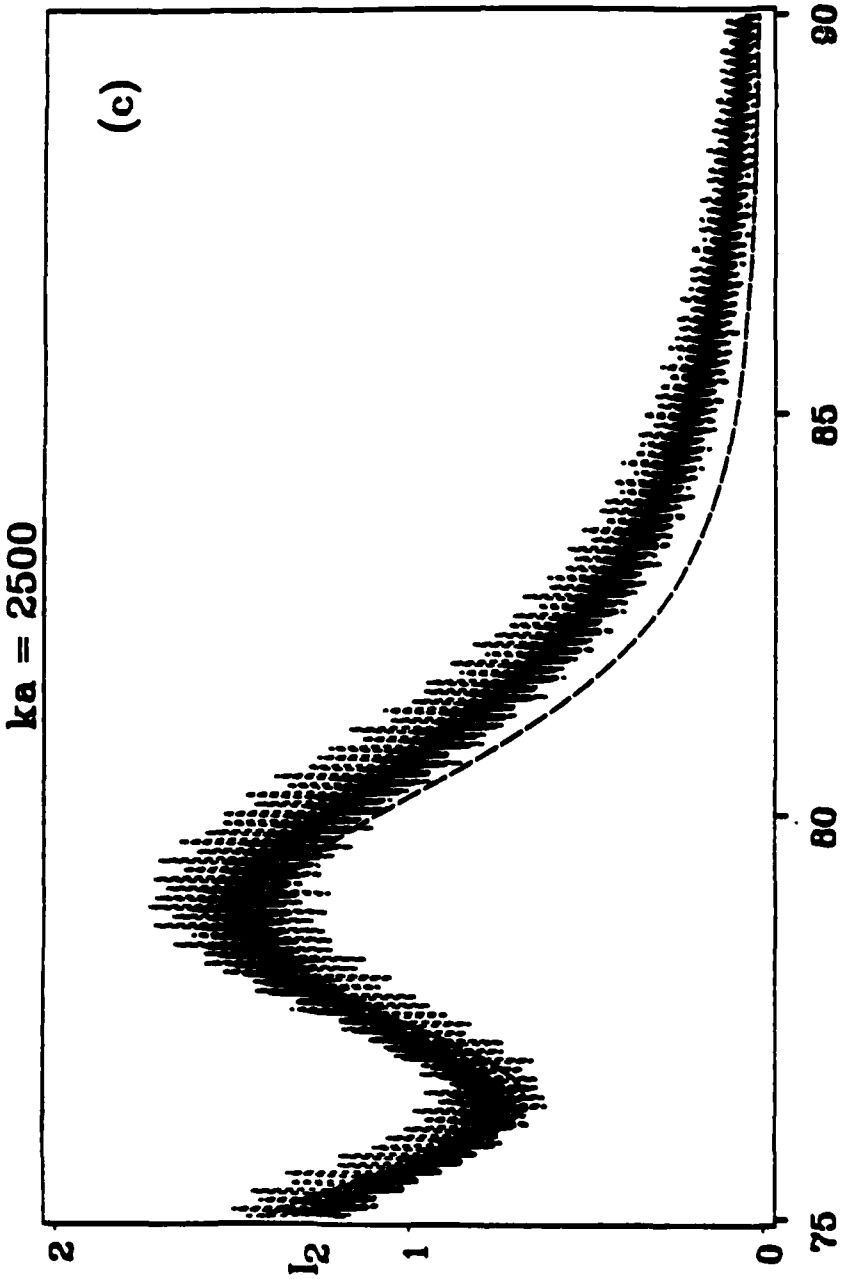

Fig. 2.10 (c)

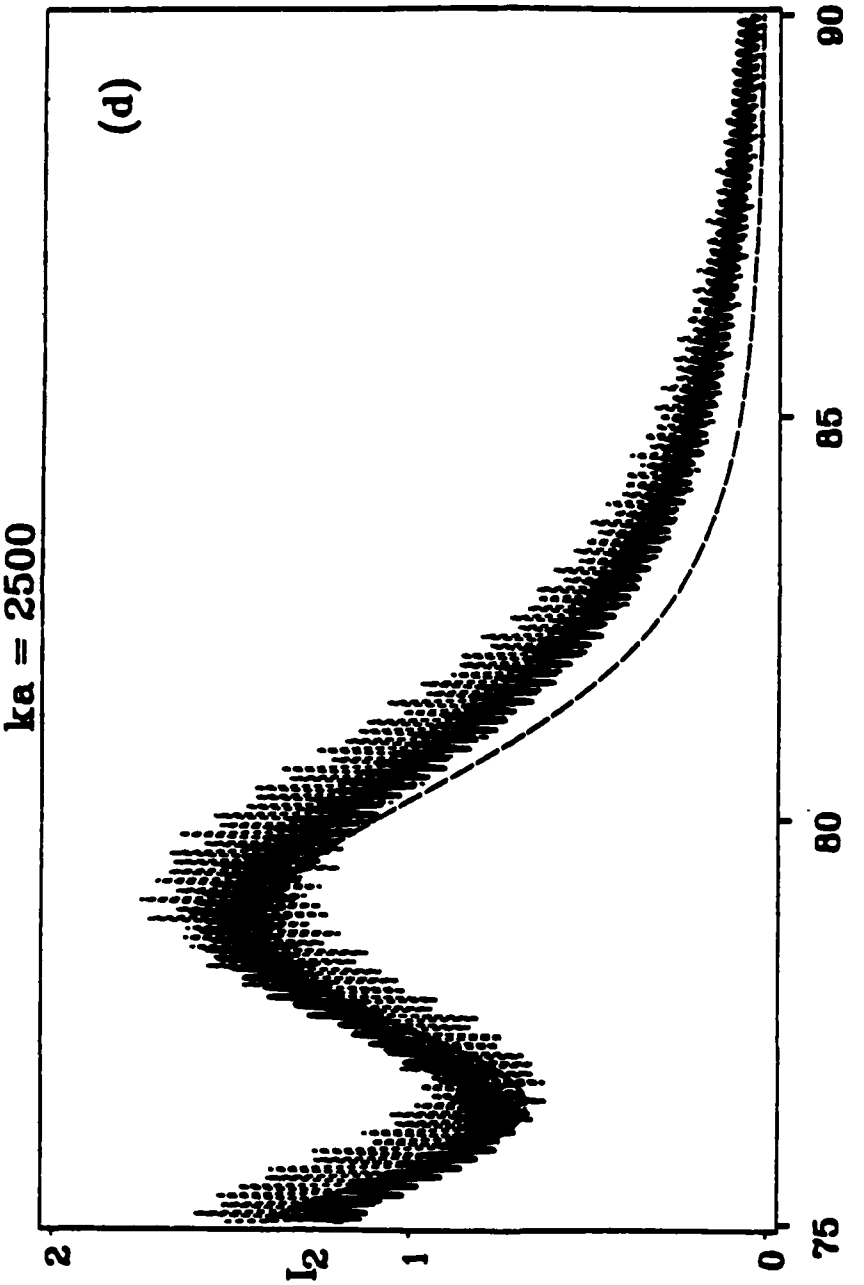

Fig. 2.10 (d)

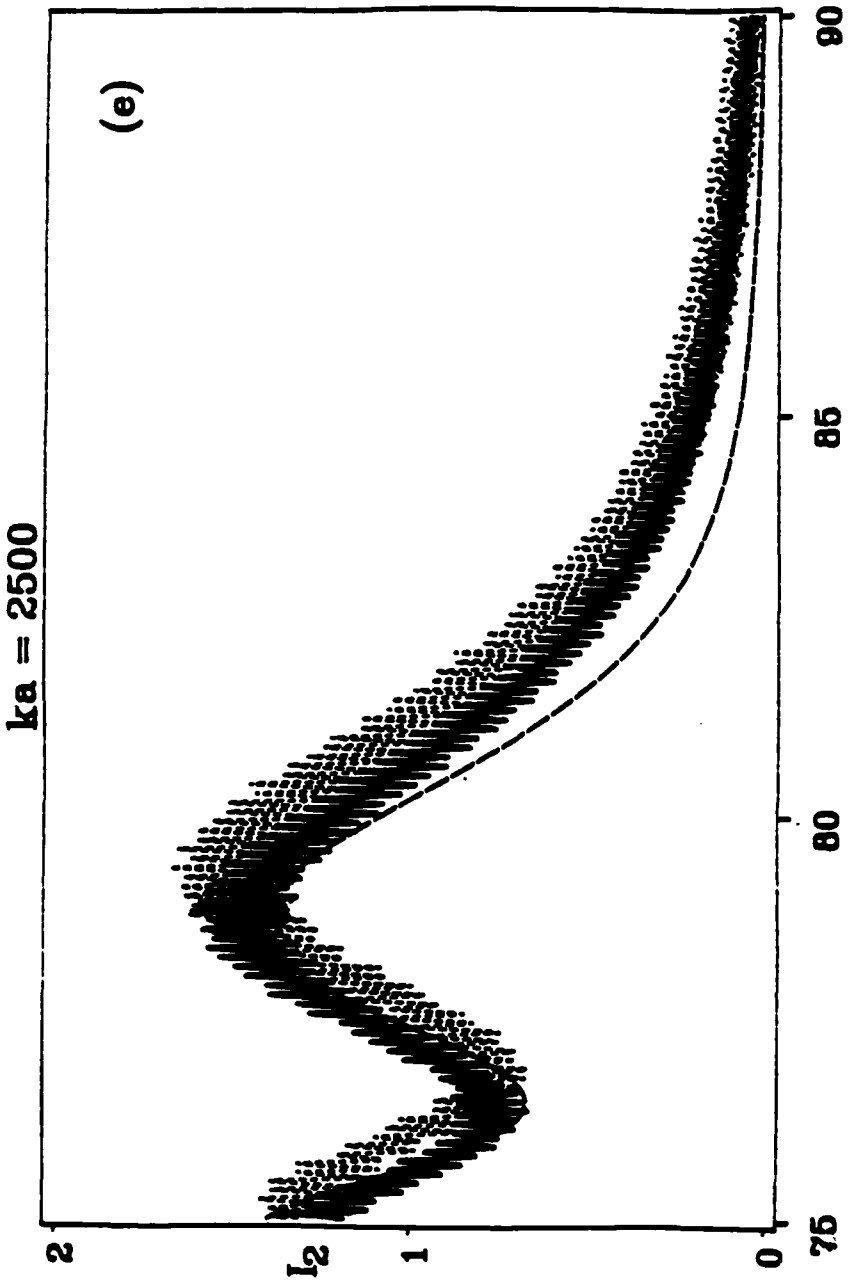

Fig. 2.10 (e)

D. Absorbing Coatings

Results for absorbing coatings are shown in Figs. 2.11 - 2.14. The range of absorbing coatings tested was $n_c = 1.5 + i1E\text{-}9$ (weakly absorbing) to $n_c = 1.5 + i1E\text{-}2$ (very strong absorption). The results in Figs. 2.11 - 2.13 indicate that the effects of absorbing coatings are negligible until the strong absorbing cases are reached ($n_c = 1.5 + i1E\text{-}3$). In Fig. 2.14 a typical result for the effects of increasing absorbing coating thickness is shown. As can be seen even with a 3.0 μm coat the effects are still small. This was even more apparent for the perpendicular case which is given in Appendix B. One notable effect was the decrease of the irradiance amplitude, which was greater at smaller values of θ and approached non-absorbing results near the critical angle. It should also be pointed out that the coarse structure angular shift is present in the absorbing coating cases also. Severe angle shift changes in the coarse structure amplitude and structure were observed in all cases for $n_c = 1.5 + i1E\text{-}2$ (Fig. 2.13).

In analyzing the absorbing coating results it was found that the effects of absorption were minimal. Since most liquids have very low absorption values[15] and coating thickness values are generally presumed to be small it is doubtful whether absorption will have a major effect on actual coated-bubble measurements. Thus, modeling could be done using the non-absorbing cases. This would speed up computation time considerably as the imaginary components would not be involved in the calculations. Another point of interest is that coatings would have to be extremely thick (> 3 μm), especially for larger bubbles, in order to have any major effects even for strongly absorbing cases. Finally, the absorption value for water is in the $I_m(n_w) \approx 1E\text{-}9$ region and the effects of such a small value of $Im(n_w)$ on the scattering pattern are expected to be small. Hence n_w is always taken to be real.

Figure 2.11. Calculated normalized irradiance for ka = 500 and n_c = 1.5 + i1E-3. The solid curve is the non-absorbing case at h = 1.01 μm, the thick-dashed curve is the physical-optics approximation, and the thin-dashed curve is the calculated absorbing coating result for h = 1.01 μm.

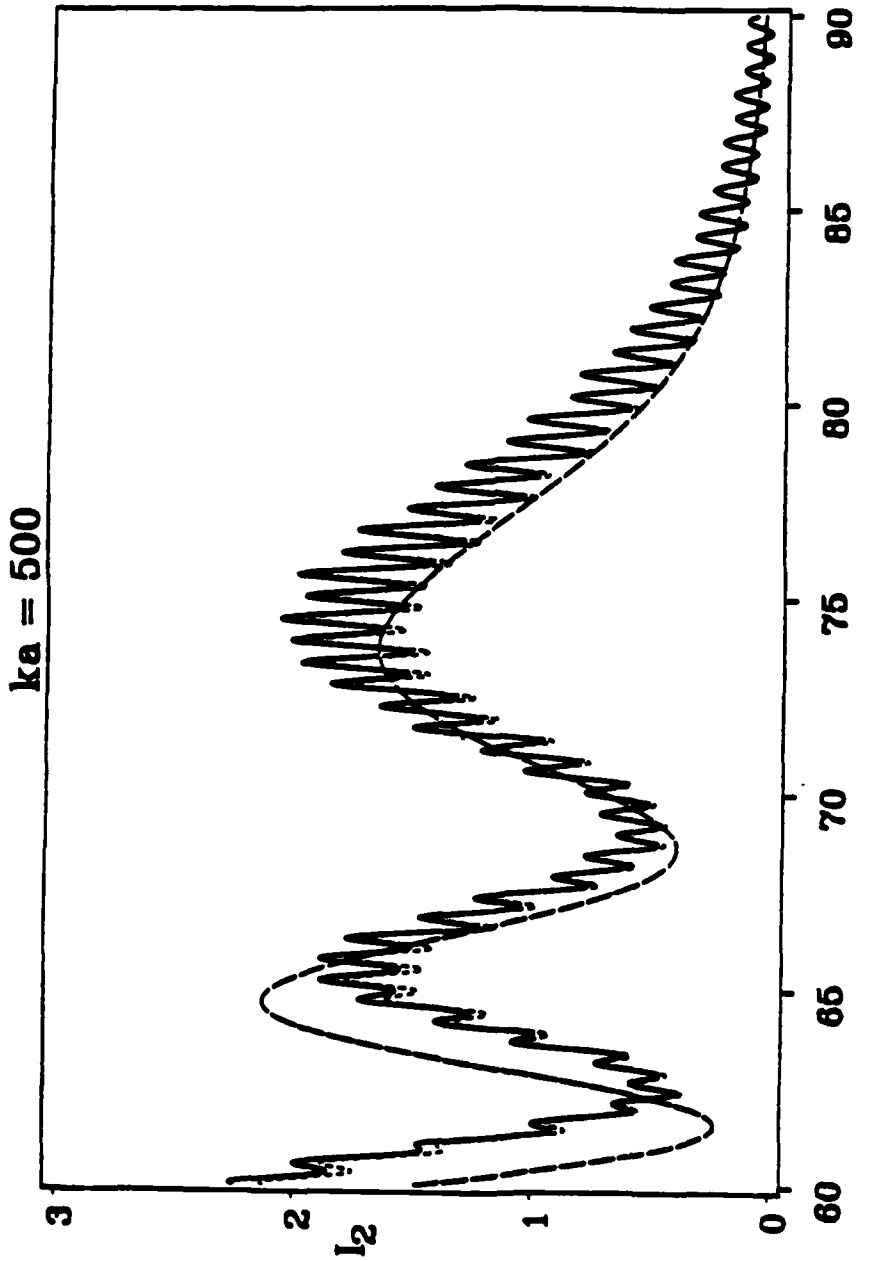

Fig. 2.11

Figure 2.12. Like Figure 2.11 but the thin-dashed curve represents n_c = 1.5 + i5E-3 at h = 1.01 μm.

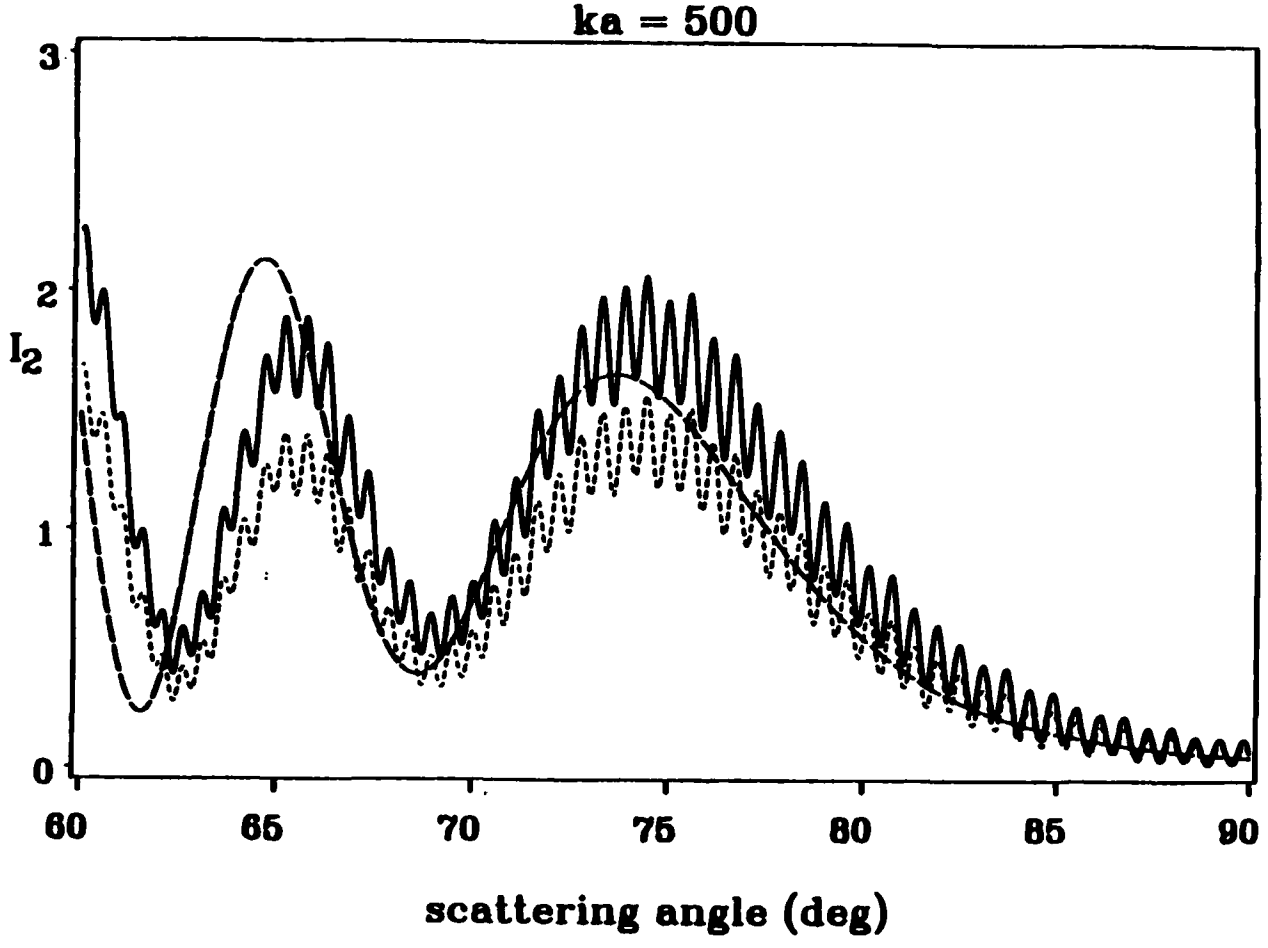

Fig. 2.12

Figure 2.13. Like Figure 2.11 but the thin-dashed curve represents $n_c = 1.5 + i1E\text{-}2$ at h = 1.01 μm.

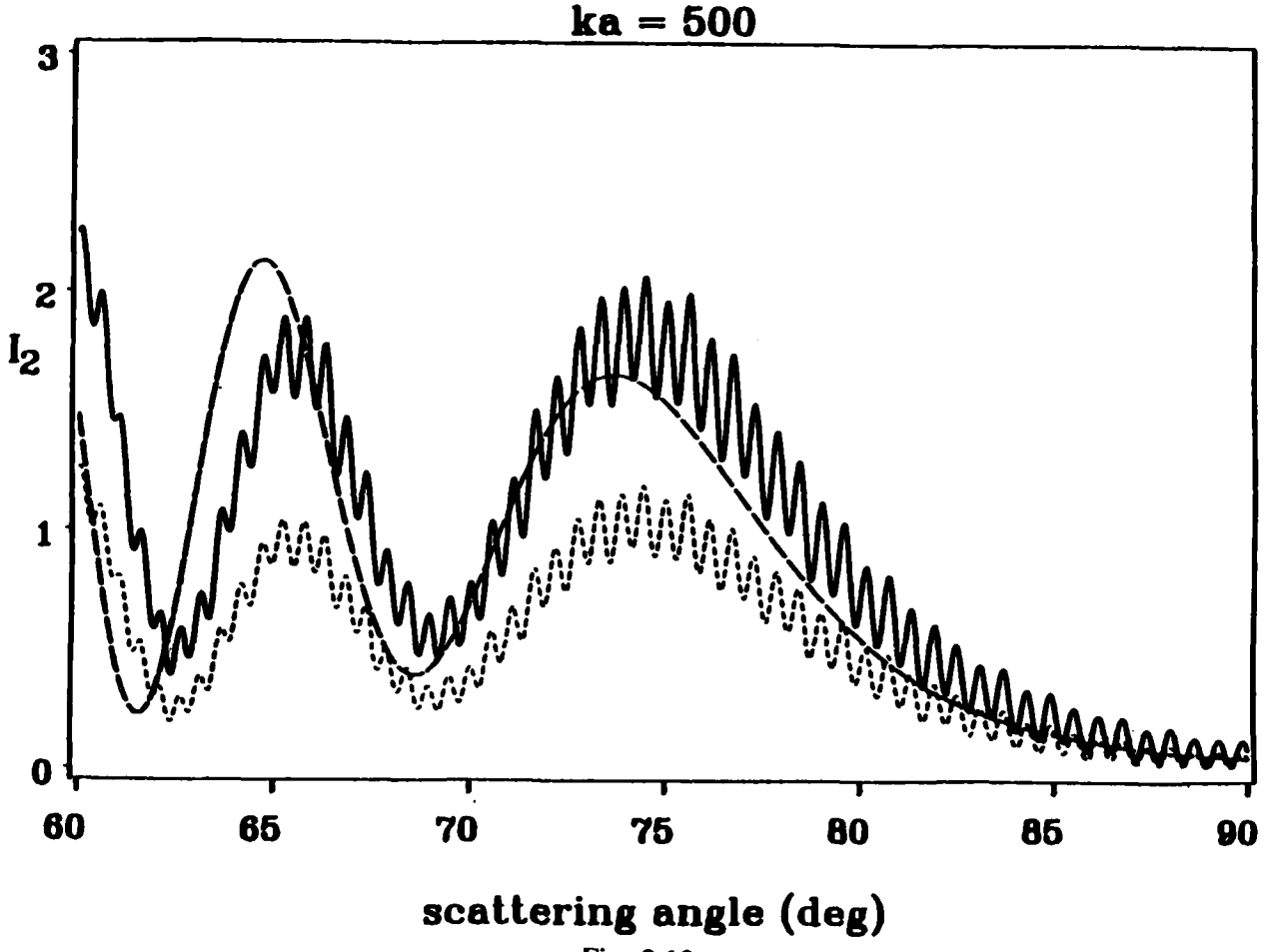

Fig. 2.13

Figure 2.14. Calculated normalized irradiances for ka = 1000 and n_c = 1.5 + i1E-3 for (a) h = 0.99 μm, (b) h = 2.01 μm, (c) h = 3.14 μm, and (d) h = 5.00 μm. The solid curves are non-absorbing results at the given values of h and the thin-dashed curve is the calculated absorbing coating results.

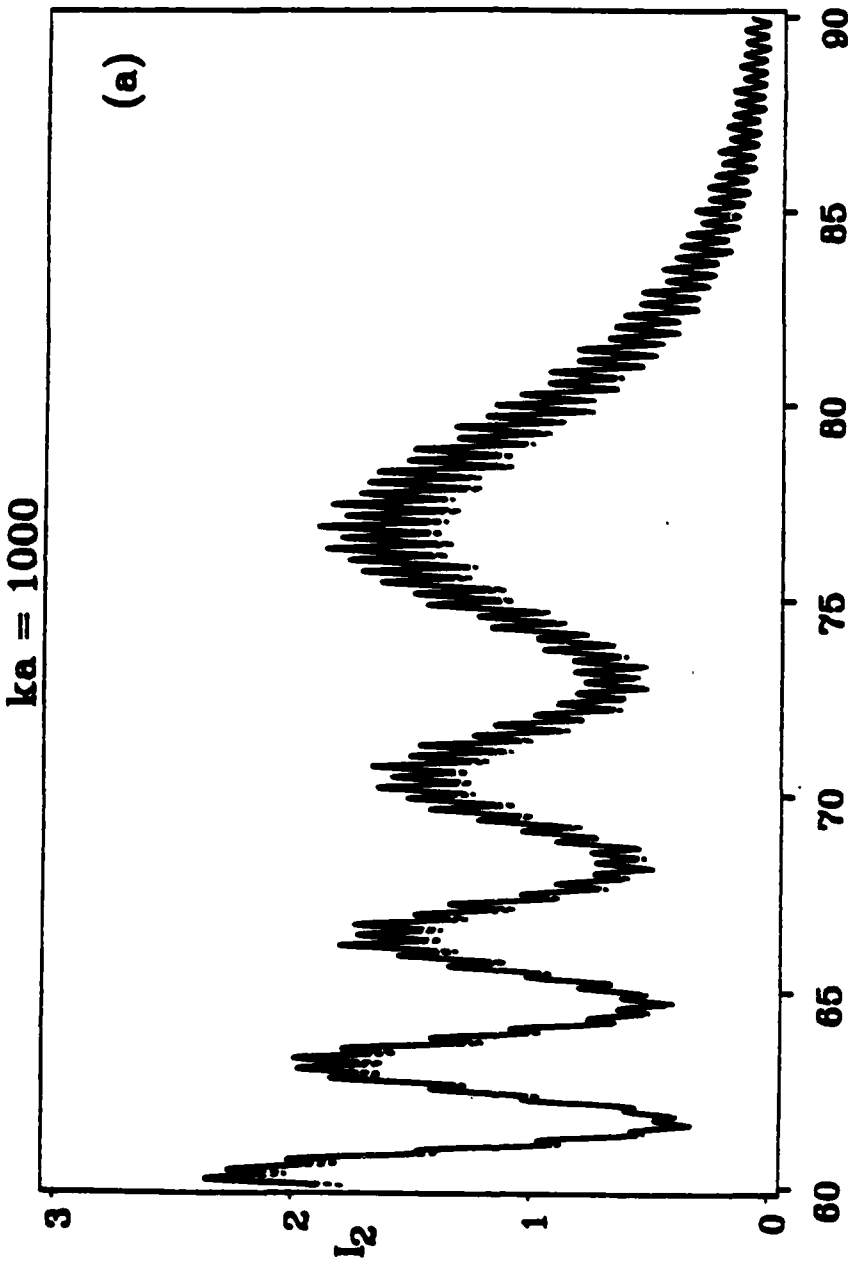

Fig. 2.14 (a)

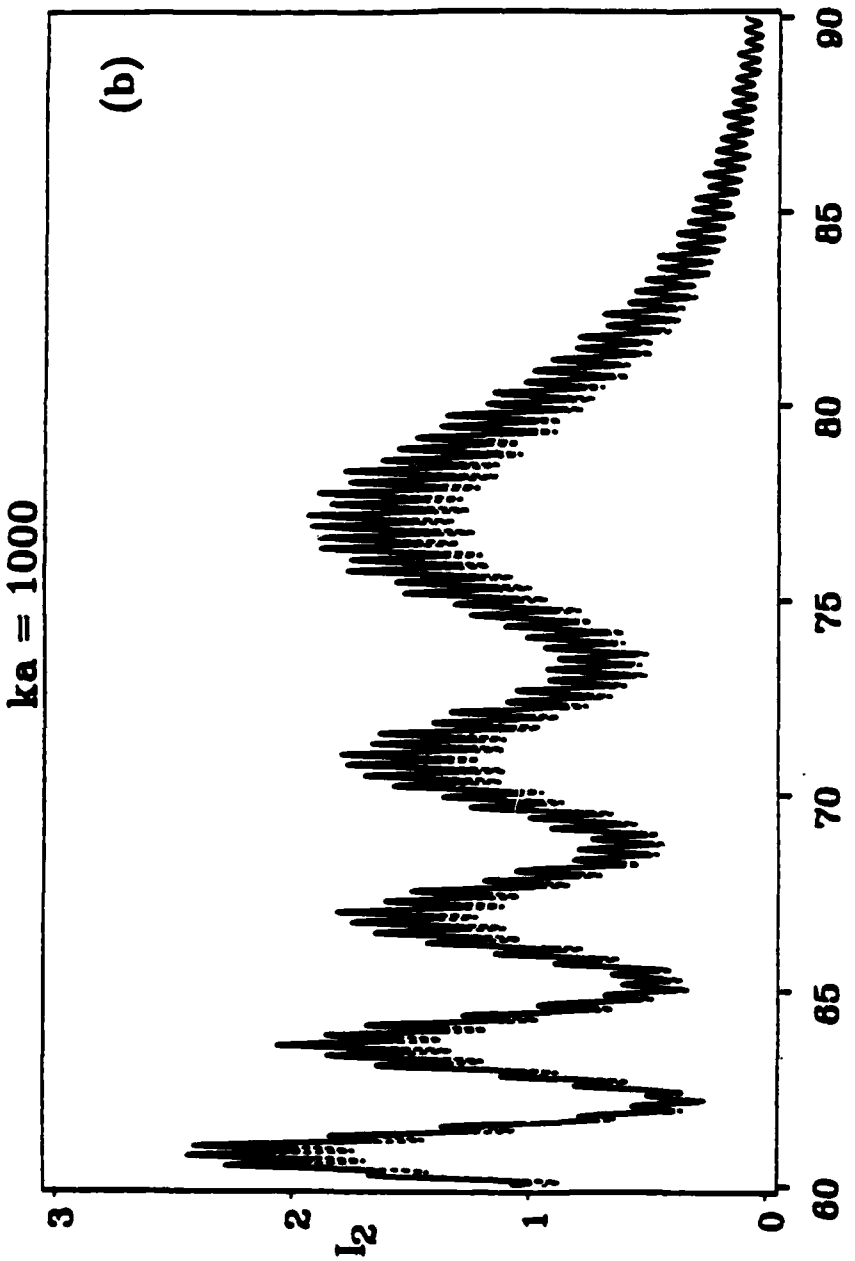

Fig. 2.14 (b)

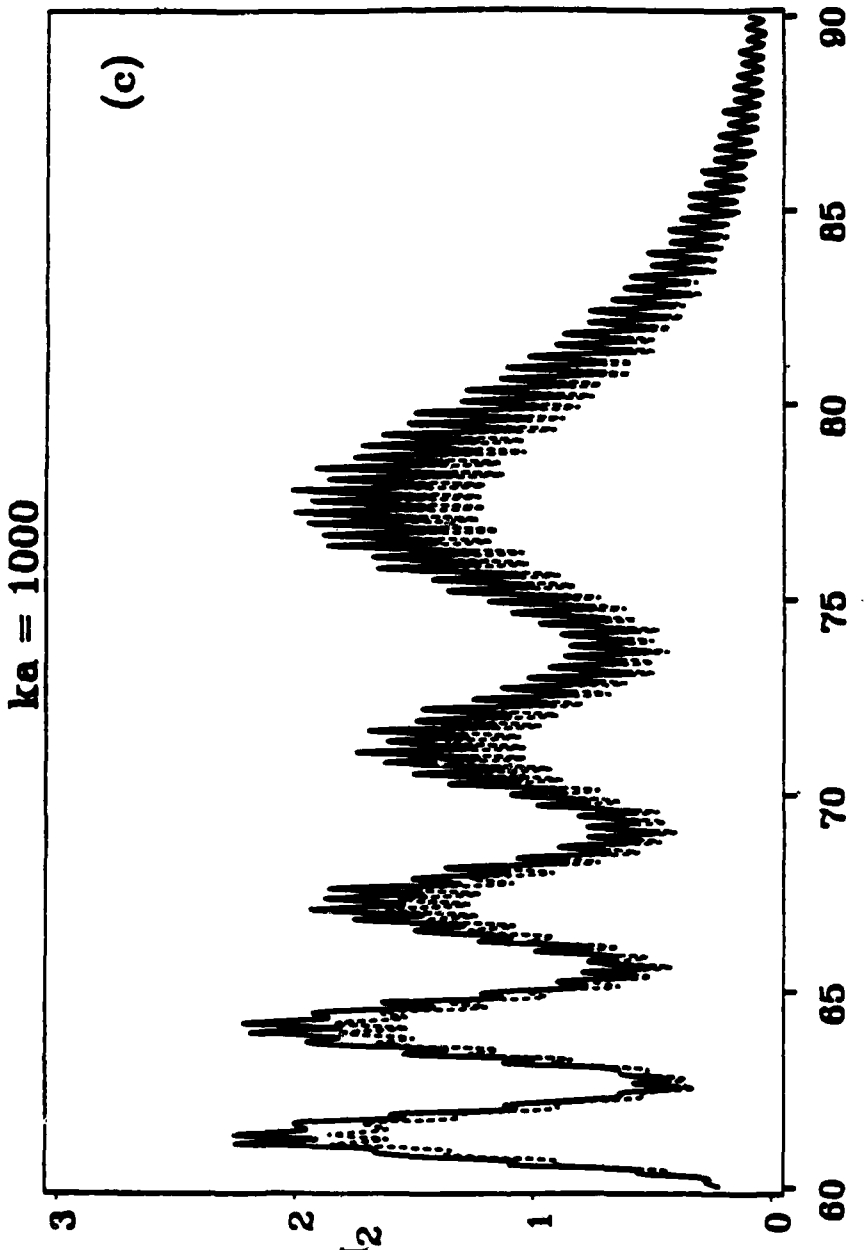

Fig. 2.14 (c)

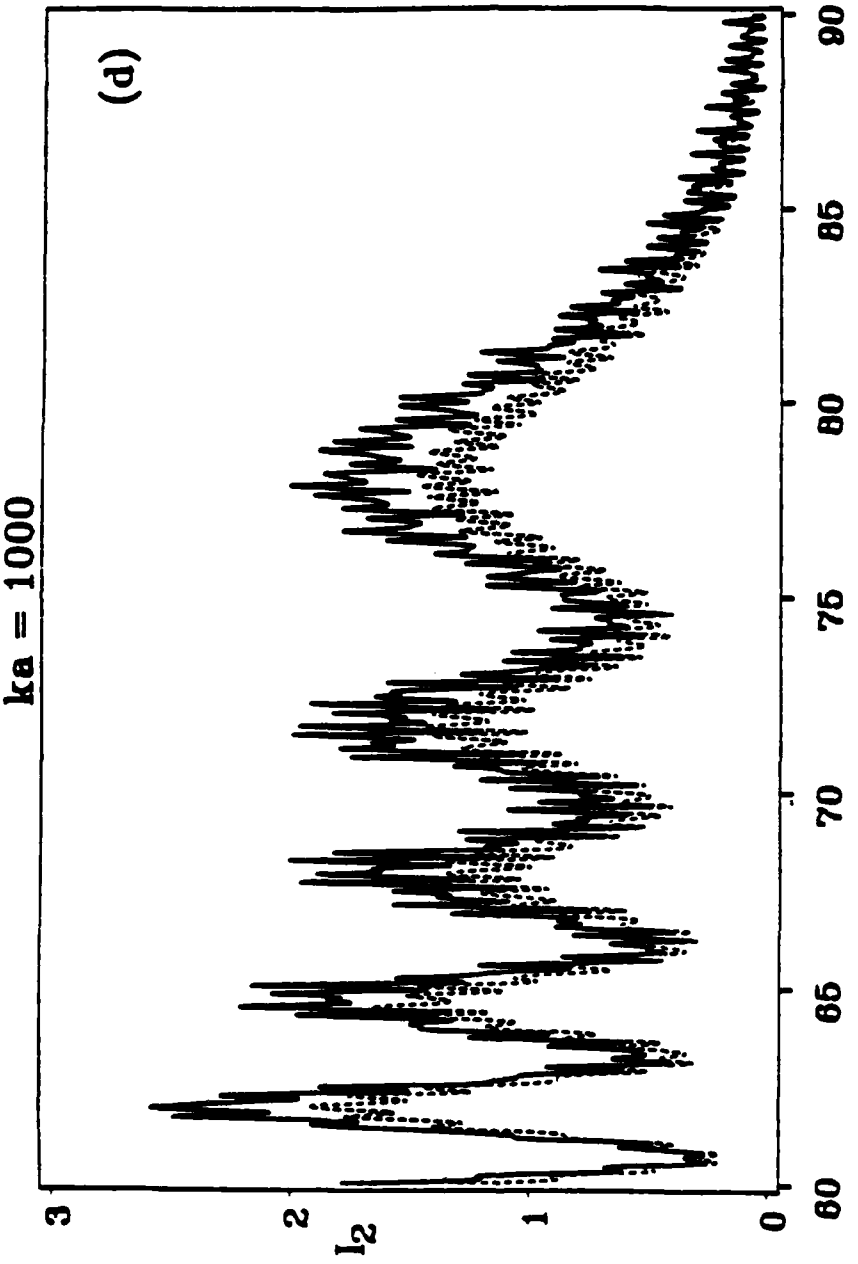

Fig. 2.14(d)

E. Effect of Varying n_c Values

The final parameter investigated was the effect of varying real values n_c. Figures 2.15 - 2.18 show the differences between the $n_c = 1.5$ case generally used and those of n_c equal to 1.45 and 1.55, respectively. In general, the effect of coatings with indices of refraction less than 1.5 was to diminish the changes in structure until the value $n_c = n_w$ in which case the shell was water and gave Mie results. For $n_c < n_w$ an angular shift of the coarse structure in the opposite direction towards lower values of θ occurred. In the cases where $n_c > 1.5$ the effect was one of accelerating both the shift and breakdown in structure. The difference between values $n_c = 1.45$, 1.5, and 1.55 was very slight for thin coatings at all size parameters; i.e., Figs. 2.15 and 2.16 and even less noticeable at larger values of ka for thicker coatings (Figs. 2.17 and 2.18).

In general most surfactants found in sea water will most likely have indices of refraction in the 1.45 to 1.55 range.[16] Based on the results in this section, the use of the value $n_w = 1.5$ will yield representative results. Although there are some small changes in the amplitude of the fine structure, the amount of coarse structure angular shift in this region is negligible for thinly coated bubbles at all sizes and thickly coated bubbles at large values of ka. Using the results characterized here it would be difficult to determine from near-critical angle scattering data alone if the coating had a 1.45, 1.55, or 1.5 index of refraction.

Figure 2.15. The effect of changing n_c with ka = 100 and h = 0.26 μm. The thick-dashed curve represents $n_c = 1.45$, the thin-dashed curve is for $n_c = 1.5$, and the solid curve represents the noncoated case.

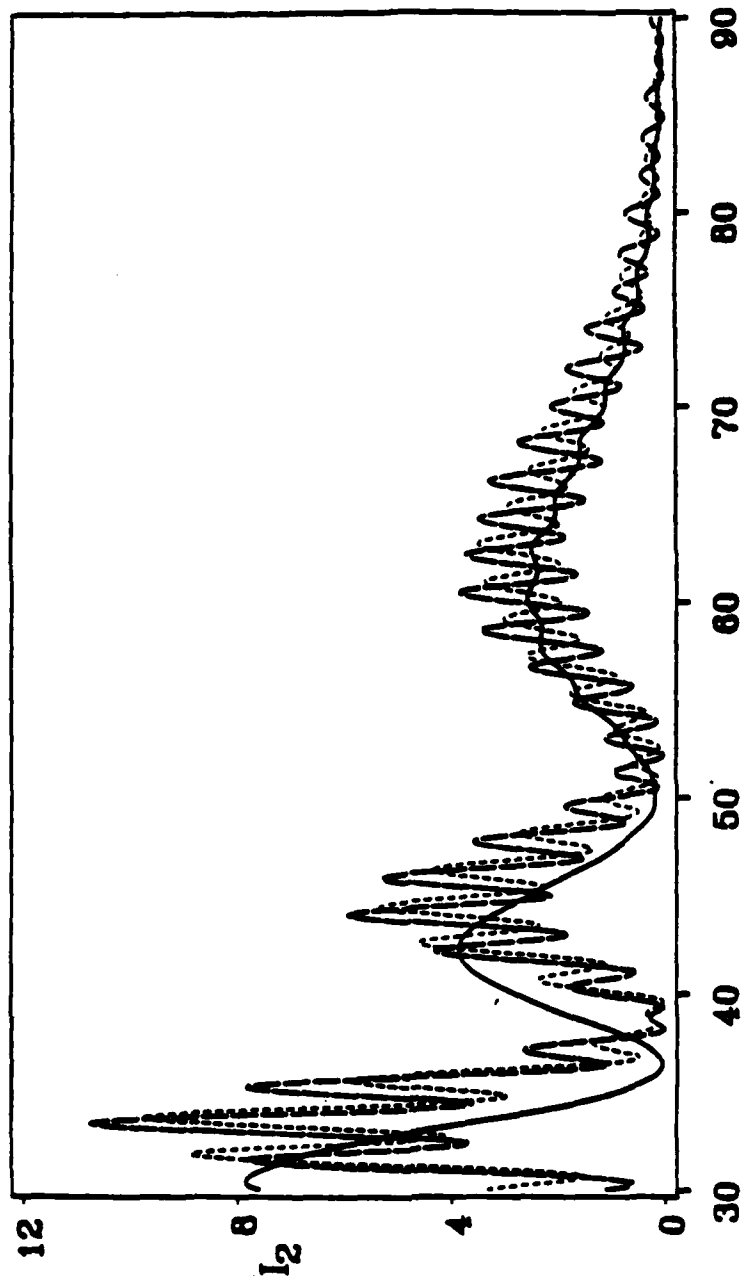

Fig. 2.15

Figure 2.16. Like Figure 2.15 but the thick-dashed curve represents $n_c = 1.55$.

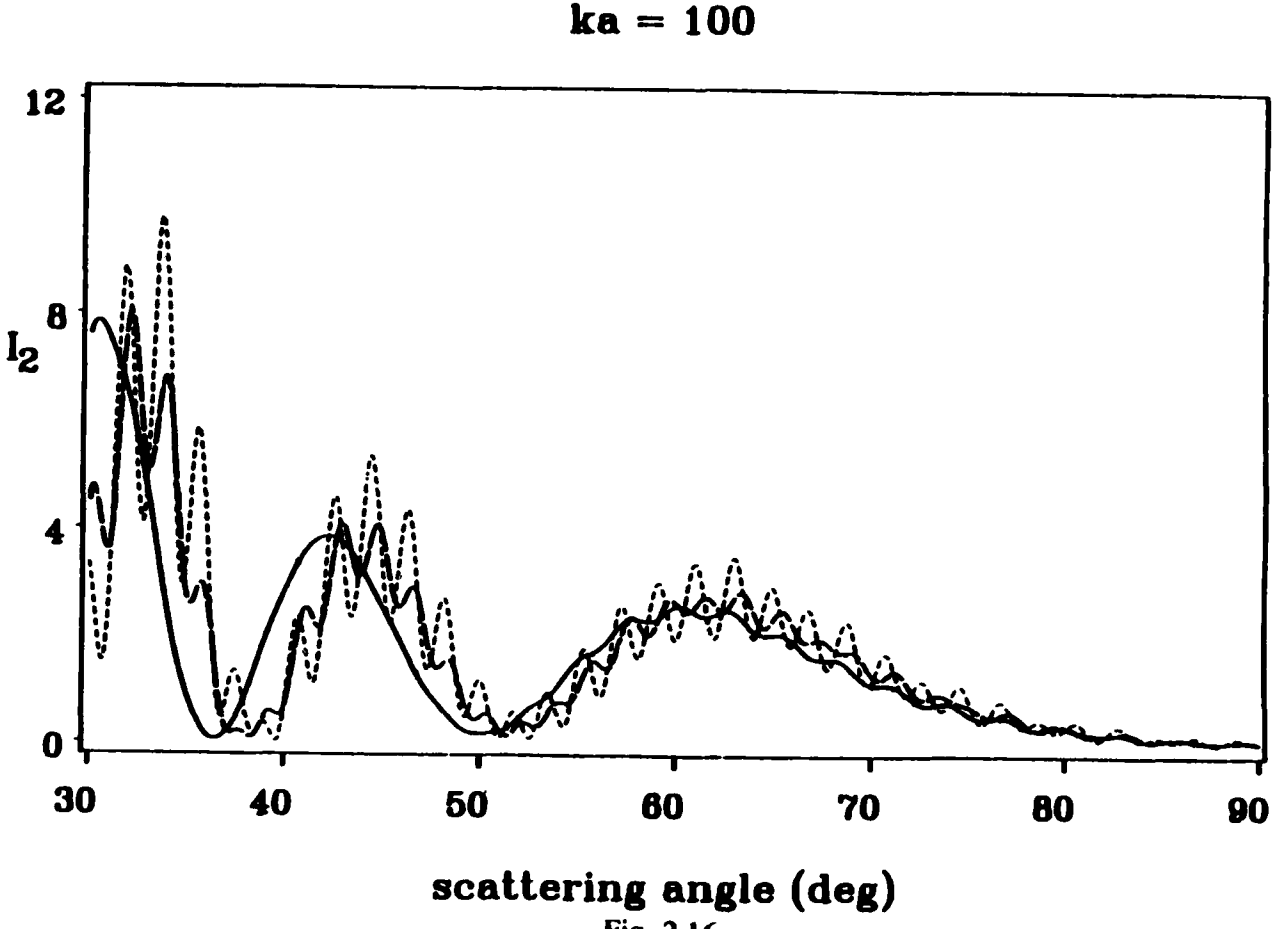

Fig. 2.16

Figure 2.17. The effect of changing n_c with ka = 1000 and h = 3.14 μm. The short-dashed curve represents n_c = 1.5, the long dashed curve represents n_c = 1.45, and the solid curve is for the noncoated case.

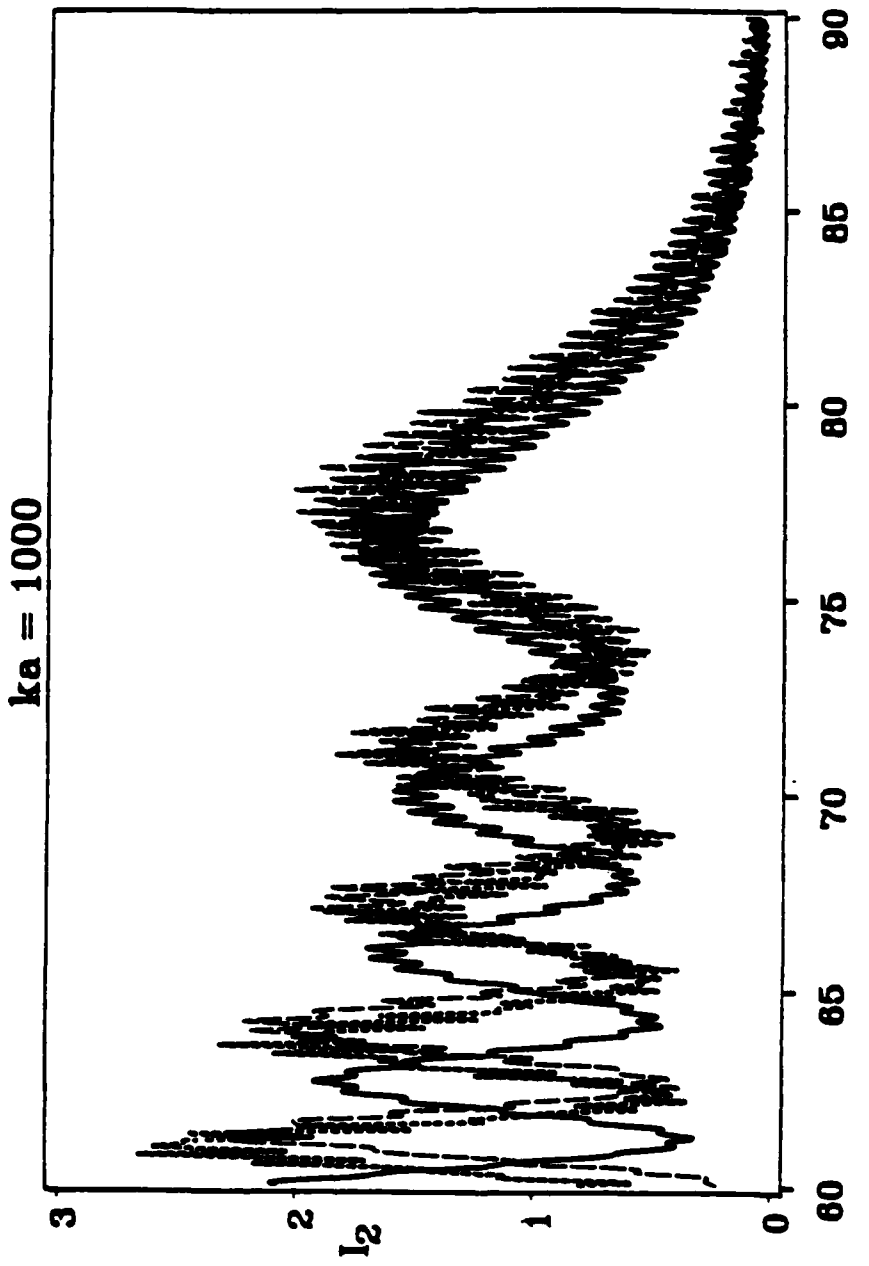

Fig. 2.17

Figure 2.18. Like Figure 2.17 but for $n_c = 1.55$ (long-dashed curve).

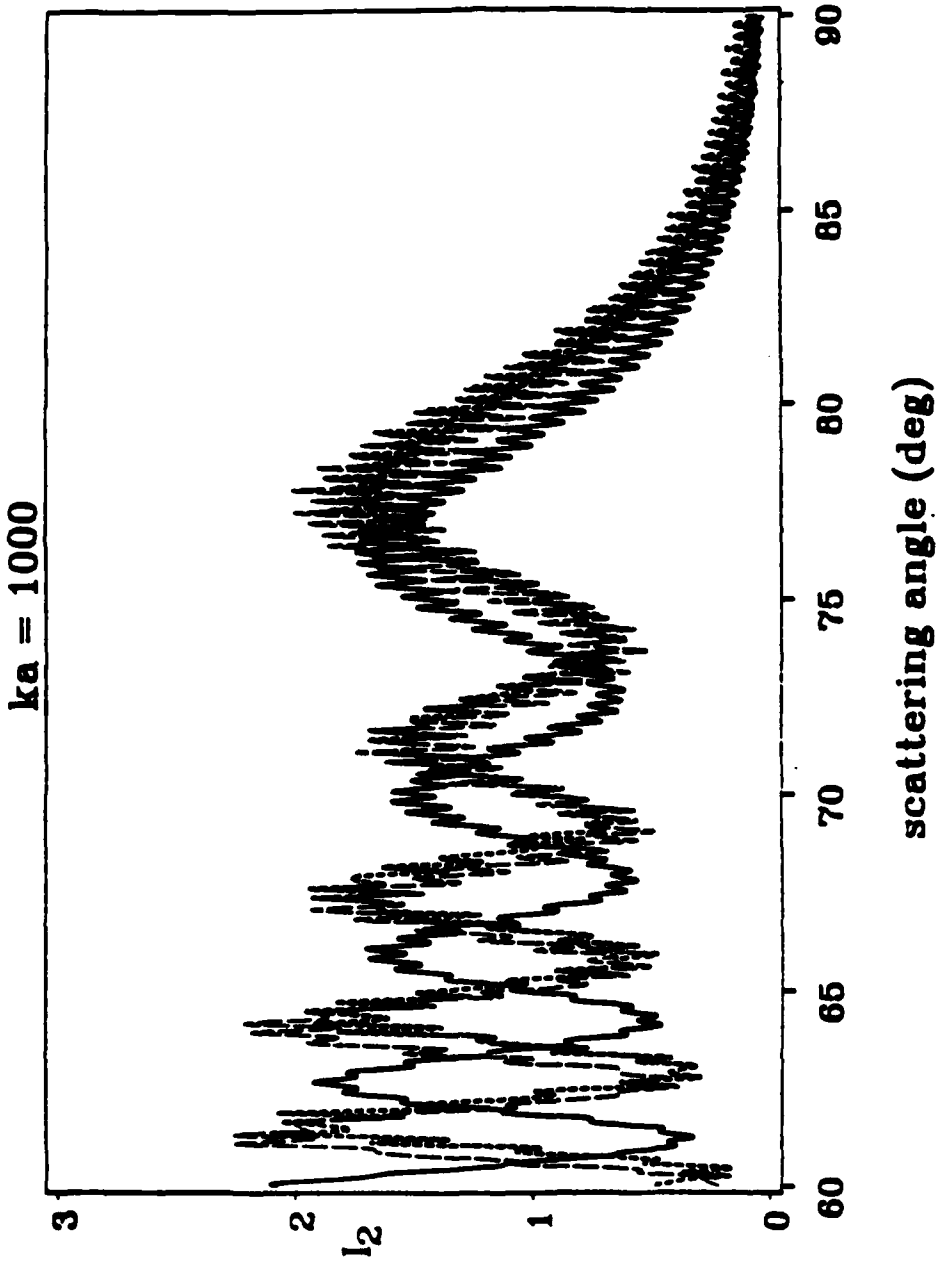

Fig. 2.18

REFERENCES TO CHAPTER 2

1. W. J. Wiscombe, Mie Scattering Calculations: Advances in Technique and Fast, Vector-Speed Computer Codes, NCAR Technical Note, June 1979.
2. W. J. Wiscombe, "Improved Mie scattering algorithms," App. Opt. 19, 1505-1509 (1980).
3. C. Bohren and D. Huffman, Absorption and Scattering of Light by Small Particles (Wiley, N.Y., 1983) Appendix B.
4. D. L. Kingsbury and P. L. Marston, "Mie scattering near the critical angle of bubbles in water," J. Opt. Soc. Am. 71, 358-361 (1981).
5. See Ref. 4.
6. D. E. Cooper, Dau-Sing Wang, and Milton Kerker, "Scattering of light by laser fusion targets with small defects," App. Opt. 22, 83-94 (1983).
7. A. Brunsting, Computer Analysis of Differential Light Scattering from Coated Spheres, Los Alamos Scientific Report LA-5032, November 1972.
8. See Ref. 3.
9. P. L. Marston and D. L. Kingsbury, "Scattering by a bubble in water near the critical angle: interference effects," J. Opt. Soc. Am. 71, 192-196 (1981); 71, 917(E) (1981).
10. G. E. Davis, "Scattering of light by an air bubble in water," J. Opt. Soc. Am. 45, 572-581 (1955).
11. See Ref. 4.
12. P. L. Marston, D. S. Langley, D. L. Kingsbury, "Light scattering by bubbles in liquids: Mie theory, physical-optics approximations, and experiments," Appl. Sci. Res. 38, 373-383 (1982).

13. D. S. Langley and P. L. Marston, "Critical-angle scattering of laser light from bubbles in water: measurements, models, and application to sizing of bubbles," App. Opt. 23 (1984).

14. See Ref. 13.

15. See Ref. 3, p. 279.

16. CRC Handbook of Chemistry and Physics, 72nd edition (CRC Press, Inc., Florida, 1981) pp. E 376-377, F166.

CHAPTER 3

DISCUSSION

3.1. Interpretation and Analysis

Computational results indicate that for both perpendicular and parallel polarizations, I_1 and I_2 respectively, the irradiance patterns of the scattered light for coated bubbles in water are noticeably altered from noncoated results. While both the coarse and fine structure oscillations previously evident in noncoated Mie results remain, a prominent angular shift toward θ_c occurs in the coarse structure oscillations due to the coating. The degree of this shift is dependent upon three factors; the size of the bubble a, the index of refraction of the coating n_c and finally the coating thickness h. For large bubbles (i.e., Fig. 2.10) the amount of shift is much less than for the smaller sized bubble (i.e., Fig. 2.5). The shift has been calculated by Professor Marston in the thin coating limit to be directly proportional to h/a.

Other effects induced by the coating are changes in the period and amplitude of the fine structure oscillations. As an illustration of this effect consider the fine structure oscillations evident in Fig. 2.6 at fixed scattering angle, say 60 degrees. In Fig. 2.6(b) ($h = 0.08\ \mu m$) the angle between the two fine structure maxima peaks is roughly 2.6° while in Fig. 2.6(i) ($h = 1.12\ \mu m$) the distance is roughly 1.7°. Thus, in general, this indicates that the fine structure quasi-period $\Delta\theta_{fs}$ tends to decrease with increasing h. The plausible reason for this decrease is that the transverse distance between the far side, or (2,1) ray, and the surface reflected ray (0,0) appears to increase with h. Inspection of Fig. 2.6 also indicates that except for 2.6(g) the amplitude of the fine structure oscillations

AD-A173 992 COMPUTATIONAL ANALYSIS OF THE EFFECTS OF SURFACE FILMS ON THE SCATTERING..(U) WASHINGTON STATE UNIV PULLMAN DEPT OF PHYSICS S C BILLETTE ET AL. 01 OCT 86 2/2

UNCLASSIFIED N00014-86-K-0242 F/G 20/6 NL

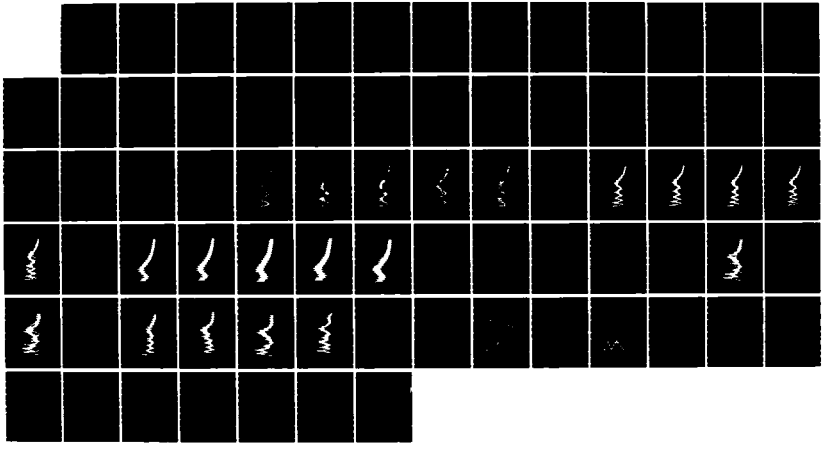

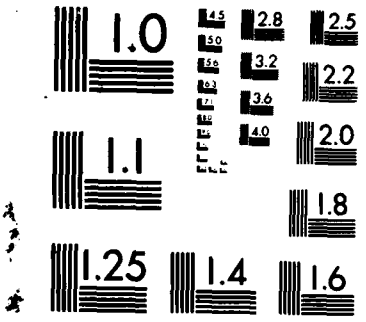

MICROCOPY RESOLUTION TEST CHART
NATIONAL BUREAU OF STANDARDS-1963-A

tends to increase with increasing h. It is possible that this could be accounted for by a shift in the effective reflection or transmission coefficients for the (2,1) ray shown in Fig. 2.7. The observations made here were shown to be valid for both absorbing and non-absorbing coatings.

The computation results for the case of coatings with absorption may be understood as follows: analyzing Figs. 2.11 to 2.14 one finds that it is possible on physical grounds to anticipate that the effects of absorption are governed by the magnitude of a unitless parameter $\sigma \equiv 4\pi h \mathrm{Im}(n_c)/\lambda_{air}$. The irradiance of a wave propagating through an absorbing medium a distance h is related to σ by the relation $I = I_0 e^{-\sigma}$ where I_0 is the initial irradiance. This is explained in Section 2.8 of Ref. 1. Let us now illustrate the use of this parameter σ by looking at an actual case presented in the data. Analyzing Fig. 2.12 we find that $h = 1.0\ \mu m$ and $\mathrm{Im}(n_c) = 5E\text{-}3$ giving a value of $\sigma = 9.93E\text{-}2$. Calculating σ for Fig. 2.14(d) with $h = 5.0\ \mu m$ we obtain the same value of $\sigma = 9.93E\text{-}2$. Note that the effect on the irradiance curves is similar. Finally, it should be noted that for higher σ values the effects due to absorption become more drastic. Comparing Fig. 2.13 ($\sigma = 1.99E\text{-}1$) with Figs. 2.11 and 2.14(a) ($\sigma = 1.99E\text{-}2$) we find this is indeed the case. Thus for coatings with σ less than approximately 0.02 the effects of absorption are negligible and real values for n_c would best be used in computations since the use of real values reduces the computation time significantly.

Based on the results presented here and in Chapter 2, the following conclusions are noted for the case of $j = 2$ scattering from bubbles having nonabsorbing coatings. First, for a coating less than 1 μm in thickness on bubbles having $ka \geq 500$ there is very little effect of the coating on the principal features of the scattering pattern. As noted in Appendix B, the effect of a given coating on the coarse features of the scattering pattern is usually smaller for $j = 2$ than for $j = 1$. This may be because the reflection of light from the coating-water interface is smaller for $j = 2$ than $j = 1$ in the angular region of

interest. (See Appendix B.) For bubbles with $ka = 100$, changes in the fine structure can be pronounced for coating thickness values between 0.25 μm and 1.0 μm.

3.2. Experimental Applications

If microbubbles in the ocean are proven to be coated by a thin film of surfactant, then it becomes important to determine if such parameters as thickness and complex refractive index of the coatings affect the reliability where by light scattering techniques can be used to determine the radius a of a gas bubble. Calculations given here for both coated and noncoated bubbles indicate that for their sizing and detection the coarse structure oscillations for the $j = 2$ case in the critical angle scattering region are best used for sizing. The basis for this observation is three-fold; first, the fine structure is generally much smaller in magnitude for both coated and noncoated bubbles for $j = 2$ than for $j = 1$. Secondly, the $j = 2$ case for coated values does not have the change in coarse structure (other than the angular shift which was noted for both cases) as was observed for $j = 1$; see e.g., Fig. B.3(e). Thirdly, unless coatings are found to be quite thick or highly absorbing previous observations and conclusions made using Mie theory and the physical-optics approximation could be used as an aid in the general design of apparatus. Thus, it is recommended that sizing and detecting of coated bubbles in experimental applications is best done by making use of the $j = 2$ coarse-structure and placing the maximum number of detectors as close as possible to the critical angle scattering region.

REFERENCES TO CHAPTER 3

1. C. Bohren and D. Huffman, Absorption and Scattering of Light by Small Particles (Wiley, N.Y. 1983) pp. 36-41.

APPENDIX A

COMPUTER PROGRAMS

Two programs were used to generate our plots. COATSPHR, using modified versions of Wiscombe's Mievo, and Bohren and Huffman's coated sphere subroutines produced the coated sphere results and ESCAT the approximation results. The data was stored in system files and manipulated using a Statistical Analysis System (SAS) routine which generated the plots presented. All plots were done on an HP7475a plotter using 0.5 mm and 0.7 mm Hewlett Packard drafting plotter pens. All programs are written in IBM FORTRANVS.

COATSPHR

To use COATSPHR the following values must be input in the main calling program:

1. DT is the angle increment to be sampled. Typically it must be less than ($\lambda/7a$) rad where a is the inner sphere radius.
2. ANG(N) is the initial angle at which scattering calculations begin. All calculations are symmetric about 90° meaning that if ANG(N) = 30° the range of 30° to 150° will be calculated.
3. NANG is the number of angles for which the coefficients are calculated. Typically for the entire range it is determined by NANG = 1/DT x (90° - ANG(N)) + 1. Note that for this particular program version NANG must be less than 1800. (This number may be increased by increasing all array sizes but for the cases presented 1800 was adequate.) If only a small region is

desired then the variable NANG should be determined by NANG = 1/DT x (last angle) + 1 (for example, to compute 0° to 5° and 175° to 180° with DT = 1/20 use NANG = 20 x 5 + 1 = 101; ANG(N) = 0°.

In addition to this the following values must be input in subroutine BHCP(X,Y).

1. REFMED is the refractive index of the surrounding medium.
2. REFRE1 is the real part of the index of refraction of the inner sphere medium.
3. REFIM1 is the imaginary component of the index of refraction of the inner sphere medium.
4. REFRE2 is the real part of index of refraction of the coating.
5. REFIM2 is the imaginary component of the coating index of refraction.
6. AOB is the ratio of the inner radius a divided by the outer radius b (see Fig. 1.1). The coating value is given by the relation h = b(1 - AOB).
7. X is the inner sphere size parameter $ka = 2\pi a/\lambda_o$ where λ_o is the wavelength in the outer medium.

Once these values are input COATSPHR generates the following output:

1. Y is size parameter of the outer shell of radius b.
2. $I_1(\theta)$ is the intensity for the electric field perpendicular to the scattering plane. It is given for each value of θ input. It is normalized such that $I_j(\theta) = 1$ represents perfect reflection according to geometric optics.
3. $I_2(\theta)$ is the intensity for the parallel case.
4. $S_1(\theta)$ and $S_2(\theta)$ are the partial wave angular scattering functions.
5. The average intensity.
6. Efficiency factors:
   a) Extinction coefficient $Q_{ext} = C_{ext}/G$ where C_{ext} is the extinction cross section and G is defined below.

b) Scattering coefficient $Q_{sca} = C_{sca}/G$ where C_{sca} = scattering cross section and G is the particle cross sectional area projected onto a plane perpendicular to the incident beam (e.g., $G = \pi b^2$ for coated sphere).

c) Absorption coefficient Q_{abs} which is simply $Q_{ext} - Q_{sca}$.

7. The asymmetry factor is the average cosine of the scattering angle. For a particle that scatters light isotropically the asymmetry factor would be zero.

Being that the author is a novice in FORTRAN programming no claim is made as to the efficiency or lack thereof in COATSPHR. The program requires close to 1 Megabyte of virtual memory to run as there are 3 large arrays and the use of quadruple precision to contend with. Fortunately this is well within the IBM 3090-200's capability range and so no attempt was made to economize the program.

ESCAT

Values for the physical-optics approximation were generated using ESCAT FORTRAN. The program is virtually unchanged from the version used by Langley in 1982. Only a few modifications were necessary to convert it for use on the FORTVS compiler. To use ESCAT the following values must be entered:

1. M is the relative refractive index of the non-coated bubble.
2. KA is size parameter of the noncoated bubble.
3. PHIBGN is the value of the first scattering angle (in degrees) to be evaluated.
4. PHIEND is the last scattering angle (in degrees).
5. DPHI is the angle step size (analagous to DT in COATSPHR).

The output gives the irradiances I_j for both the $j = 1$ and $j = 2$ cases, with or without diffraction effects. The program only determines the coarse structure as has been shown in the figures but has the advantage that it executes extremely quickly for all bubble sizes, whereas similar Mie calculations require significantly more computation time.

```
FILE: COATSPHR FORTRAN  A1

C          SCATTERING PROGRAM FOR COATED SPHERES
C
C          S. C. BILLETTE    NOVEMBER 1985
C
C          ANGULAR DIMENSIONS
C
      COMPLEX*8 SBACK, S1, S2
      REAL*16 ANG(3600),XMU,PI,CON,DT,XX,CONV,YY
      REAL*16 I1,I2,INTEN,ANGLE,N2CUT
      COMMON/INOUT/S1(3600),S2(3600),XMU(3600),SBACK,XX,YY,
     *     QEXT,QSCA,GQSC,NUMANG,N2CUT
C
C     USE SUBROUTINE BHCP TO INITIALIZE FOR AN AND BN CALCULATIONS
C               AND OBTAIN CORE AND COAT SIZE PARAMETERS
C
      CALL BHCP(XX,YY)
C
      N2CUT = 0.0Q0
      PI = 3.14159265358979323846264338327950Q0
      CON = PI/180.Q0
      NANG = 301
      CONV = XX**2
      DT = 1.0Q0/20.0Q0
      N = 1
      ANG(N) = 75.0Q0
C
      DO 1 J = 1, NANG
         XMU(N) = QCOS(CON*ANG(N))
         ANG(N+1) = ANG(N)+DT
    1    N = N+1
      NUMANG = 2*(N-1)
      J = NUMANG+1
C
      DO 2 I = N,NUMANG
         ANG(I) = 180.-ANG(J-I)
    2    XMU(I) = -XMU(J-I)
C
C     CALL SUBROUNTINE MIEV0 TO DETERMINE S1 AND S2
C
         CALL MIEV0
C
      CONTINUE
C
      QABS = QEXT-QSCA
      WRITE(6,1000) XX,YY
C
      DO 10 I = 1,NUMANG
          I1 = 4.0Q0*((REAL(S1(I)))**2+(AIMAG(S1(I)))**2)/CONV
          I2 = 4.0Q0*((REAL(S2(I)))**2+(AIMAG(S2(I)))**2)/CONV
          INTEN = .5Q0*(I1+I2)
          ANGLE = ANG(I)
C
C         WRITE STATEMENTS
C
   10 WRITE(6,1001) ANGLE,I1,I2,S1(I),S2(I),INTEN
```

FILE: COATSPHR FORTRAN A1

```
      WRITE(6,1002) QEXT,QSCA,QABS,GQSC
      WRITE(6,1003) SBACK
      STOP
C
C           FORMAT STATEMENTS
C
 1000 FORMAT(5X,'CORE PARAMETER =',D16.6,3X,'COAT PARAMETER =',D16.6,
     *  //,'  ANGLE',8X,'I1',11X,'I2',20X,'S1',26X,
     *  'S2',15X,'INTENSITY')
 1001 FORMAT(F8.3,8E14.6)
 1002 FORMAT( /30X,'EXTINCTION    SCATTERING    ABSORPTION'/7X,
     *  'EFFICIENCY FACTORS',3F14.6/ 7X,'ASYMMETRY FACTOR =',F9.6)
 1003 FORMAT(7X,'S BACKSCATTER =',2E14.6)
C
      END
      SUBROUTINE MIEV0
C
C         ************************************************
C         NOTE: THIS SUBROUTINE USES THE SAME VARIABLE NAMES
C          AS THOSE FOUND IN WISCOMBE'S MIEV0 FROM WHICH IT
C            IS DERIVED. SEE MIEV0 FOR A COMPLETE LISTING.
C         ************************************************
C
      COMMON/INOUT/S1(3600),S2(3600),XMU(3600),SBACK,XX,YY,
     *    QEXT,QSCA,GQSC,NUMANG,N2CUT/BLOCK2/AN,BN/BLOCK3/NT
      REAL*16 NP1DN,N2CUT
      REAL*16 XX,YY,XINV,FN,FNP1,RN,RNP1,TWONP1,COEFF
      REAL*16 PIN,PINM1,TMP,TAUN,XMU
      LOGICAL NOIMAG, NOANGS
      COMPLEX*8 SBACK, S1, S2
      COMPLEX*32 SP,SM,SPS,SMS
      COMPLEX*32 ANPM,BNPM,ANP,BNP,ANM1,BNM1
      COMPLEX*32 AN,BN
      DIMENSION SP(1800),SM(1800),SPS(1800),SMS(1800),
     *    PIN(1800),PINM1(1800),TAUN(1800),TMP(1800)
C
      XINV = 1.0Q0/XX
      NN2 = NUMANG+1
      NN = NN2/2
      NOANGS = NUMANG.EQ.0
C
C        CALCULATE NUMBER OF TERMS IN PARTIAL WAVE SERIES
C         USING EMPIRICAL FORMULAE WHICH WERE FITTED FOR
C                 SIZE PARAMETERS UP TO 20,000
C
      IF(YY.LE.8.0Q0) NT = YY+4.00Q0*YY**(1.0Q0/3.0Q0)+1.0Q0
      IF(YY.GT.8.0Q0) NT = YY+4.05Q0*YY**(1.0Q0/3.0Q0)+2.0Q0
      NTP1 = NT+1
      NTP2 = NT+2
C
      WRITE(6,8001) NT
 8001 FORMAT(4X,' NT =',I6/4X)
C
C        INITIALIZE QUANTITIES USED FOR EFFICIENT CALCULATION OF
C             NUMERICAL COEFFICIENTS IN PARTIAL WAVE SERIES
```

FILE: COATSPHR FORTRAN A1

```
C
      FN = 1.0Q0
      RN = 1.0Q0
      MM = 1
      ANM1 = (0.0Q0,0.0Q0)
      BNM1 = (0.0Q0,0.0Q0)
C
C        INITIALIZE SUMS FOR EFFICIENCIES, ASYMMETRY FACTOR, AND
C        BACKSCATTERING AMPLITUDE
C
      QEXT = 0.0Q0
      QSCA = 0.0Q0
      GQSC = 0.0Q0
      SBACK = (0.0Q0,0.0Q0)
C
C        INITIALIZE ANGULAR FCN PIN AND SUMS FOR S+,S- AT ALL ANGLES
C
      DO 250 J = 1,NN
         SP(J) = (0.0Q0,0.0Q0)
         SM(J) = (0.0Q0,0.0Q0)
         SPS(J) = (0.0Q0,0.0Q0)
         SMS(J) = (0.0Q0,0.0Q0)
         PINM1(J) = 0.0Q0
  250 PIN(J) = 1.0Q0
C
      DO 500 N = 1,NT
C
C        COMPUTE THE VARIOUS NUMERICAL COEFFICIENTS NEEDED
C
         FNP1 = FN+1.0Q0
         TWONP1 = FN+FNP1
         RNP1 = 1.0Q0/FNP1
         COEFF = RN+RNP1
         NP1DN = 1.0Q0+RN
C
C        CALCULATE THE PARTIAL WAVE SERIES COEFFICIENTS AN AND BN
C
         CALL SCOAT1
C
C        INCREMENT SUMS FOR ASYMMETRY FACTOR, EXTINCTION EFFICIENCY,
C                 AND BACKSCATTERING AMPLITUDE
C
      IF(NOANGS) GO TO 450
C
C        PUT SERIES COEFFICIENTS IN FORM NEEDED FOR COMPUTING S+, S-
C
      GQSC = GQSC + (FN-RN)*REAL(ANM1*QCONJG(AN)-BNM1*QCONJG(BN))
     *       + COEFF*REAL(AN*QCONJG(BN))
      QSCA = QSCA + TWONP1*((REAL(AN))**2 + (QIMAG(AN))**2
     *       + (REAL(BN))**2 + (QIMAG(BN))**2)
      QEXT = QEXT + TWONP1*REAL(AN+BN)
      SBACK = SBACK + (MM*TWONP1)*(AN-BN)
C
      ANP = COEFF*(AN+BN)
      BNP = COEFF*(AN-BN)
```

```
FILE: COATSPHR FORTRAN  A1


      ANPM = MM*ANP
      BNPM = MM*BNP
C
      DO 400 J = 1,NN
C
C       ADD UP SUMS WHILE UPWARD RECURSING ANGULAR FUNCTIONS
C                 LITTLE PI AND LITTLE TAU
C
         TMP(J) = (XMU(J)*PIN(J)) - PINM1(J)
         TAUN(J) = FN*TMP(J) - PINM1(J)
         SP(J)  = SP(J)  +  ANP*(PIN(J)-TAUN(J))
         SMS(J) = SMS(J) +  BNPM*(PIN(J)-TAUN(J))
         SM(J)  = SM(J)  +  BNP*(PIN(J)-TAUN(J))
         SPS(J) = SPS(J) +  ANPM*(PIN(J)-TAUN(J))
         PINM1(J) = PIN(J)
         PIN(J) = (XMU(J)*PIN(J)) + NP1DN*TMP(J)
  400 CONTINUE
C
C        UPDATE RELEVANT QUANTITIES FOR NEXT PASS THROUGH LOOP
C
  450 MM = -MM
      FN = FNP1
      RN = RNP1
      ANM1 = AN
      BNM1 = BN
  500 CONTINUE
C
C        MULTIPLY SUMS BY APPROPRIATE FACTORS TO GET QEXT, QSCA, GQSC
C
      QEXT = 2.0Q0*(XINV**2)*QEXT
      QSCA = 2.0Q0*(XINV**2)*QSCA
      IF(NOIMAG) QSCA = QEXT
      GQSC = 4.0Q0*(XINV**2)*GQSC
      SBACK = 0.5Q0*SBACK
C
      IF(NOANGS) RETURN
      DO 800 J = 1,NN
         S1(J) = 0.5Q0*(SP(J)-SM(J))
         S2(J) = 0.5Q0*(SP(J)-SM(J))
         S1(NN2-J)= 0.5Q0*(SPS(J)-SMS(J))
  800 S2(NN2-J)= 0.5Q0*(SPS(J)-SMS(J))
      RETURN
C
      END
      SUBROUTINE BHCP(X,Y)
C
C        SUBROUTINE TO INPUT COATED SPHERE PARAMETERS AND TO
C              INITIALIZE FOR LATER ENTRY INTO BCOAT1
C
      REAL*16 X,Y,PI,AOB
      REAL*16 QEXT,QSCA,QBACK
      REAL*16 REFMED,REFRE1,REFIM1,REFRE2,REFIM2
      COMPLEX*32 RFREL1, RFREL2
C
C           REFMED = REFRACTIVE INDEX OF SURROUNDING MEDIUM
```

```
FILE: COATSPHR FORTRAN  A1


C           REFRACTIVE INDEX OF CORE = REFRE1 - I*REFIM1
C           REFRACTIVE INDEX OF COAT = REFRE2 - I*REFIM2
C           AOB = RATIO OF CORE RADIUS TO COAT RADIUS
C           X = CORE SIZE PARAMETER
C           Y = COAT SIZE PARAMETER
C
      REFMED = 4.0Q0/3.0Q0
      REFRE1 = 1.00Q0
      REFIM1 = 0.00Q0
      REFRE2 = 1.50Q0
      REFIM2 = 0.00Q0
      AOB = 0.99Q0
      X = 100.0Q0
      Y = X/AOB
C
C           DEFINE VARIABLES RFREL1, RFREL2
C
      RFREL1 = QCMPLX(REFRE1,REFIM1)/REFMED
      RFREL2 = QCMPLX(REFRE2,REFIM2)/REFMED
C
C     USE SUBROUTINE BHCOAT TO CALC. EFFICIENCIES FOR COATED SPHERES
C
      CALL BHCOAT (X,Y,RFREL1,RFREL2)
C
C           WRITE STATEMENTS
C
      WRITE (6,9)
      WRITE (6,11)
      WRITE (6,9)
      WRITE (6,4)
      WRITE (6,12) REFMED,REFRE1,REFIM1,REFRE2,REFIM2
      WRITE (6,14) AOB
C
C           FORMAT STATEMENTS
C
    4 FORMAT('    ')
    9 FORMAT(19X,'*******************************')
   11 FORMAT(19X,'COATED SPHERE SCATTERING PROGRAM')
   12 FORMAT(5X,'REFMED =',E14.9/5X,'REFRE1 =',E14.9,
     *3X,'REFIM1 =',E14.9/5X,'REFRE2 =',E14.9,3X,'REFIM2 =',E14.9)
   14 FORMAT(5X,'AOB =',E14.9)
      RETURN
   87 STOP
C
      END
      SUBROUTINE  BHCOAT (X,Y,RFREL1,RFREL2)
C
C           SUBROUTINE BHCOAT TO CALCULATE LITTLE AN AND BN FOR
C           GIVEN SIZE PARAMETERS OF CORE AND COAT AND RELATIVE
C           REFRACTIVE INDICES. BASED ON SUBROUTINE GIVEN IN AP-
C           PENDIX B OF ABSORPTION AND SCATTERING OF LIGHT BY C.
C           BOHREN AND D. HUFFMAN (WILEY, 1983)
C
C           **********************CAUTION**********************
C           BHCOAT SHOULD NOT BE USED FOR LARGE, HIGHLY ABSORBING
```

```
FILE: COATSPHR FORTRAN  A1

C           COATED SPHERES X*REFIM1, X*REFIM2 AND Y*REFIM2 SHOULD
C           BE LESS THAN ABOUT 10.
C           **********************CAUTION**********************
C
      COMMON/BLOCK2/AN,BN/BLOCK3/YSTOP
      REAL*16 QSCA,QBACK,QEXT,PSIY,CHIY,DEL,RN,YSTOP
      REAL*16 X,Y,PSI0Y,PSI1Y,CHI0Y,CHI1Y
      COMPLEX*32 RFREL1,RFREL2,X1,X2,Y2,REFREL
      COMPLEX*32 D1X1,D0X1,D1X2,D0X2,D1Y2,D0Y2
      COMPLEX*32 XI0Y,XI1Y,XIY,CHI0Y2,CHI1Y2,CHIY2,CHI0X2,CHI1X2,CHIX2
      COMPLEX*32 CHIPX2,CHIPY2,ANCAP,BNCAP,DNBAR,GNBAR,AN,BN,CRACK,BRACK
      COMPLEX*32 XBACK,AMESS1,AMESS2,AMESS3,AMESS4,
      COMPLEX*32 DBIGD1,BIGD1,DBIGD2,BIGD2,DBIGD3,BIGD3
      COMPLEX*32 ZINV,ZINV2,ZINV3
      DIMENSION BIGD1(10150),BIGD2(10150),BIGD3(10150)
C
C           DEL IS THE INNER SPHERE DIVERGENCE CRITERION
C
      DEL = 1.0Q-8
      X1 = RFREL1*X
      X2 = RFREL2*X
      Y2 = RFREL2*Y
      YSTOP = Y + 4.05Q0*Y**(1.0Q0/3.0Q0) + 2.0Q0
      REFREL = RFREL2/RFREL1
      NSTOP = YSTOP
      NTP1 = NSTOP + 1
      NTP2 = NSTOP + 2
C
C           SERIES TERMINATED AFTER NSTOP TERMS
C
C     SUBROUTINE TO CALCULATE INITIAL HIGH ORDER BIGD1-N
C
      CALL BIGD(X,RFREL1,DBIGD1)
C
      BIGD1(NSTOP) = DBIGD1
      ZINV = 1.0Q0/(RFREL1*X)
C
      DO 70 N = 2,NSTOP
          DBIGD1 = (NTP2-N)*ZINV-1.0Q0/(((NTP2-N)*ZINV)-DBIGD1)
   70 BIGD1(NTP1-N) = DBIGD1
C
C     SUBROUTINE TO CALCULATE INITIAL HIGH ORDER BIGD2-N
C
      CALL BIGD(X,RFREL2,DBIGD2)
C
      BIGD2(NSTOP) = DBIGD2
      ZINV2 = 1.0Q0/(RFREL2*X)
C
      DO 80 N = 2,NSTOP
          DBIGD2 = (NTP2-N)*ZINV2-1.0Q0/(((NTP2-N)*ZINV2)-DBIGD2)
   80 BIGD2(NTP1-N) = DBIGD2
C
C     SUBROUTINE TO CALCULATE INITIAL HIGH ORDER BIGD3-N
C
      CALL BIGD(Y,RFREL2,DBIGD3)
```

FILE: COATSPHR FORTRAN A1

```
C
      BIGD3(NSTOP) = DBIGD3
      ZINV3 = 1.0Q0/(REFREL2*Y)
C
      DO 90 N = 2,NSTOP
          DBIGD3 = (NTP2-N)*ZINV3-1.0Q0/(((NTP2-N)*ZINV3)-DBIGD3)
   90 BIGD3(NTP1-N) = DBIGD3
C
      D0X1 = CQCOS(X1)/CQSIN(X1)
      D0X2 = CQCOS(X2)/CQSIN(X2)
      D0Y2 = CQCOS(Y2)/CQSIN(Y2)
      PSI0Y = QCOS(Y)
      PSI1Y = QSIN(Y)
      CHI0Y = -QSIN(Y)
      CHI1Y = QCOS(Y)
C
      XI0Y = QCMPLX(PSI0Y,-CHI0Y)
      XI1Y = QCMPLX(PSI1Y,-CHI1Y)
      CHI0Y2 = -CQSIN(Y2)
      CHI1Y2 =  CQCOS(Y2)
      CHI0X2 = -CQSIN(X2)
      CHI1X2 =  CQCOS(X2)
C
      QSCA = 0.0Q0
      QEXT = 0.0Q0
      XBACK = QCMPLX (0.0Q0,0.0Q0)
      N = 1
      IFLAG = 0
C
      RETURN
      ENTRY BCOAT1
  200 RN = N
      PSIY = (2.0Q0*RN-1.0Q0)*PSI1Y/Y - PSI0Y
      CHIY = (2.0Q0*RN-1.0Q0)*CHI1Y/Y - CHI0Y
      XIY = QCMPLX(PSIY,-CHIY)
      D1Y2 = BIGD3(N)
      IF (IFLAG.EQ.1) GO TO 999
      D1X1 = BIGD1(N)
      D1X2 = BIGD2(N)
C
      CHIX2 = (2.0Q0*RN - 1.0Q0)* CHI1X2/X2 -CHI0X2
      CHIY2 = (2.0Q0*RN - 1.0Q0)* CHI1Y2/Y2 -CHI0Y2
      CHIPX2 = CHI1X2 - RN*CHIX2/X2
      CHIPY2 = CHI1Y2 - RN*CHIY2/Y2
C
      ANCAP = REFREL*D1X1-D1X2
      ANCAP = ANCAP/(REFREL*D1X1*CHIX2 - CHIPX2)
      ANCAP = ANCAP/(CHIX2*D1X2 - CHIPX2)
      BRACK = ANCAP*(CHIY2*D1Y2 - CHIPY2)
C
      BNCAP = REFREL*D1X2 - D1X1
      BNCAP = BNCAP/(REFREL*CHIPX2 - D1X1*CHIX2)
      BNCAP = BNCAP/(CHIX2*D1X2 - CHIPX2)
      CRACK = BNCAP*(CHIY2*D1Y2 - CHIPY2)
C
```

```
FILE: COATSPHR FORTRAN  A1

      AMESS1 = BRACK*CHIPY2
      AMESS2 = BRACK*CHIY2
      AMESS3 = CRACK*CHIPY2
      AMESS4 = CRACK*CHIY2
C
      IF(CQABS(AMESS1).GT.DEL*CQABS(D1Y2)) GO TO 999
      IF(CQABS(AMESS2).GT.DEL) GO TO 999
      IF(CQABS(AMESS3).GT.DEL*CQABS(D1Y2)) GO TO 999
      IF(CQABS(AMESS4).GT.DEL) GO TO 999
C
      BRACK = QCMPLX (0.0Q0,0.0Q0)
      CRACK = QCMPLX (0.0Q0,0.0Q0)
      IFLAG = 1
  999 DNBAR = D1Y2 - BRACK*CHIPY2
      DNBAR = DNBAR/(1.0Q0 - BRACK*CHIY2)
      GNBAR = D1Y2 - CRACK*CHIPY2
      GNBAR = GNBAR/(1.0Q0 - CRACK*CHIY2)
C
      AN = (DNBAR/RFREL2+RN/Y)*PSIY - PSI1Y
      AN = AN/((DNBAR/RFREL2+RN/Y)*XIY - XI1Y)
      BN = (RFREL2*GNBAR+RN/Y)*PSIY - PSI1Y
      BN = BN/((RFREL2*GNBAR+RN/Y)*XIY-XI1Y)
C
      PSI0Y = PSI1Y
      PSI1Y = PSIY
      CHI0Y = CHI1Y
      CHI1Y = CHIY
      XI1Y = QCMPLX(PSI1Y,-CHI1Y)
C
      CHI0X2 = CHI1X2
      CHI1X2 = CHIX2
      CHI0Y2 = CHI1Y2
      CHI1Y2 = CHIY2
C
      D0X1 = D1X1
      D0X2 = D1X2
      D0Y2 = D1Y2
      N = N - 1
C
      RETURN
      END
      SUBROUTINE BIGD(XX,IOR,DBIGD)
C
C     SUBROUTINE TO CALCULATE LOGARITHMIC DERIVATIVES BY LENZ'S
C                METHOD USING DOWN RECURSION
C
      COMMON/BLOCK3/YSTOP
      REAL*16 XINV,XX,YSTOP
      COMPLEX*32 ZINV,IOR,FF,AK,DEN,NUM,NTN,DTD,TT,DBIGD
      DATA EPS1/1.Q-2/EPS2/1.Q-8/
      DATA MAXIT/10000/
      NT = YSTOP
      NTP1 = NT + 1
      NTP2 = NT + 2
C
```

FILE: COATSPHR FORTRAN A1

```
C     MAKE SURE BIGD ARRAY WILL BE BIG ENOUGH
C
      IF(NTP1.LE.20150) GO TO 10
      WRITE(6,8000)NT
 8000 FORMAT(///'ESTIMATED LENGTH OF MIE SERIES NT=',I6)
      STOP
C
C     COMPUTE BIGD
C
   10 XINV = 1.0Q0/XX
      ZINV = XINV/IOR
C
C     PREPARE FOR DOWN RECURRANCE-COMPUTE INITIAL HIGH ORDER
C               BIGD-N USING LENTZ METHOD
C
      FF = NTP1*ZINV
      MM = -1
      KK = 2*NT+3
      AK = (MM*KK)*ZINV
      DEN = AK
      NUM = DEN + 1.0Q0/FF
      KOUNT = 1
C
   20 KOUNT = KOUNT+1
      IF(KOUNT.GT.MAXIT) GO TO 40
      IF(CQABS(NUM/AK).GT.EPS1.AND.CQABS(DEN/AK).GT.EPS1) GO TO 30
      MM = -MM
      KK = KK+2
      AK = (MM*KK)*ZINV
      NTN = AK*NUM + 1.0Q0
      DTD = AK*DEN + 1.0Q0
      FF = (NTN/DTD)*FF
      MM = -MM
      KK = KK+2
      AK = (MM*KK)*ZINV
      NUM = AK + NUM/NTN
      DEN = AK + DEN/DTD
      KOUNT = KOUNT + 1
      GO TO 20
C
   30 TT = NUM/DEN
      FF = TT*FF
C
C     CHECK FOR CONVERGENCE
C
      IF(QABS(QREAL(TT)-1.0Q0).LT.EPS2 .AND. QABS(QIMAG(TT)).LT.EPS2)
     *     GO TO 50
      MM = -MM
      KK = KK+2
      AK = (MM*KK)*ZINV
      NUM = AK + 1.0Q0/NUM
      DEN = AK + 1.0Q0/DEN
      GO TO 20
C
   40 WRITE(6,8001) NT,XX,IOR,AK,NUM,DEN,TT,FF
```

```
FILE: COATSPHR FORTRAN  A1


 8001 FORMAT(///'CONTINUED FRACTION FOR A-SUB-NT FAILED TO CONVERGE'/
     *    ' NT=',I6/' X=',E20.8/' REFR INDEX=',2E20.8/' AK=',2E20.8/
     *    ' NUM=',2E20.8/' DEN=',2E20.8/' TT=',2E20.8/'FF=',2E20.8)
      STOP
   50 OBIGD = FF
      RETURN
C
      END
```

```
FILE: ESCAT    FORTRAN  A1

C          PROGRAM ESCAT TO COMPUTE COMPLEX SCATTERING
C          AMPLITUDES S1 AND S2 USING A PHYSICAL OPTICS
C          APPROXIMATION AND DIFFRACTION.
C
C          D.L. KINGSBURY AND P.L. MARSTON 1980
C          D.S. LANGLEY 1982
C          MODIFIED FOR CMS BY S.C.BILLETTE APRIL 7, 1986
C
C          ************************************************
C                        INPUT PARAMETERS
C
C            M = RELATIVE REFRACTIVE INDEX OF BUBBLE
C            KA = SIZE PARAMETER
C            PHIBGN = STARTING ANGLE IN DEGREES
C            PHIEND = LAST ANGLE (DEGREES)
C            DPHI = ANGLE STEP SIZE (DEGREES)
C
C          ************************************************
C
      REAL M,KA,I1,I2,ID,IT1,IT2
      COMPLEX S1,S2,S01,S02,S11,S12,F01,F02,F11,F12,SD1,SD2
      DOUBLE PRECISION N,THC,ST1
      DATA RMIN/0.0/
      M = .75
      KA = 100.0
      PHIBGN = 30.0
      PHIEND = 90.0
      DPHI = 1.0/18.0
C
C
C           II > 1 GIVES P.O.A RESULTS USING ONLY (0,0) & (1,0) RAYS
      II = 2
C           JJ > 1 GIVES DIFFRACTION ONLY RESULTS
      JJ = 0
C           KK > 1 GIVES P.O.A. INCLUDING DIFFRACTION RESULTS
      KK = 0
C
      WRITE(1,1000) M,KA
 1000 FORMAT('M = ',F6.4,'   KA = ',F6.2)
C
C           COMPUTE CRITICAL ANGLES FOR GIVEN REFRACTIVE INDEX
C
      PI = 4.0D0*DATAN(1.0D0)
      N = 1.0D0/M
      THC = DATAN(1.0D0/DSQRT(N**2 - 1.0D0))
      PHC = PI - 2.0*THC
C
C           BEGIN COMPUTATION FOR SCATTERING ANGLE PHI (RADIANS)
C
      L = 0
      PHID = PHIBGN
      IF(PHID.GT.PHIEND) STOP
   50 PHI = PHID*PI/180.0
C
C           COMPUTE (0,0  RAY PARAMETERS
```

```
FILE: ESCAT    FORTRAN  A1


C
C   TH0 = INCIDENCE ANGLE
C   G01,G02 = PHASES FOR J = 1,2 (CENTER REF.)
C   F01,F02 = S.P.A. FAR ZONE COMPLEX AMPLITUDES FOR J = 1,2
C
      TH0 = (PI-PHI)/2.0
      CT0 = COS(TH0)
      ST0 = SIN(TH0)
      W = SIN(PHC-PHI)*SQRT(KA*COS(SNGL(THC))/(2.0*PI))
C
      CALL FRES(W,FC,FS)
C
      F01 = CMPLX(FC,FS)*CEXP(CMPLX(0.0,-1.0*PI/4.0))/SQRT(2.0)
      F02 = F01
      G01 = -2.0*KA*CT0
      G02 = G01
C
C           INITIALIZE (1,0) RAY SCATTERING AMPLITUDES:
C           IF PHI EXCEEDS PHC THERE IS NO (1,0) RAY, AND NO
C           (0,0) REFLECTION PHASE SHIFT.
C
      S11 = CMPLX(0.0,0.0)
      S12 = CMPLX(0.0,0.0)
      IF(PHI.GE.PHC) GO TO 60
C
C           COMPUTE (1,0) RAY PARAMETERS:
C              TH1 = INCIDENT ANGLE
C              R01 = REFRACTION ANGLE
C              G11,G12 = PHASES FOR J = 1,2 (CENTER REFERENCED)
C              D1 = GEOMETRIC DIVERGENCE FACTOR
C              R11,R12 = FRESNEL COEFFICIENTS FOR J = 1,2
C              F11,F12 = S.P.A. FAR ZONE COMPLEX AMPLITUDES
C
      PH2 = PHI/2.0
      TH1 = ATAN(M*SIN(PH2)/(1.0-M*COS(PH2)))
      CT1 = COS(TH1)
      ST1 = DSIN(DBLE(TH1))
      R01 = DATAN(N*ST1/DSQRT(1.0D0-(N*ST1)**2))
      CR1 = COS(R01)
      G11 = 2.0*KA*(M*CR1-CT1)
      G12 = G11
      TAU = N
      IF(CR1.GT.RMIN) TAU = TAU* CT1/CR1
      D1 = M*CT1**2/(4.0*(TAU-1.0)*(1.0-M*COS(PH2))*COS(PH2))
      DIF1 = R01 - TH1
      SUM1 = R01 + TH1
      SDF = SIN(DIF1)
      SSM = SIN(SUM1)
      TDF = TAN(DIF1)
      TSM = TAN(SUM1)
C
      IF(SDF.LE.RMIN) TDF = 1.0-M
      IF(SDF.LE.RMIN) TSM = 1.0+M
      IF(SDF.LE.RMIN) SSM = 1.0+M
      IF(SDF.LE.RMIN) SDF = 1.0-M
```

```
FILE: ESCAT    FORTRAN  A1

C
      R11 = (SDF/SSM)**2
      R12 = (TDF/TSM)**2
      F11 = CMPLX(2.0*(1.0-R11)*SQRT(D1),0.0)
      F12 = CMPLX(2.0*(1.0-R12)*SQRT(D1),0.0)
C
C           INCLUDE REFLECTION PHASE SHIFTS FOR (0,0) RAY:
C
      DEL = SQRT(ST0**2 - M**2)/CT0
      DEL1 = 2.0*ATAN(DEL)
      DEL2 = 2.0*ATAN(N*N*DEL)
      G01 = G01 - DEL1
      G02 = G02 - DEL2
C
C           COMPUTE (1,0) AND (0,0) RAY SCATTERING AMPLITUDES IN
C           STANDARD UNITS (E.G. VAN DE HULST, WISCOMBE)
C
      S11 = CMPLX(0.0,-1.0*KA/2.0)*F11*CEXP(CMPLX(0.0,G11))
      S12 = CMPLX(0.0,-1.0*KA/2.0)*F12*CEXP(CMPLX(0.0,G12))
   60 S01 = CMPLX(0.0,-1.0*KA/2.0)*F01*CEXP(CMPLX(0.0,G01))
      S02 = CMPLX(0.0,-1.0*KA/2.0)*F02*CEXP(CMPLX(0.0,G02))
C
C            SUM THE (0,0) AND (1,0) RAY SCATTERING AMPLITUDES
C
      S1 = S01 + S11
      S2 = S02 - S12
      ANG = PHID
      RS1 = REAL(S1)
      CS1 = AIMAG(S1)
      RS2 = REAL(S2)
      CS2 = AIMAG(S2)
      I1 = (2.0*CABS(S1)/KA)**2
      I2 = (2.0*CABS(S2)/KA)**2
      IF(II.LE.1) GO TO 888
      WRITE(1,1100)ANG,I1,I2
 1100 FORMAT(F7.4,2E14.6)
  888 CONTINUE
C
C           COMPUTE THE DIFFRACTED AMPLITUDES SD1 AND SD2
C           WITH CENTER REFERENCED PHASES
C
      ARG = KA*SIN(PHI)
      DP = 0.5
      IF(ARG.LT.0.0) ARG = ABS(ARG)
      IF(ARG.LE.RMIN) GO TO 90
      IF(ABS(PHID).GE.90.0) GO TO 95
   80 DP = COS(PHI)*BJ1X(ARG)
   90 SD1 = CMPLX(DP*KA**2,0.0)
   95 IF(ABS(PHID).GE.90.0) SD1 = CMPLX(0.0,0.0)
      SD2 = SD1
      ANG = PHID
      RSD1 = REAL(SD1)
      CSD1 = AIMAG(SD1)
      RSD2 = RSD1
      CSD2 = CSD1
```

```
FILE: ESCAT    FORTRAN  A1

      ID = (2.0*CABS(SD1)/KA)**2
      IF(JJ.LE.1) GO TO 889
      WRITE(1,1200)ANG,ID
 1200 FORMAT(F7.4,E14.6)
  889 CONTINUE
C
C           COMPUTE TOTAL AMPLITUDES FOR P.O.A. PLUS DIFFRACTION
C
      S1 = S1 + SD1
      S2 = S2 + SD2
      ANG = PHID
      RS1 = REAL(S1)
      CS1 = AIMAG(S1)
      RS2 = REAL(S2)
      CS2 = AIMAG(S2)
      IT1 = (2.0*CABS(S1)/KA)**2
      IT2 = (2.0*CABS(S2)/KA)**2
      IF(KK.LE.1) GO TO 890
      WRITE(1,1300)ANG,IT1,IT2
 1300 FORMAT(F7.4,2E14.6)
  890 CONTINUE
C
C           STEP PHI UP BY DPHI AND REPEAT UNTIL PHIEND
C
      L = L + 1
      PHID = PHIBGN + L*DPHI
      IF(PHID.LE.PHIEND) GO TO 50
      STOP
      END
      SUBROUTINE FRES(WE,FS,FC)
C
C           COMPUTES THE FRESNEL INTEGRAL FROM 0 TO WE
C
      W = ABS(WE)
      F = (1.0 + 0.926*W)/(2.0 + 1.792*W + 3.104*W**2)
      G = 1.0/(2.0 + 4.142*W + 3.492*W**2 + 6.670*W**3)
      A = 1.570796*W**2
      C = COS(A)
      S = SIN(A)
      FC = 0.5 + F*S - G*C
      FS = 0.5 - F*C - G*S
      IF(WE.LT.0) GO TO 3
      FC = FC + 0.5
      FS = FS + 0.5
      RETURN
    3 FC = 0.5 - FC
      FS = 0.5 - FS
      RETURN
      END
      FUNCTION BJ1X(X)
C
C           COMPUTES BESSEL FUNCTION J1(X), AND DIVIDES BY X:
C           USING THE POLYNOMIAL APPROXIMATIONS FROM ABRAMOWITZ
C           & STEGUN
C
```

FILE: ESCAT FORTRAN A1

```
      DIMENSION A(7),B(7),C(7)
      DATA A/0.5,-0.56249985,0.21093573,-0.03954289,0.00443319,
     *      -3.1761E-4,1.109E-5/
      DATA B/0.79788456,1.56E-6,0.01659667,1.7105E-4,-0.00249511,
     *       0.00113653,-2.0033E-4/
      DATA C/-2.35619449,0.12499612,5.65E-5,-0.00637879,7.4348E-4,
     *       7.9824E-4,-2.9166E-4/
      IF(ABS(X).LT.3.0) GO TO 20
      Z = ABS(3.0/X)
      F = B(7)
      T = C(7)
      DO 10 K = 6,1,-1
         F = B(K) + Z*F
         T = C(K) + Z*T
   10 CONTINUE
      BJ1X = F*COS(X+T)/(X*SQRT(X))
      RETURN
   20 Z = (X/3.0)**2
      BJ1X = A(7)
      DO 30 K = 6,1,-1
         BJ1X = A(K) + Z*BJ1X
   30 CONTINUE
      RETURN
      END
```

APPENDIX B

SUPPLEMENTAL I_1 EXAMPLES

Figures B.1 - B.9 give the results for calculations for the $j = 1$ case (perpendicular E-field vector polarization) similar to those performed in Chapter 2. There are several differences in the features for the I_1 case which should be mentioned. First, the fine structure variation is much more prominent than for the I_2 case as can be seen in Figs. B.1 - B.4. This behavior is also shown for coated bubble cases. Uncoated bubble results show that for $30° < \theta < 90°$ the positions of the fine-structure intensity oscillations for $j = 2$ are typically shifted from those for $j = 1$ by one half of a fine-structure quasi-period, except where θ is slightly less than θ_c. This fine structure shift is also present in the coated bubble results although it appears that the shift towards θ_c in I_1 is slightly greater than for I_2 at comparable coating thickness values.

One prominent feature seen in the $j = 1$ case and not the $j = 2$ case is the anomalous modulation in coarse structure for large values of h in the $\theta = 70°$ to $90°$ region as is shown in Figs. B.2(e) and B.3(e). This behavior was not seen in the $j = 2$ cases (compare Fig. 2.8(e) and 2.9(e)). The apparent cause of this modulation is the nature of the reflection coefficient at the water-coating interface for the two cases. Consider the reflection at the water-coating interface of ray $(0,0)_b$ shown in Fig. 2.7. From geometric considerations the local angle of incidence i is related to the scattering angle θ by

$$i = (180° - \theta)/2. \qquad (B.1)$$

The relative amplitudes of the waves associated with this ray in the two cases ($j = 1$ and

j = 2) are given by comparison of the Fresnel (or plane surface) reflection coefficients r_j,

$$r_1 = \frac{\sin(i - r)}{\sin(i + r)}, \quad r_2 = \frac{\tan(i - r)}{\tan(i + r)} \qquad \text{(B.2a,b)}$$

where r denotes the local refraction angle and is given by $r = \sin^{-1}[(n_w/n_c)\sin i]$. Consider the case $\theta = 82.82°$ for which (B.1) gives $i = 48.59°$. Then for $n_w = 4/3$ and $n_c = 1.5$ we have $r = 41.81°$ and (B.2) gives $r_1 = 0.1181$ and $r_2 = -0.0008$; clearly $|r_1| >> |r_2|$. For the case $j = 1$ it appears that the amplitude of the $(0,0)_b$ ray may be sufficient to interfere with that of the (0,0) ray in Fig. 2.7 to cause the anomalous modulations. Because this effect only occurs in the $j = 1$ case, the choice of $j = 2$ for bubble sizing and detection is further supported.

Another feature which was much more prominent in I_1 was the presence of contrast modulations created by the superposing of the (0,0) and (3,1) ray amplitudes onto the fine-structure interference pattern of the (0,0) and (2,1) ray amplitudes (e.g., $\theta \approx 67°$, $\theta \approx 85°$ in Fig. B.2(a)). These modulations were discussed by Langley and Marston for the case of an uncoated bubble in Ref. 13 of Chapter 2. Note that as the thickness of the coating is increased other modulations occur (i.e., $\theta \approx 72°$, 75° in Fig. B.2(d)) which appear to be unique to that particular coating value. This effect is most prominent for smaller bubbles ($ka < 1000$). The apparent reason for this behavior is due to the fact that the approximate angular period of the contrast modulations $(\Delta\theta)_M$ is proportional to $\lambda_0/(B_3 - B_2)$ where B_3 is the distance between the (0,0) and (3,1) ray and B_2 is the distance between the (0,0) and (2,1) ray. The introduction of a coating invariably alters the distance between B_3 and B_2 resulting in the new modulations. For most other cases the behavior of I_1 was found to be similar to the analogous cases presented in Chapter 2 for I_2. These results are presented in Figs. B.5 - B.9.

Figure B.1. Calculated normalized scattering irradiances for ka = 100, $n_w = 4/3$, $n_c = 1.5$ for the perpendicular polarization I_1 in the critical angle scattering region. The solid curve is from Mie theory, the thick-dashed curve is the physical-optics approximation, and the thin-dashed curve is the calculated coated sphere results for (a) 0.25 μm, (b) 0.5 μm, (c) 1.0 μm, (d) 2.0 μm, and (e) 3.0 μm. Note the greater amount of fine structure as compared to the I_2 case in Figures 2.5 (a) - (e).

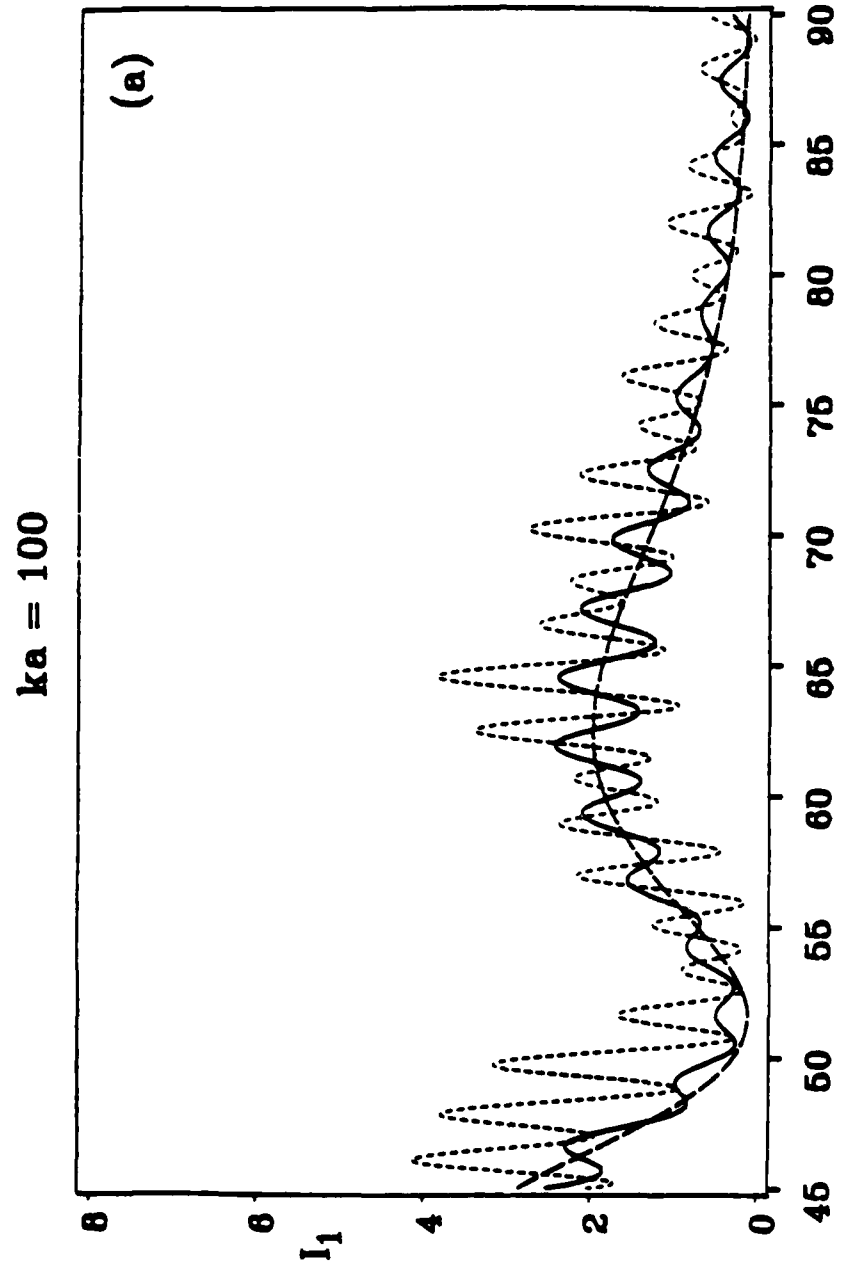
ka = 100
(a)
I_1
8
6
4
2
0
45
50
55
60
65
70
75
80
85
90
scattering angle (deg)

Fig. B.1 (a)

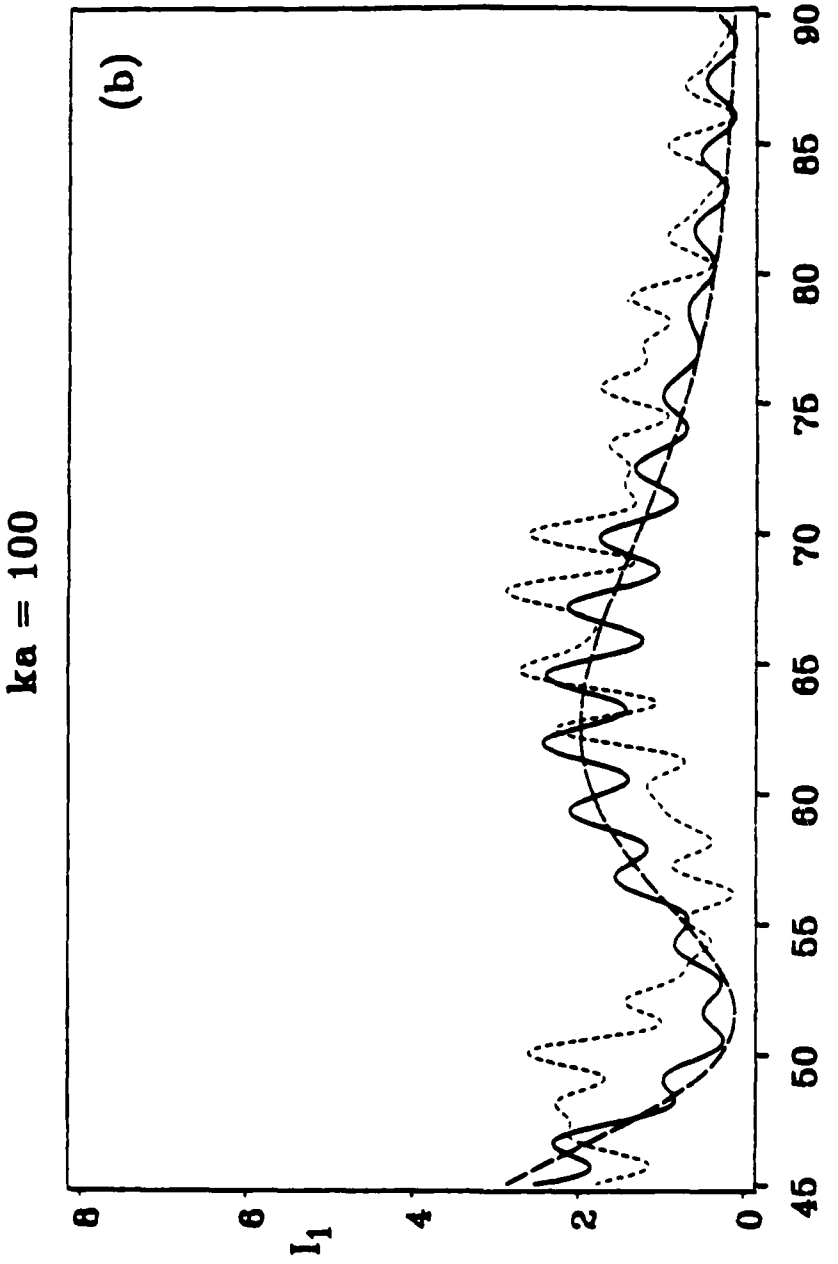
(b)
ka = 100
I_1
8
6
4
2
0
45
50
55
60
65
70
75
80
85
90
scattering angle (deg)

Fig. B.1 (b)

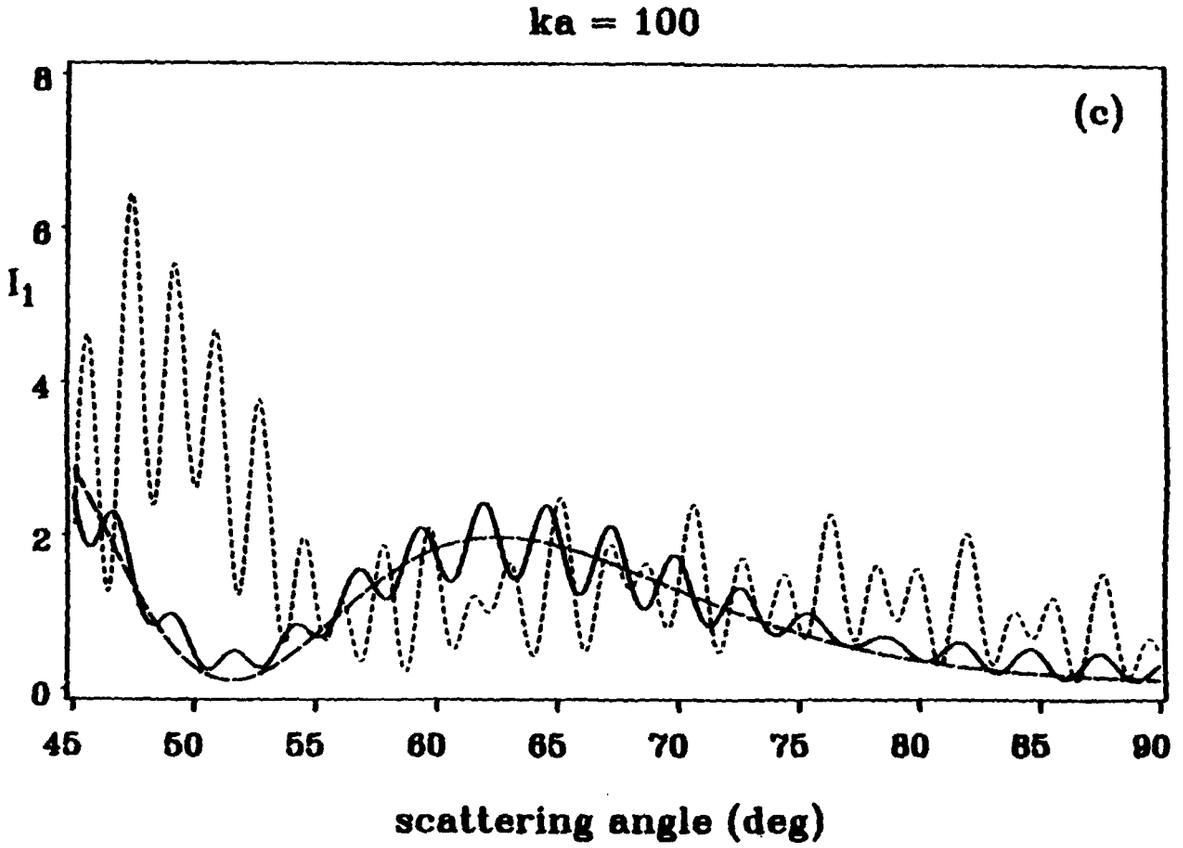
ka = 100
(c)
8
6
4
2
0
I_1
45
50
55
60
65
70
75
80
85
90
scattering angle (deg)

Fig. B.1 (c)

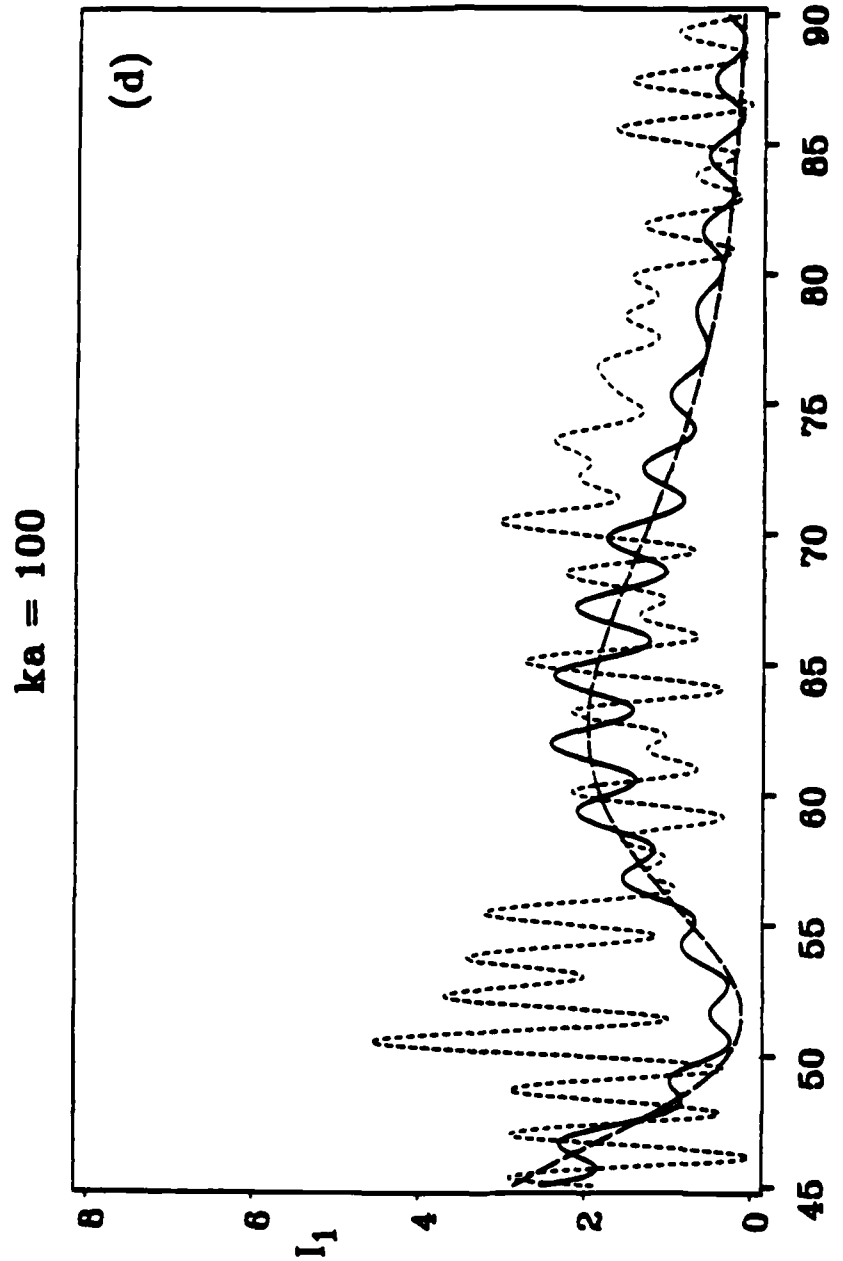
(d)
ka = 100
I_1
0
2
4
6
8
45
50
55
60
65
70
75
80
85
90
scattering angle (deg)

Fig. B.1 (d)

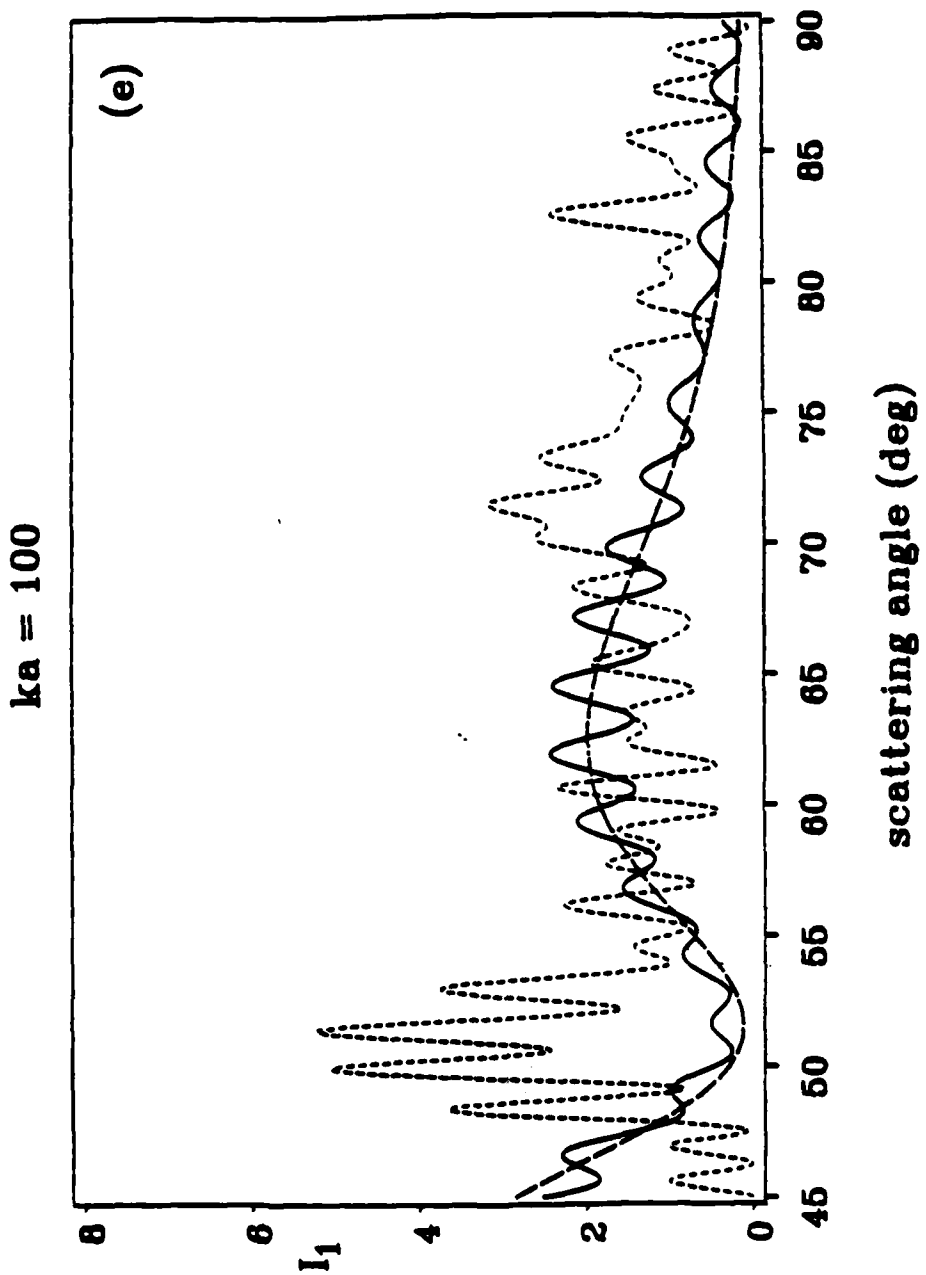
(e)
ka = 100
I_1
0
2
4
6
8
45
50
55
60
65
70
75
80
85
90
scattering angle (deg)

Fig. B.1 (e)

Figure B.2. Like Figure 2.8 but for j = 1 case.

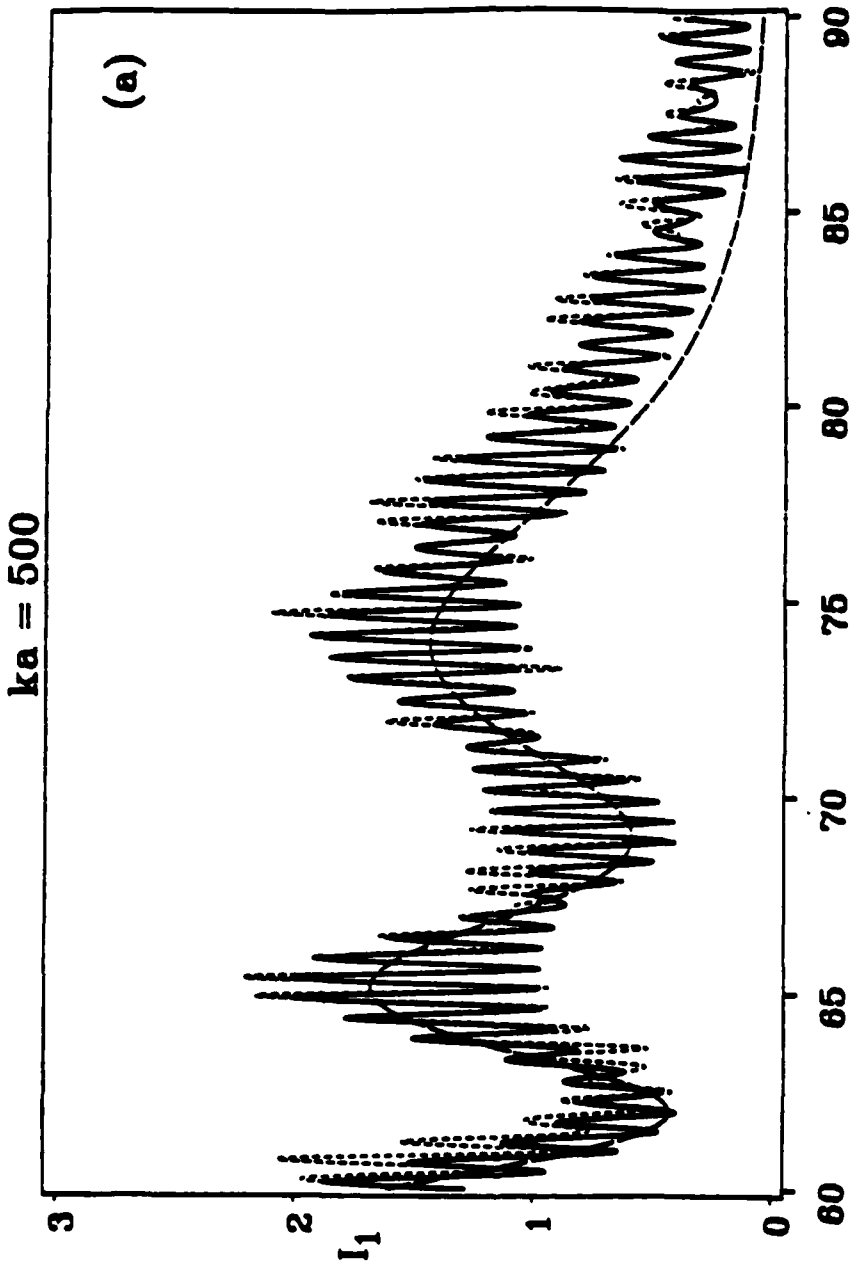

Fig. B.2 (a)

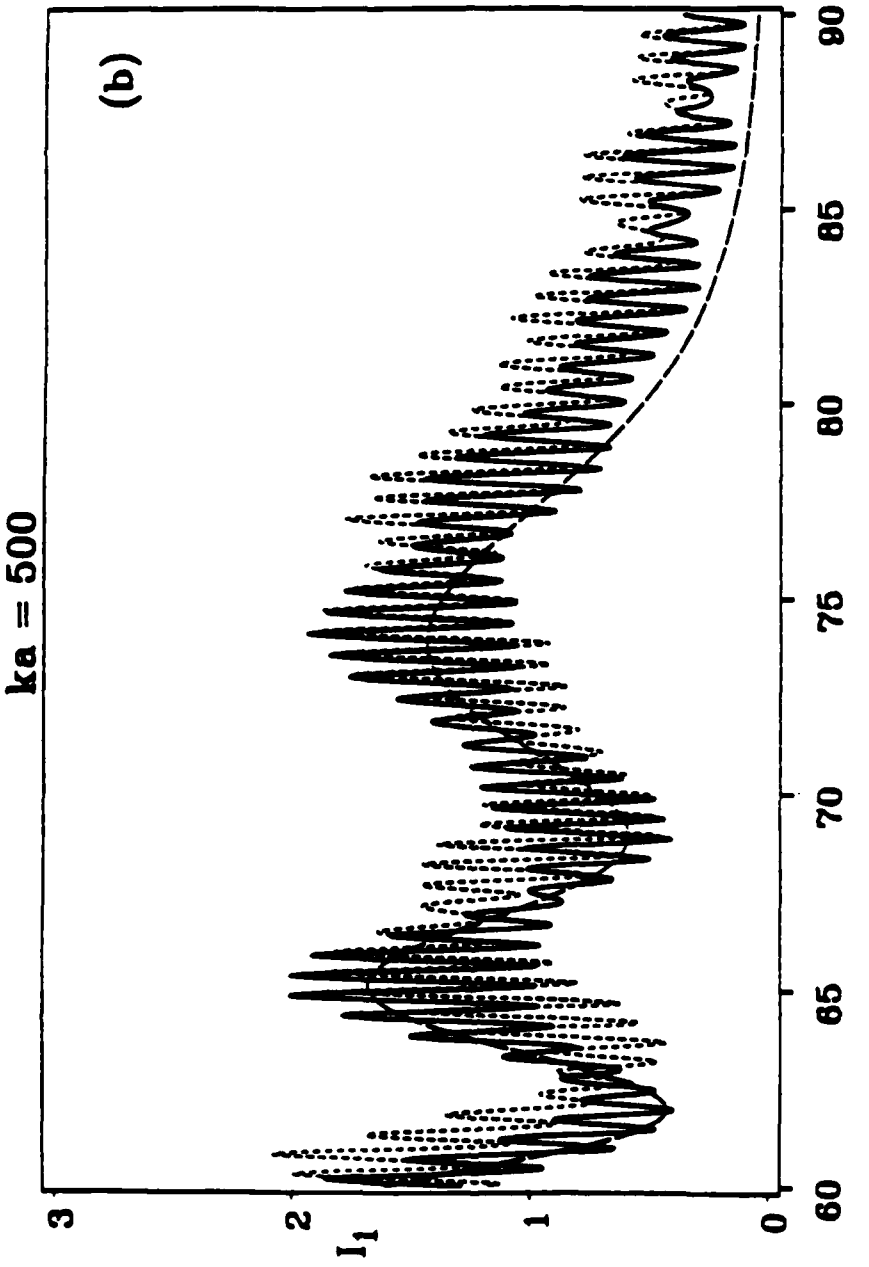

Fig. B.2 (b)

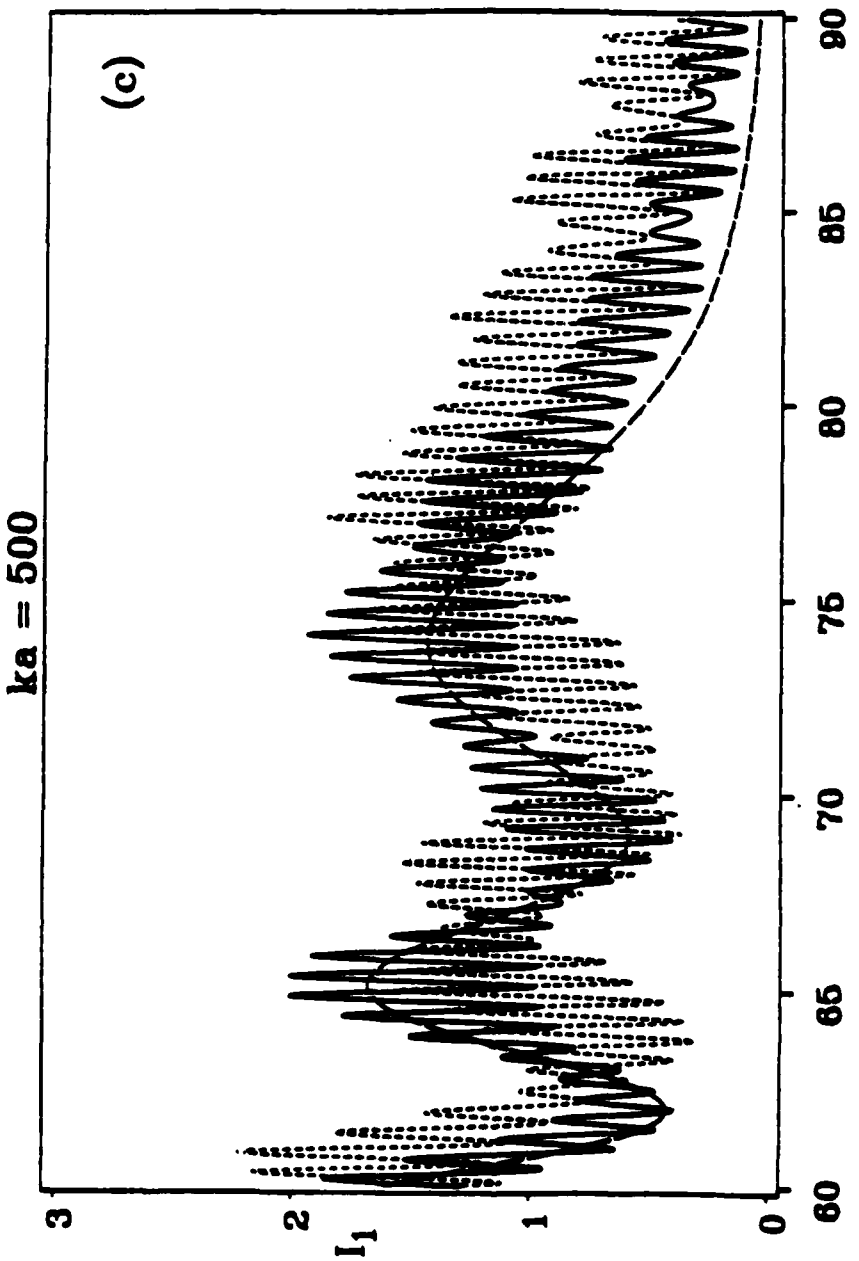

Fig. B.2 (c)

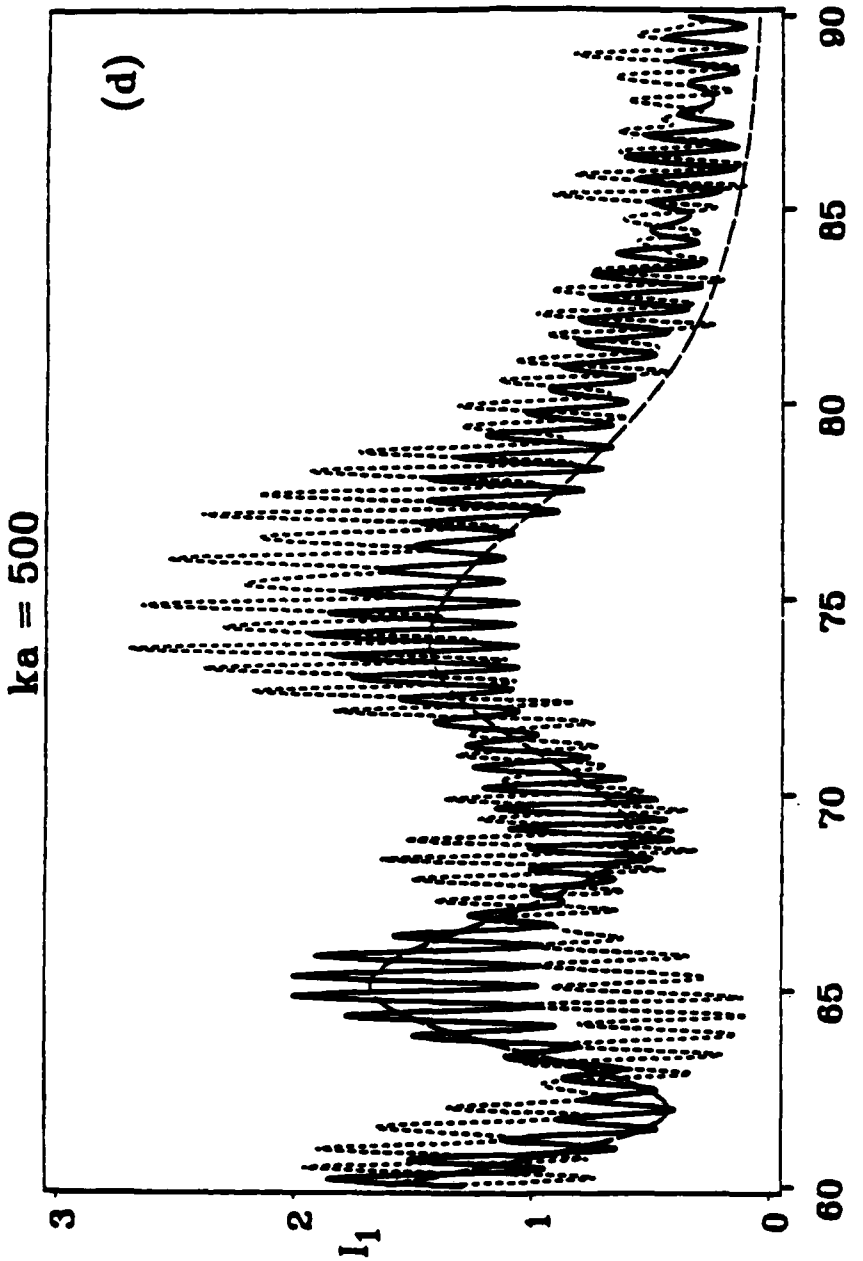

Fig. B.2 (d)

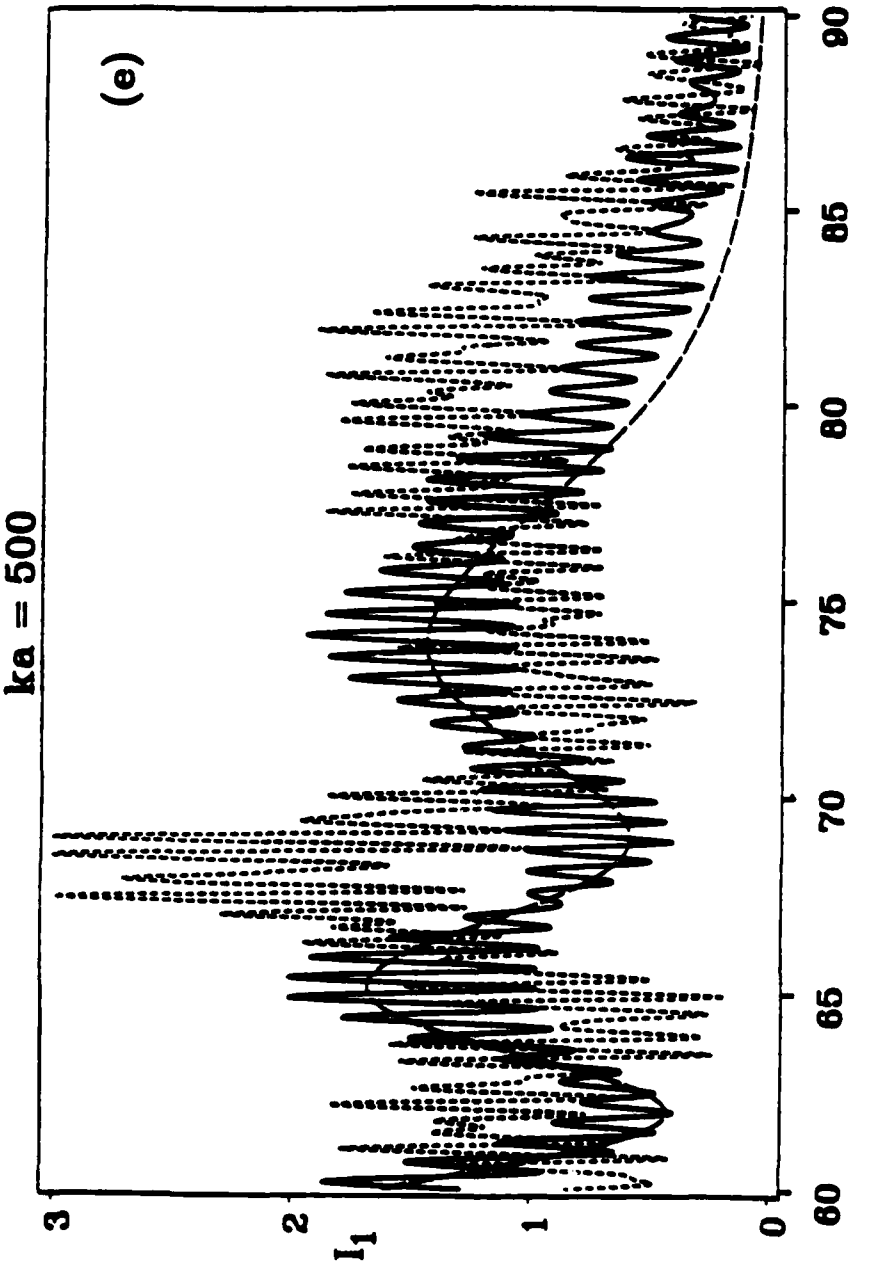

Fig. B.2 (c)

Figure B.3. Like Figure 2.9 but for j = 1 case.

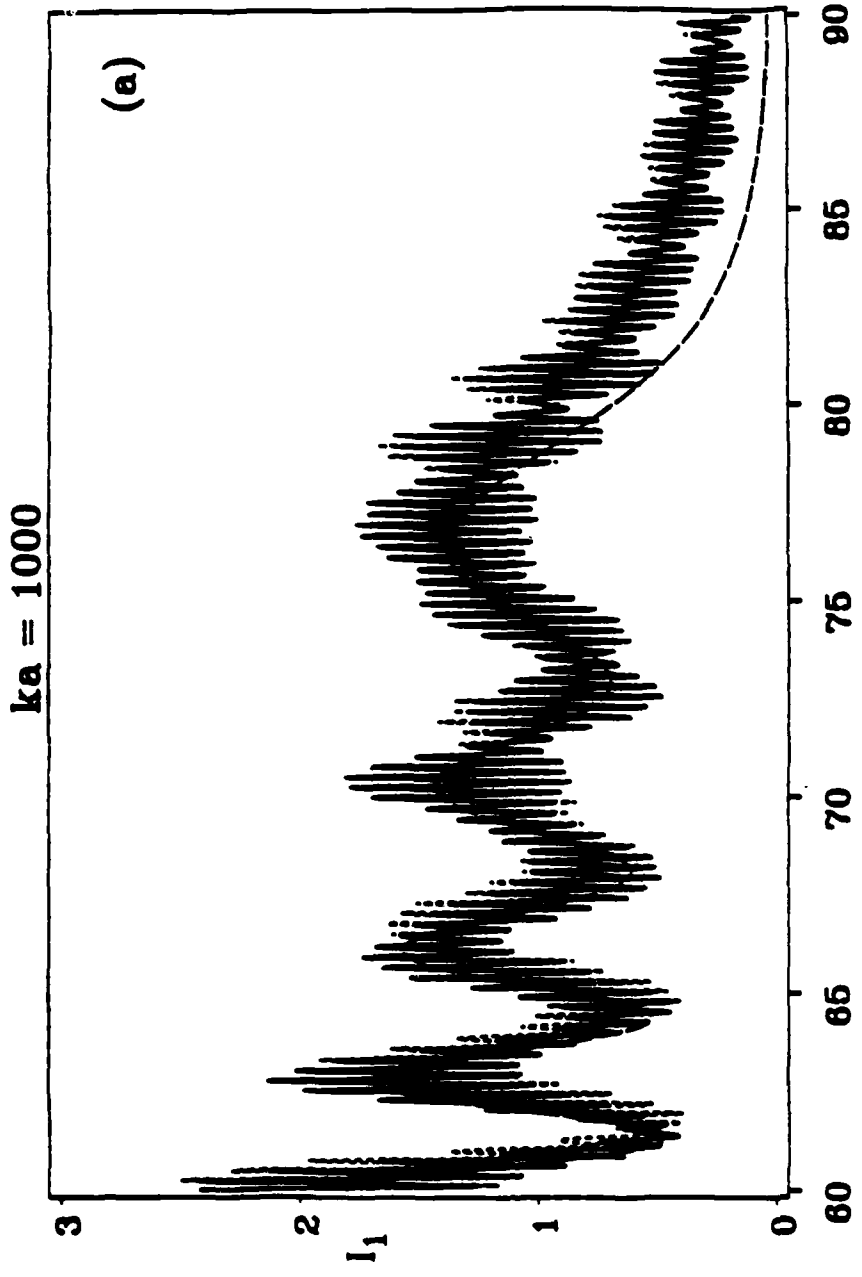

Fig. B.3 (a)

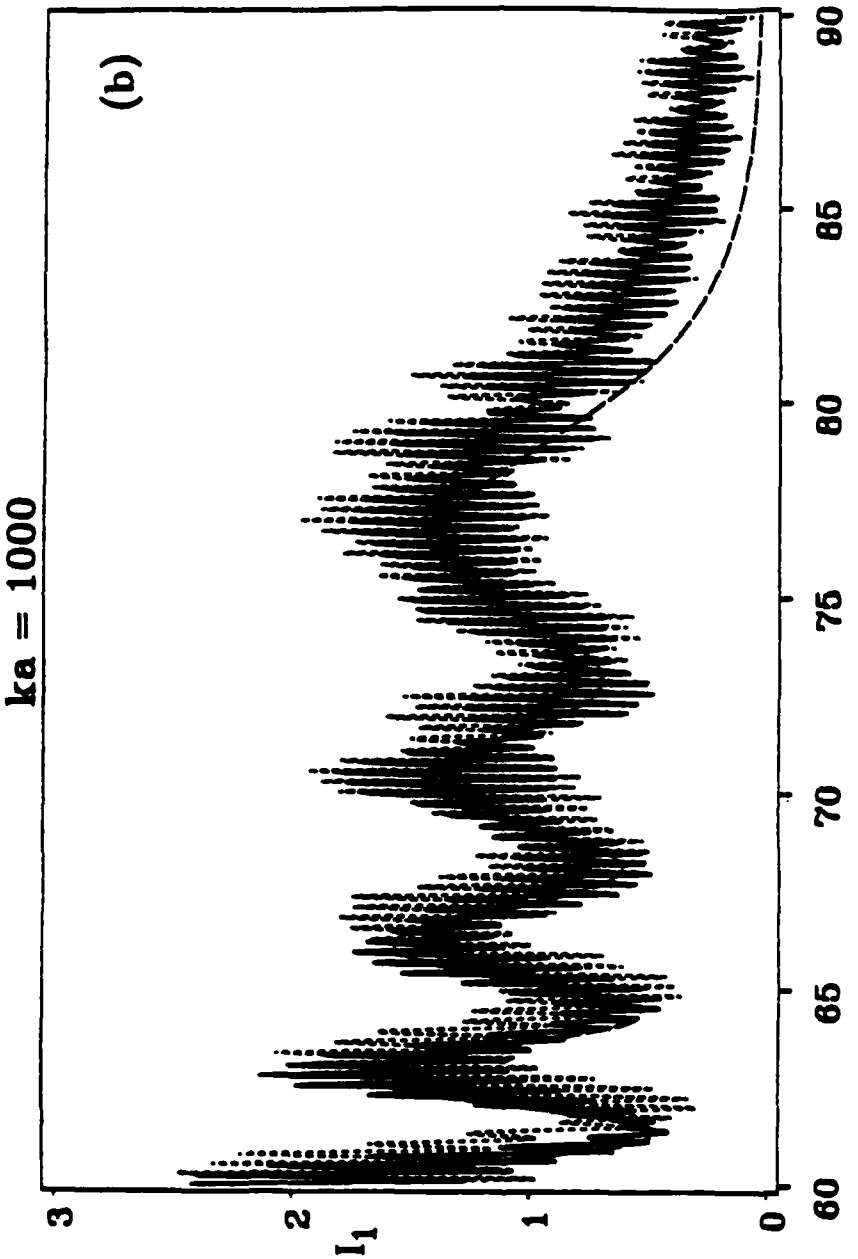

Fig. B.3 (b)

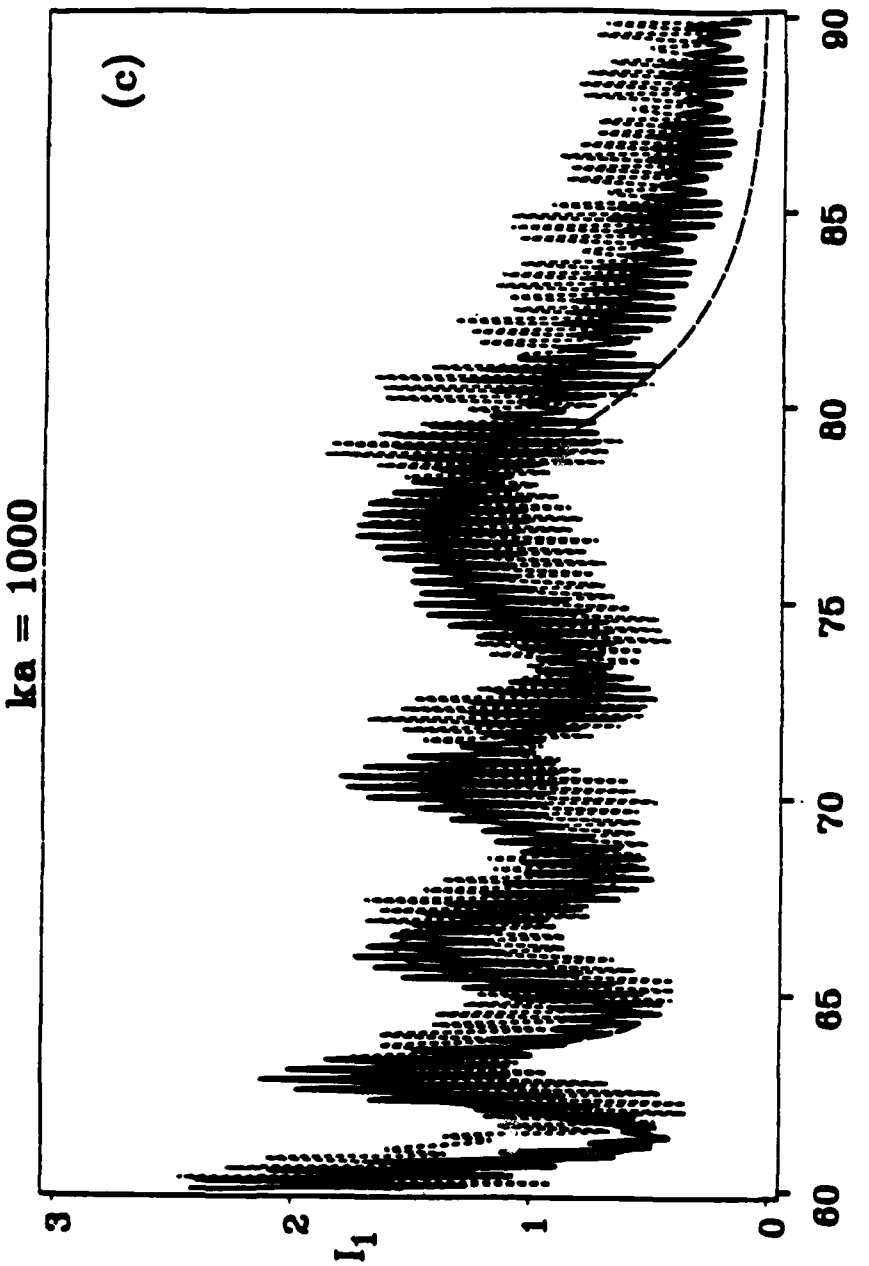

Fig. B.3 (c)

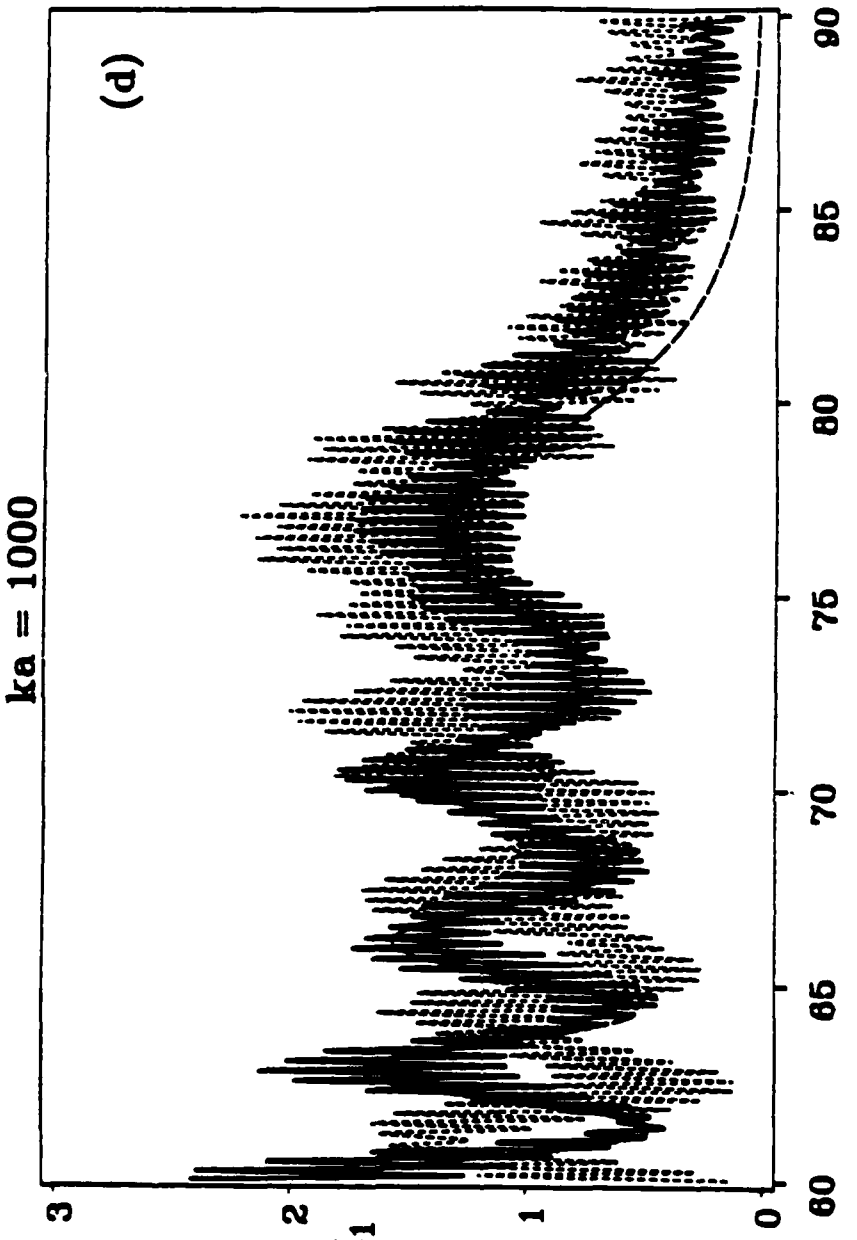

Fig. B.3 (d)

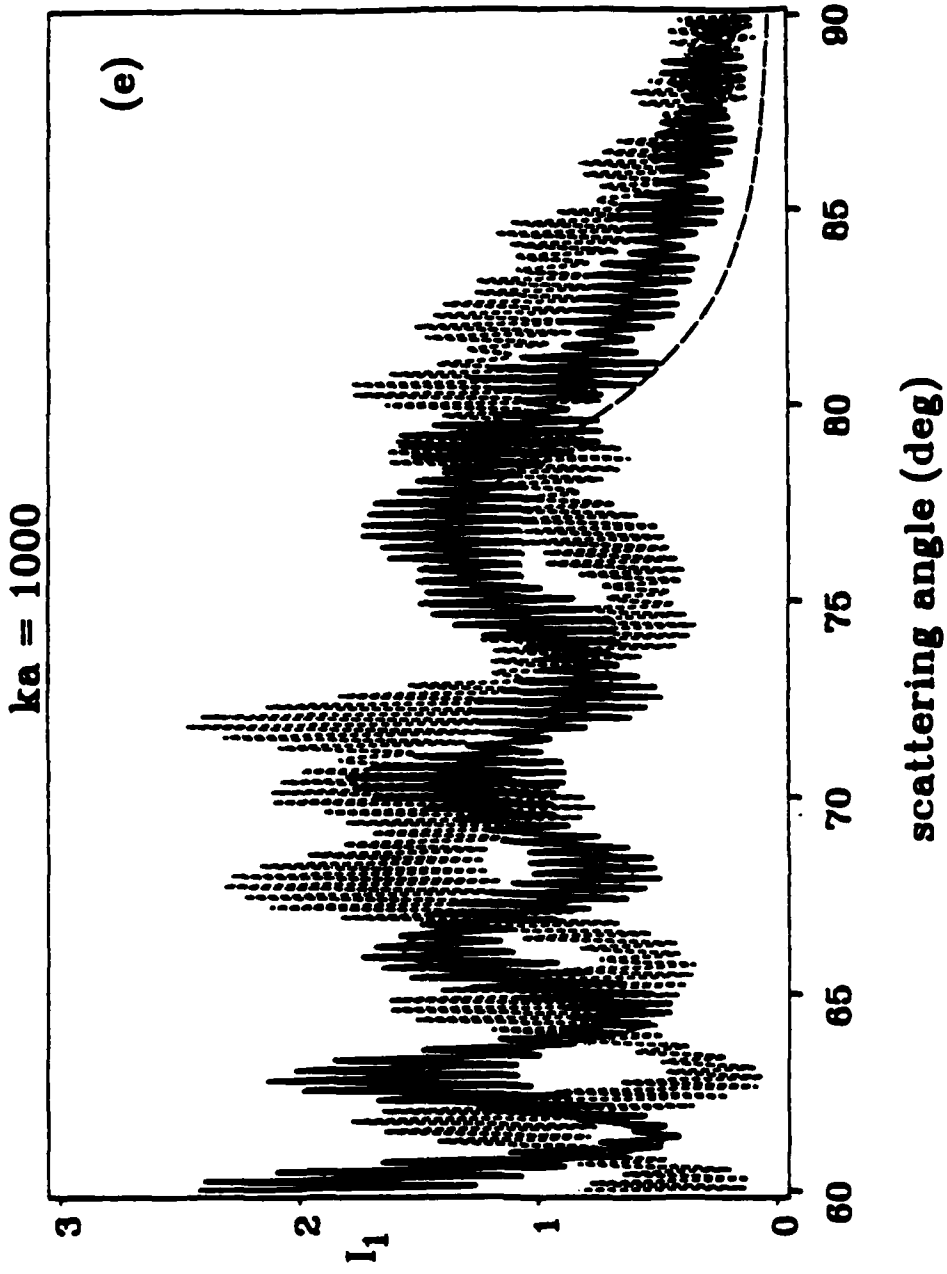

Fig. B.3 (e)

Figure B.4. Like Figure 2.10 but for j = 1 case.

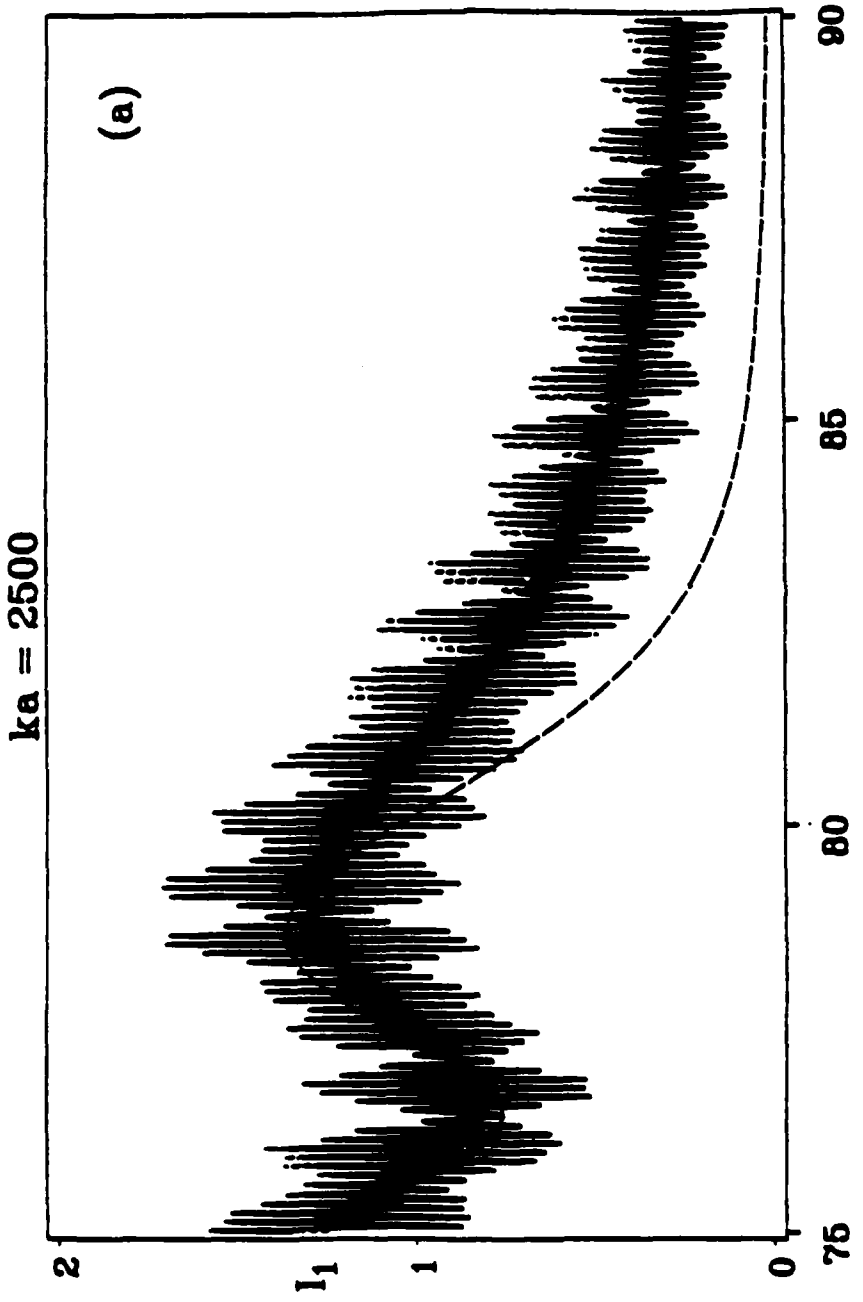

Fig. B.4 (a)

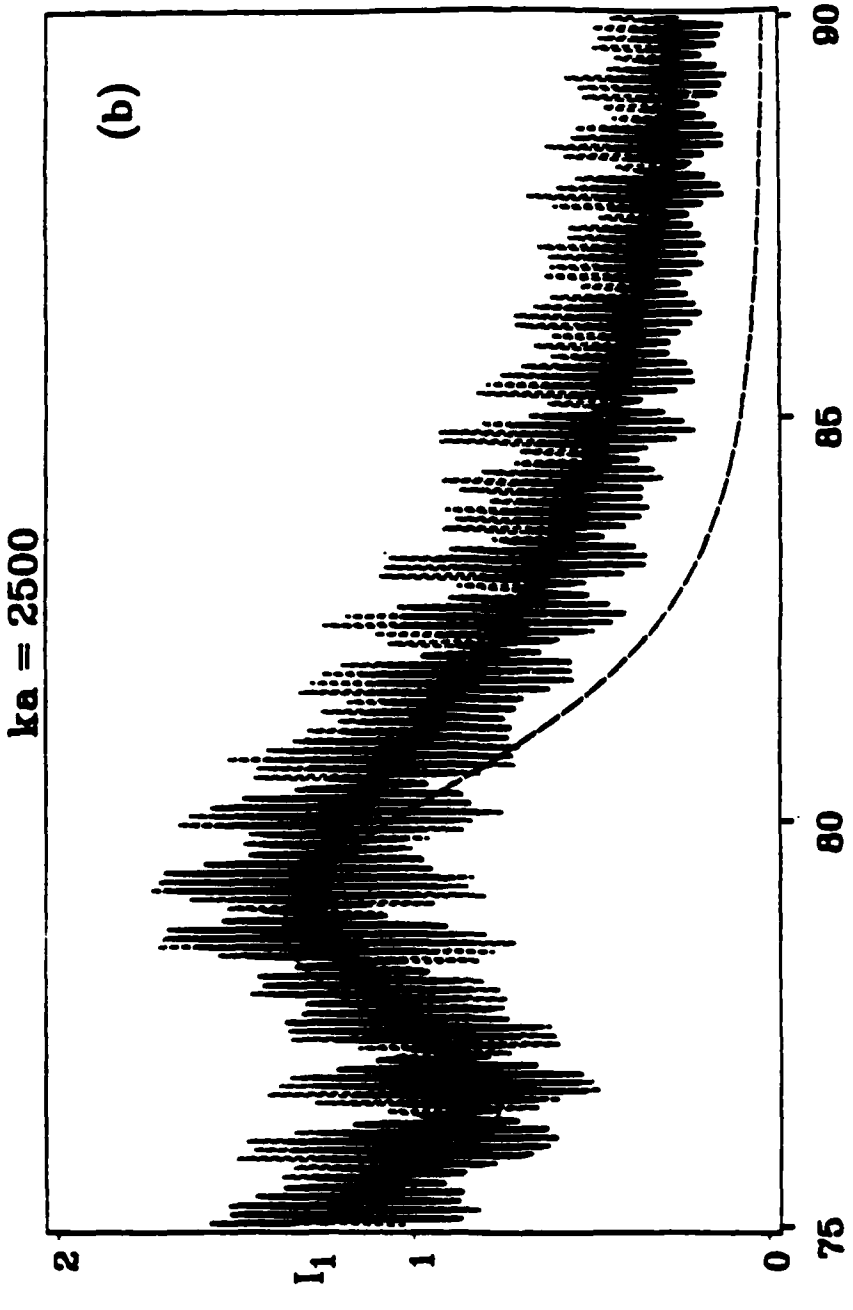

Fig. B.4 (b)

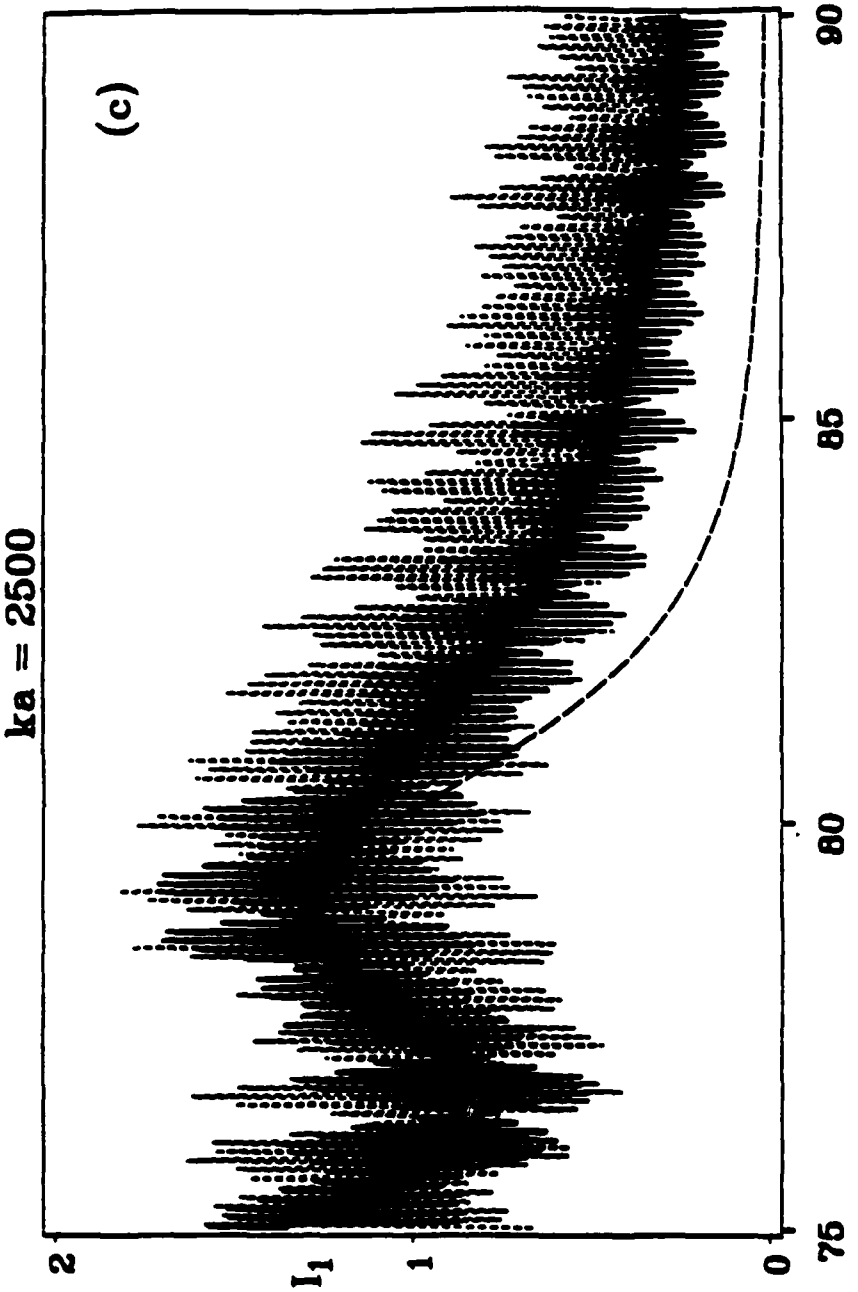

Fig. B.4 (c)

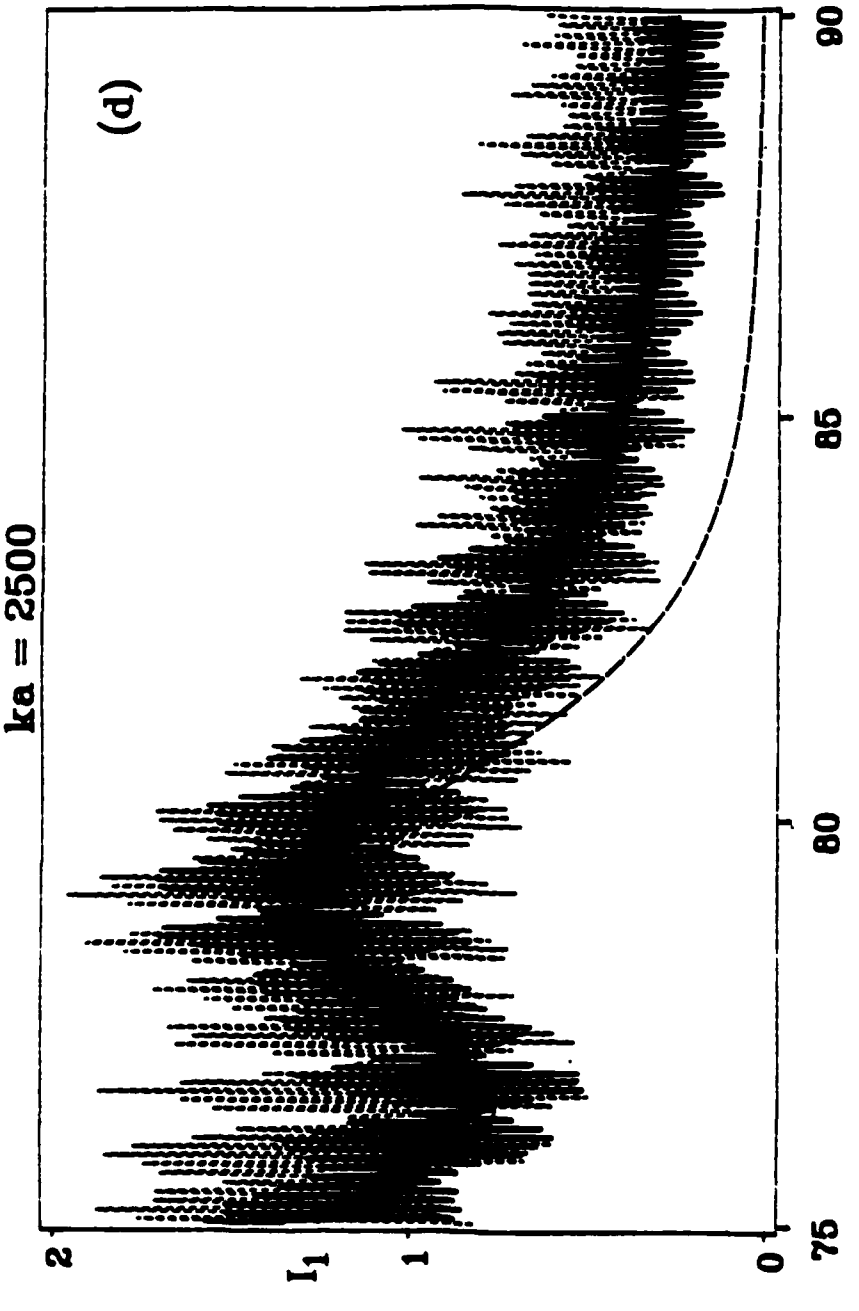

Fig. B.4 (d)

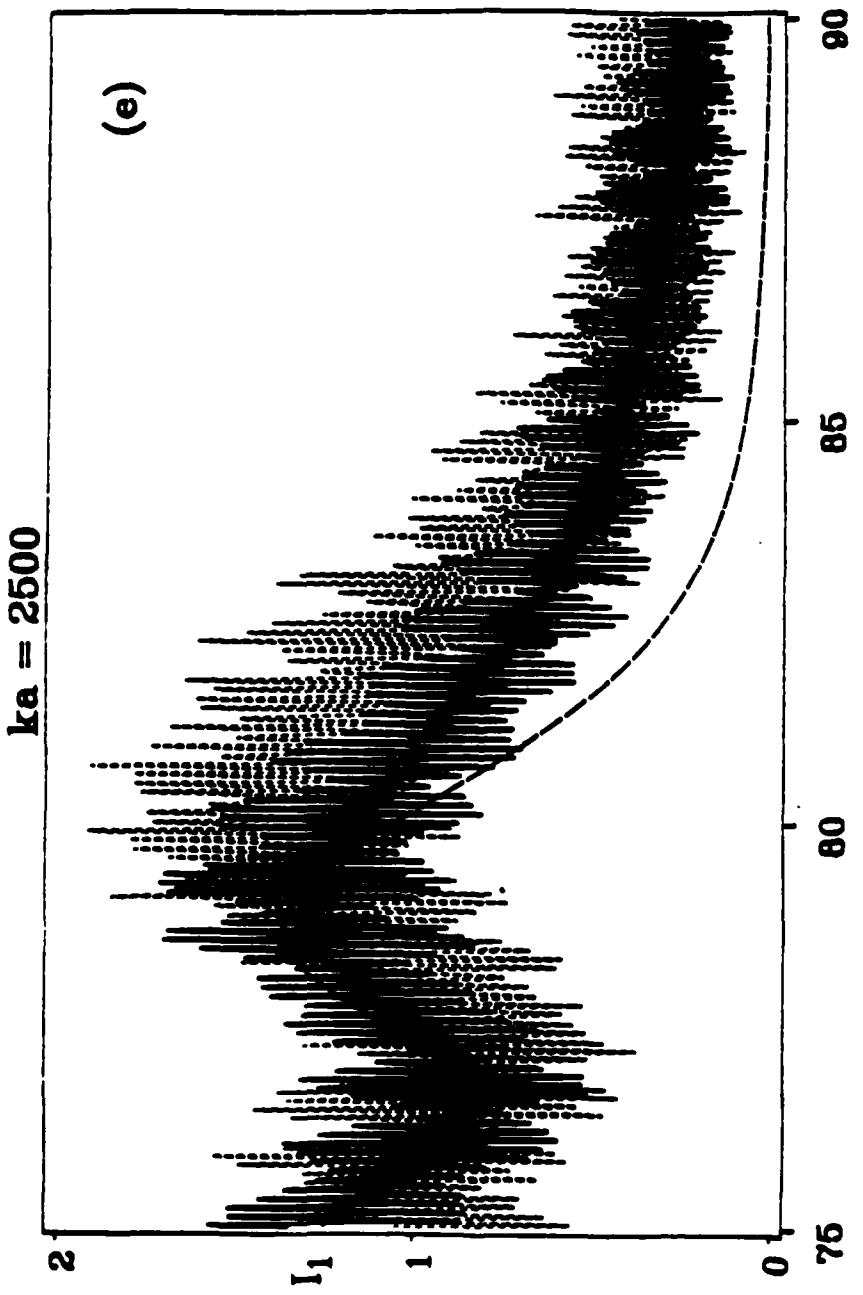

Fig. B.4 (c)

Figure B.5. The effect of changing n_c with ka = 100 and h = 0.26. The thick-dashed curve represents $n_c = 1.45$, the thin-dashed curve is for $n_c = 1.5$, and the solid curve represents the noncoated case.

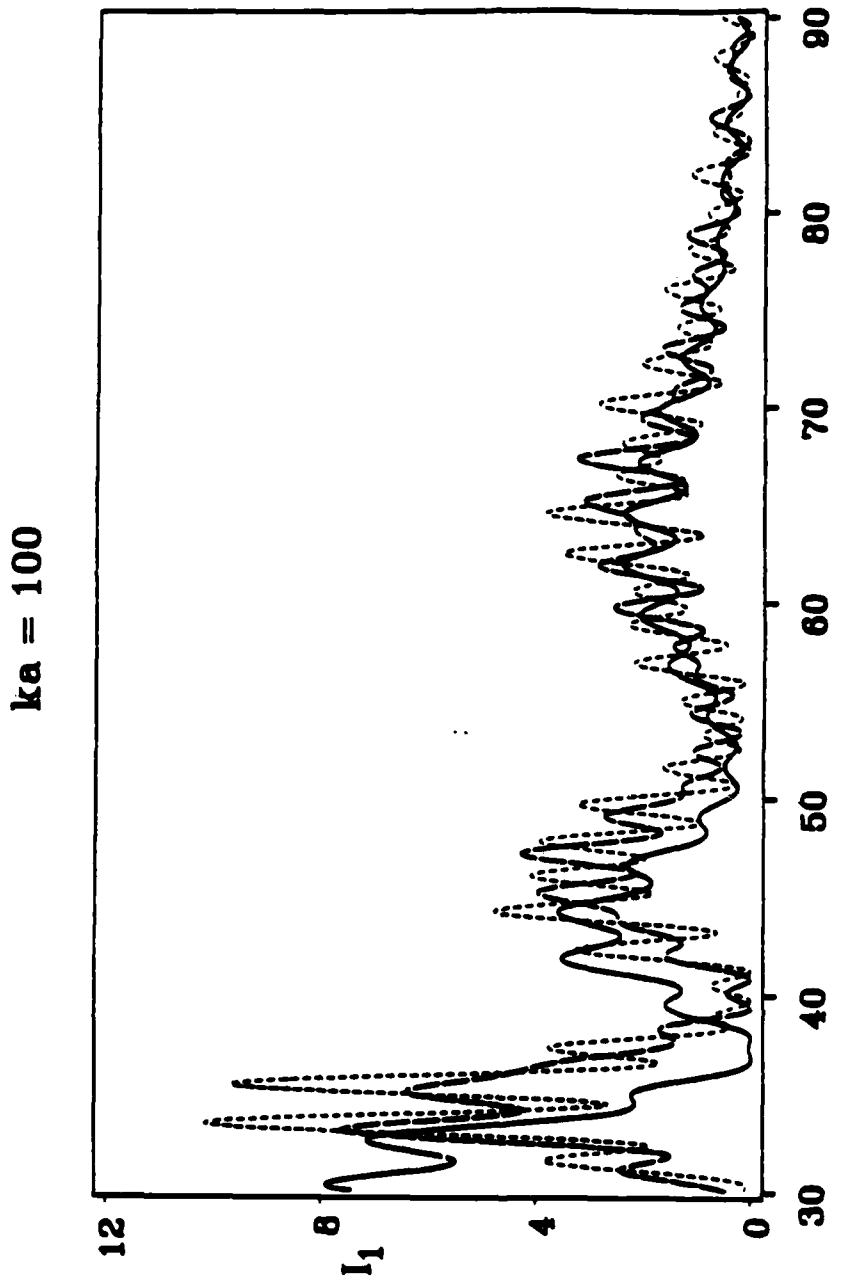

Fig. B.5

Figure B.6. Like Figure B.5 but the thick-dashed curve represents $n_c = 1.55$.

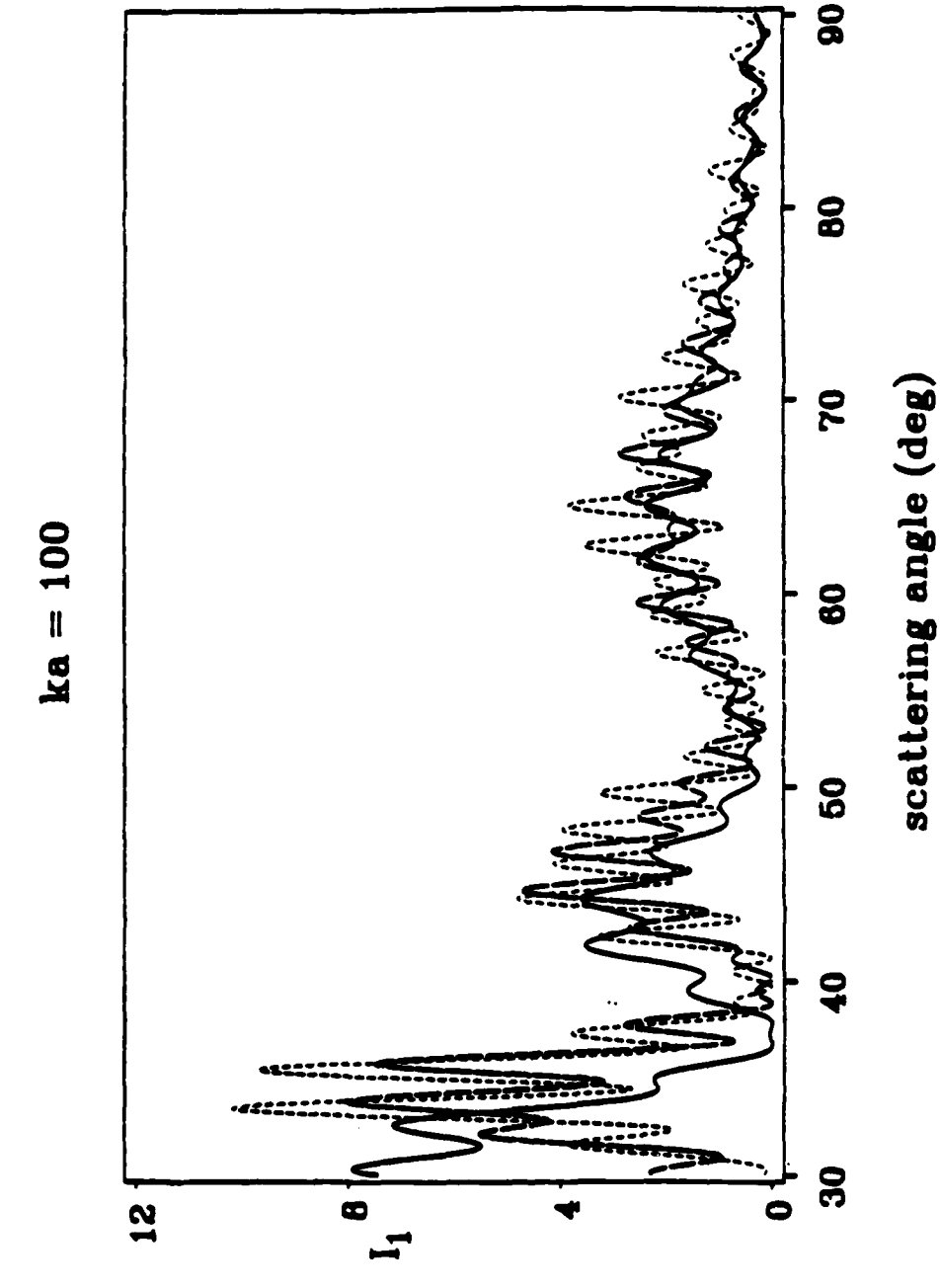

Fig. B.6

Figure B.7. The effect of changing n_c with ka = 1000 and h = 3.14 μm. The thin-dashed curve is for n_c = 1.45 and the solid curve is for n_c = 1.5. (The noncoated case is omitted.)

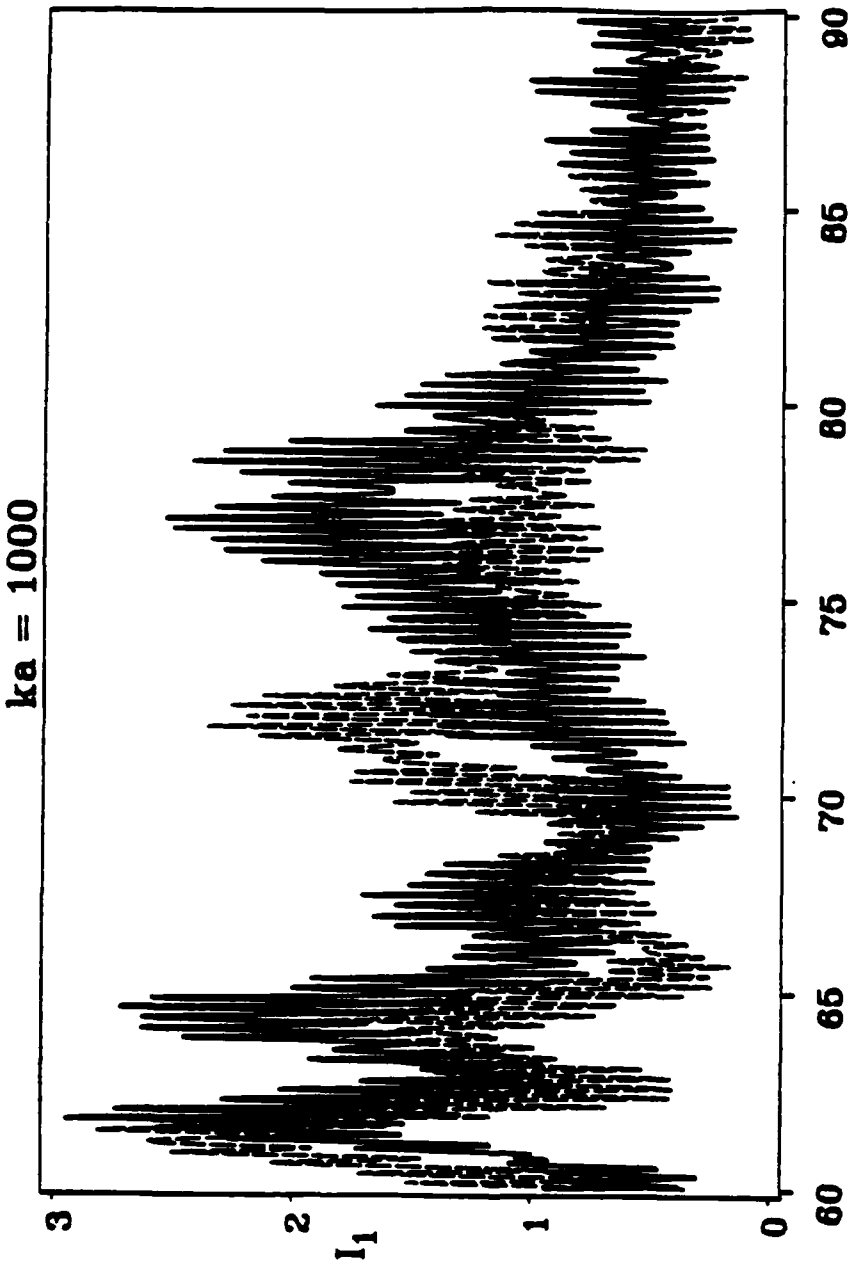

Fig. B.7

Figure B.8. Like Figure B.7 but thin-dashed curve represents $n_c = 1.55$.

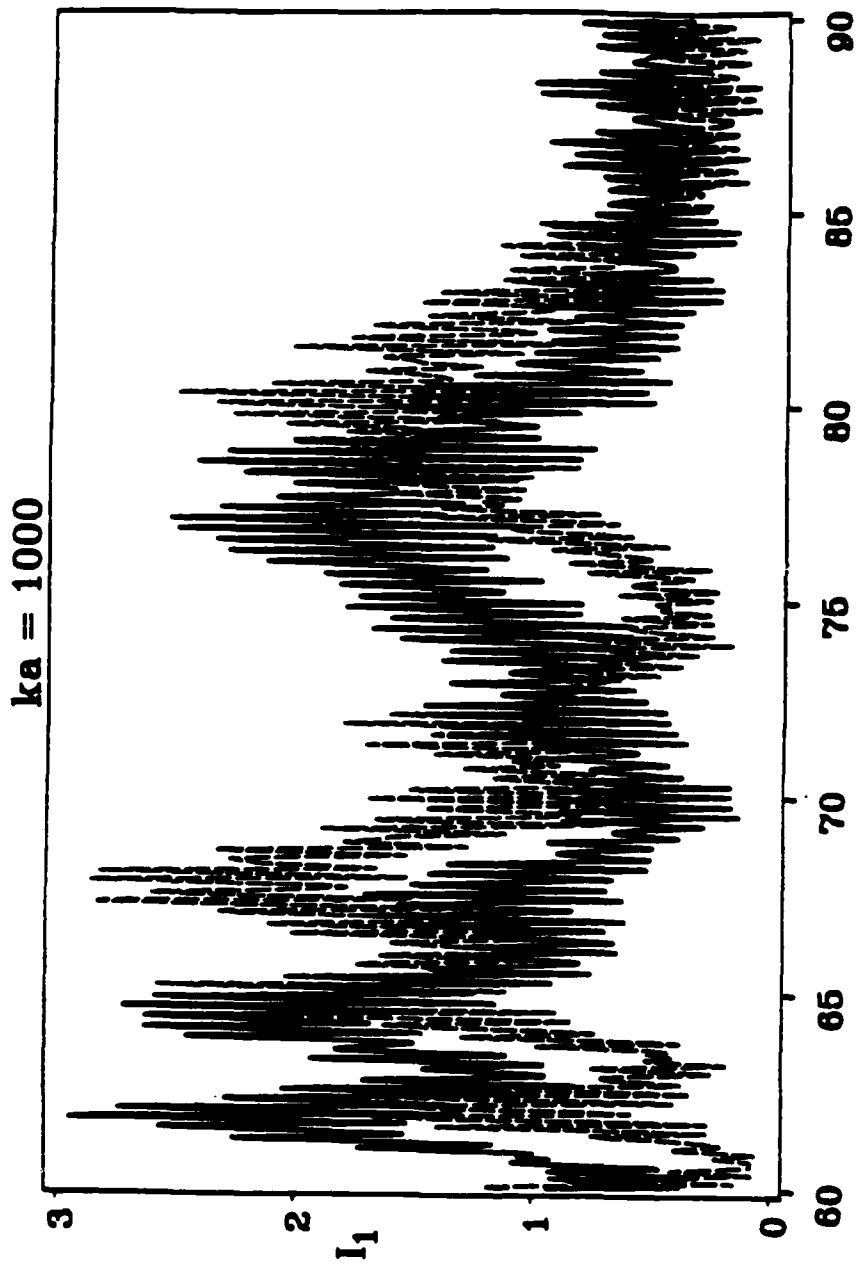

Fig. B.8

Figure B.9. Calculated normalized irradiances for a strongly absorbing coating (n_c = 1.5 + ilE - 3) for ka = 1000 and (a) h = 0.99 μm, (b) h = 2.0 μm, (c) h = 3.14 μm, and (d) h = 5.00 μm. The solid line is the non-absorbing coat result. Note that in case (a) the absorbing case (dashed) is virtually the same as the non-absorbing case.

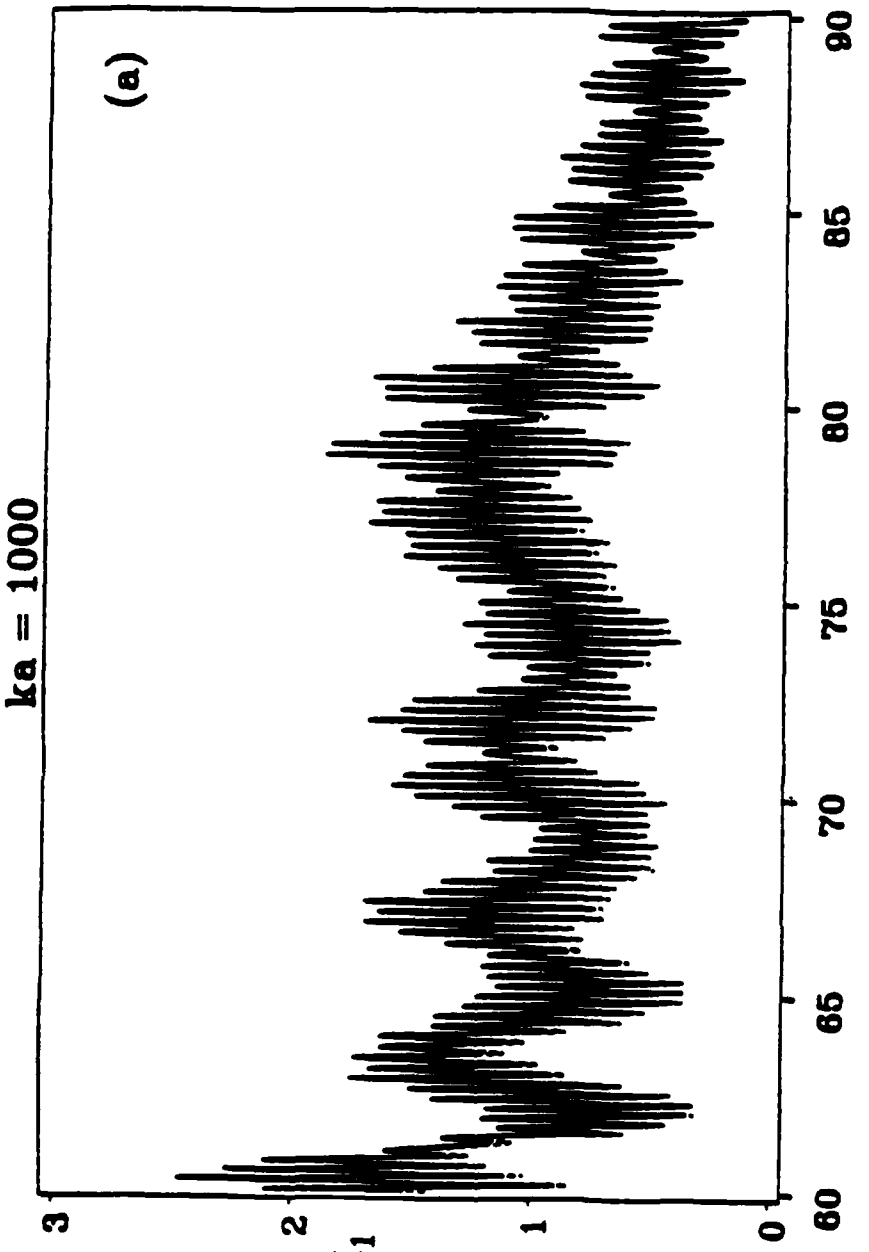

Fig. B.9 (a)

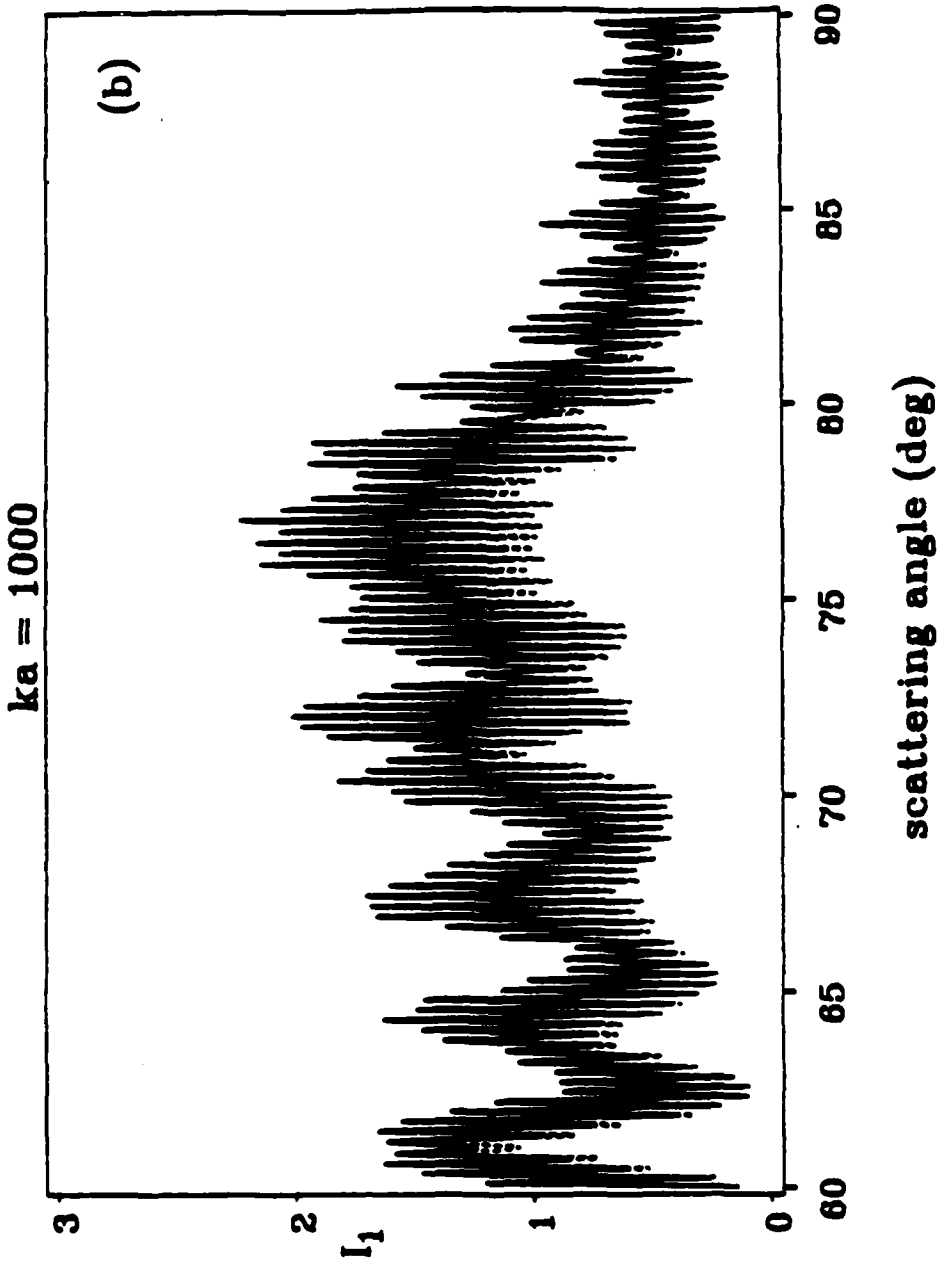

Fig. B.9 (b)

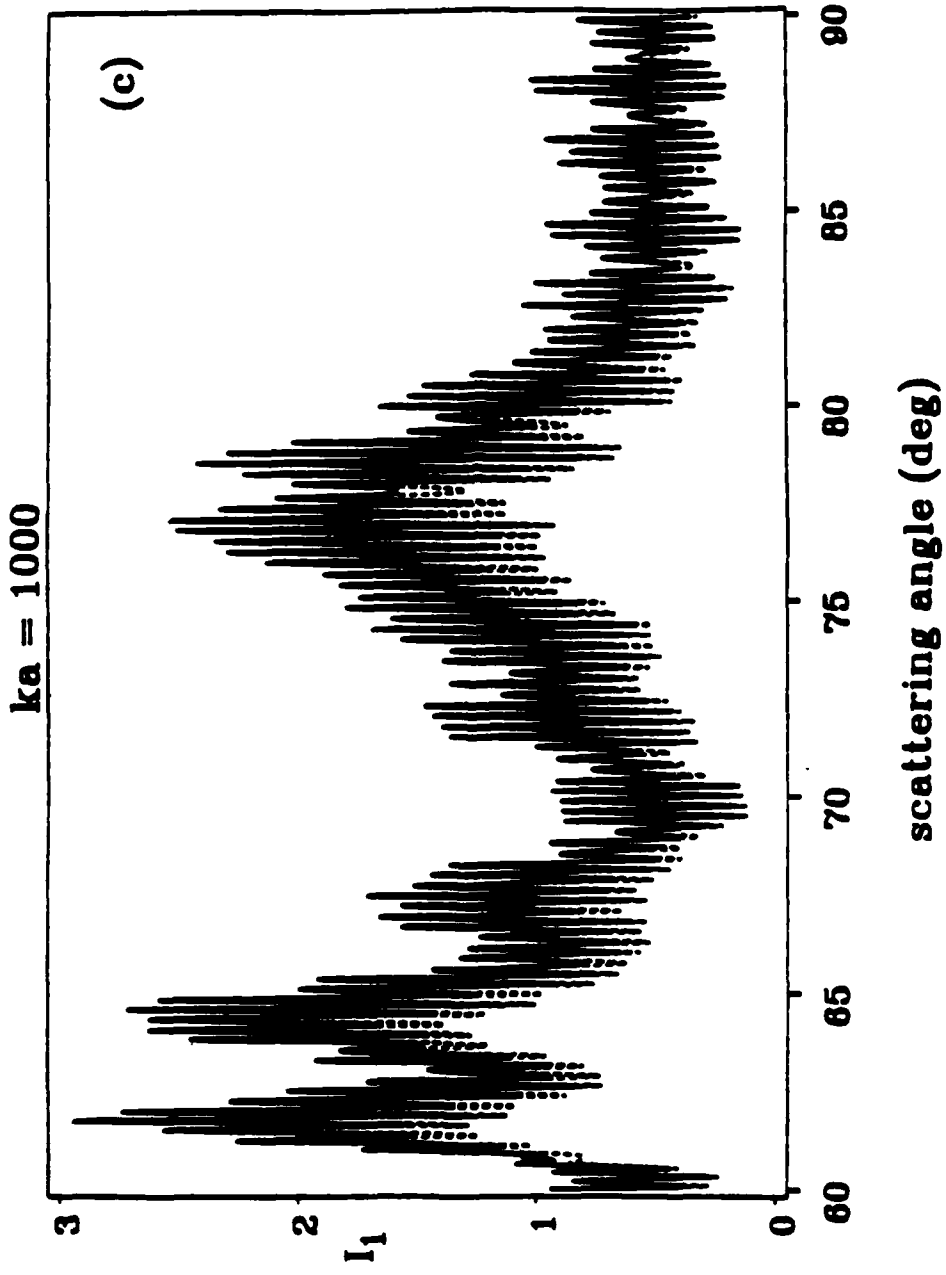

Fig. B.9 (c)

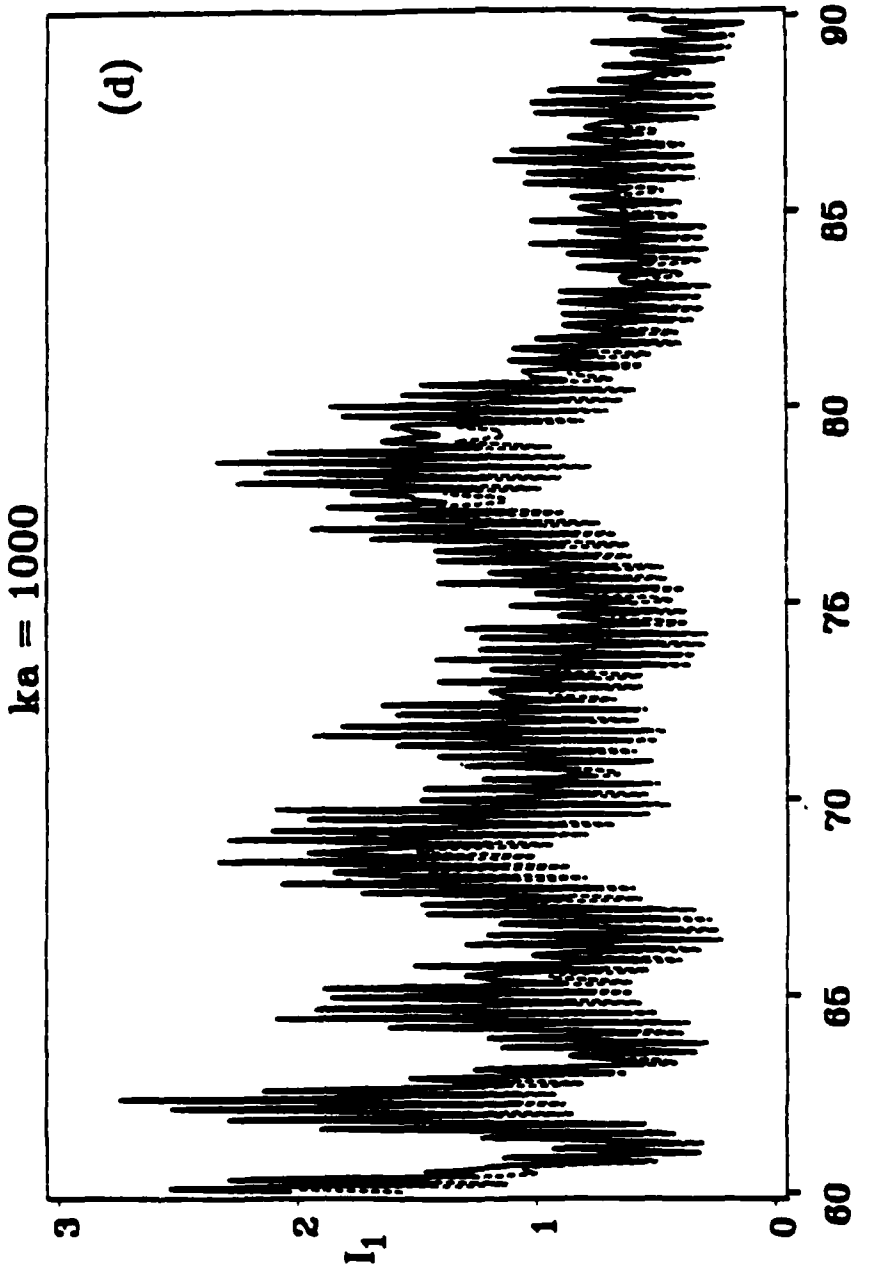

Fig. B.9(d).

APPENDIX C

EFFECTS OF THE REFRACTIVE INDEX OF WATER ON SCATTERING PATTERNS

For the computations done in Chapter 2 and Appendix B the value of $n_w = 4/3$ was used. This value was chosen as it represents roughly the typical value for conditions found both inside and outside the lab. Tests were performed over the range of $n_w = 1.332$ (pure water at a temperature ≈ 30° C) to $n_w = 1.338$ (high salinity in ocean water) in order to determine the range of validity of $n_w = 4/3$. Typical results are shown for the two extremes in Figs. C.1 and C.2. As can be seen in both cases there is a slight shift in the coarse structure while fine structure retains its approximate structure. This shift was found to be less prominent for larger bubbles. Typically values of n_w within ± 0.002 (1.332 to 1.335) were found to have a negligible effect on all but the thickest coating values where a slight amount of added coarse structure shift was noted. Under unusual conditions such as extreme water temperatures or high salinity where variation of n_w is greater than 0.002 the measured value of n_w given in the tables is best used.

Figure C.3 compares the $j = 2$ irradiance values for $n_w = 1.332$, and $n_w = 1.338$ to $n_w = 4/3$ for a non-coated air bubble over the entire 180° range. As can be seen from the figure the critical angle region shows good agreement between all three values. In the majority of cases the approximation of $n_w = 4/3$ was valid for both coated and non-coated air bubble calculations as the behavior of all earlier described effects was unaltered. Since most values of sea water are within the ± 0.002 range of $n_w = 4/3$ the results presented here may be used as accurate models of possible coating effects.

Figure C.1. Water index of refraction evaluation for the lower extreme case of $n_w = 1.332$, (dashed curve). The solid curve is for $n_w = 4/3$. The other parameters were $ka = 500$, $n_c = 1.5$. Note that the 4/3 value is a very good approximation in most cases.

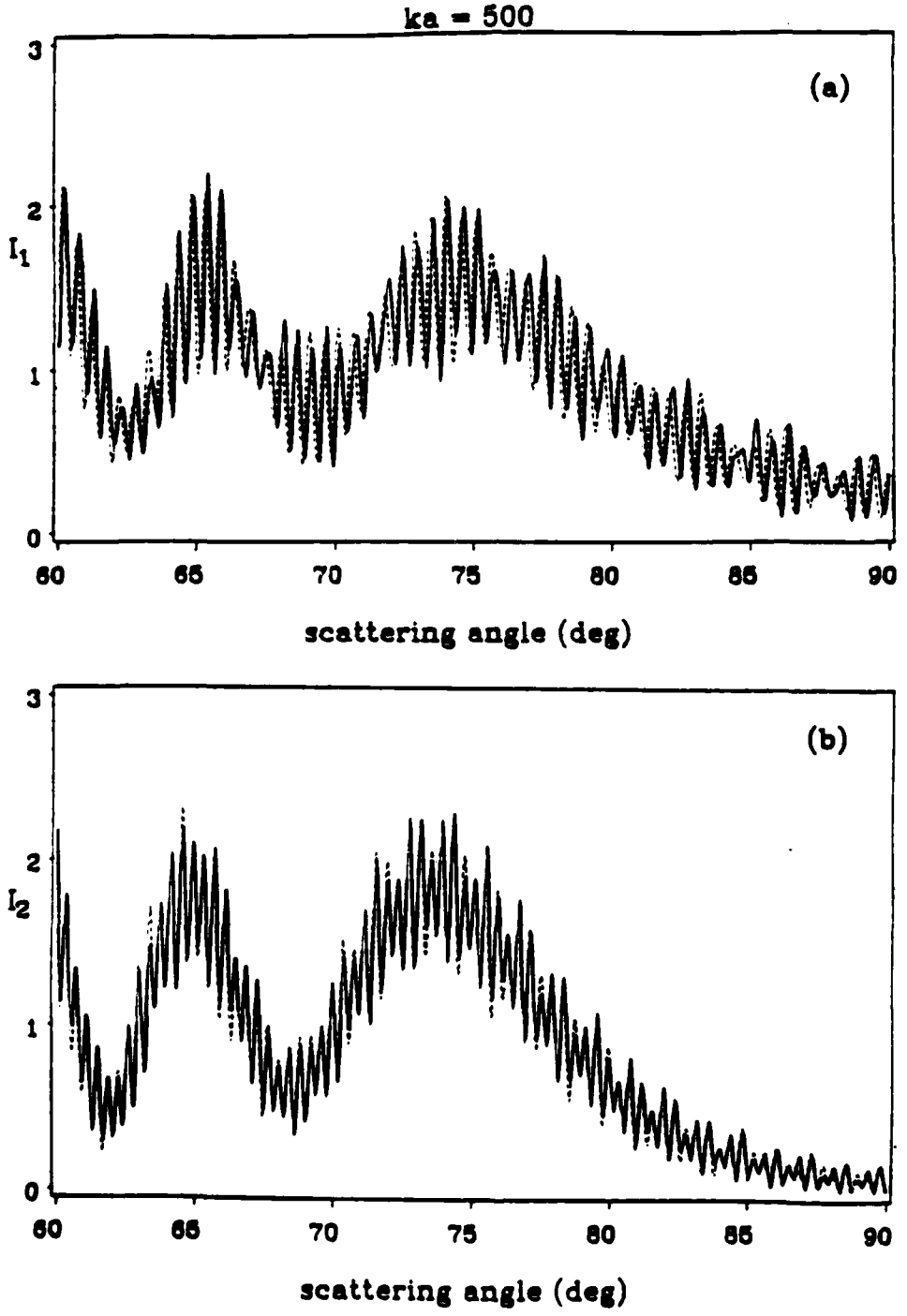
ka = 500
(a)
I_1
3
2
1
0
60
65
70
75
80
85
90
scattering angle (deg)
(b)
I_2
3
2
1
0
60
65
70
75
80
85
90
scattering angle (deg)

Fig. C.1 (a) and (b)

Figure C.2. Like Figure C.1 but for $n_w = 1.338$

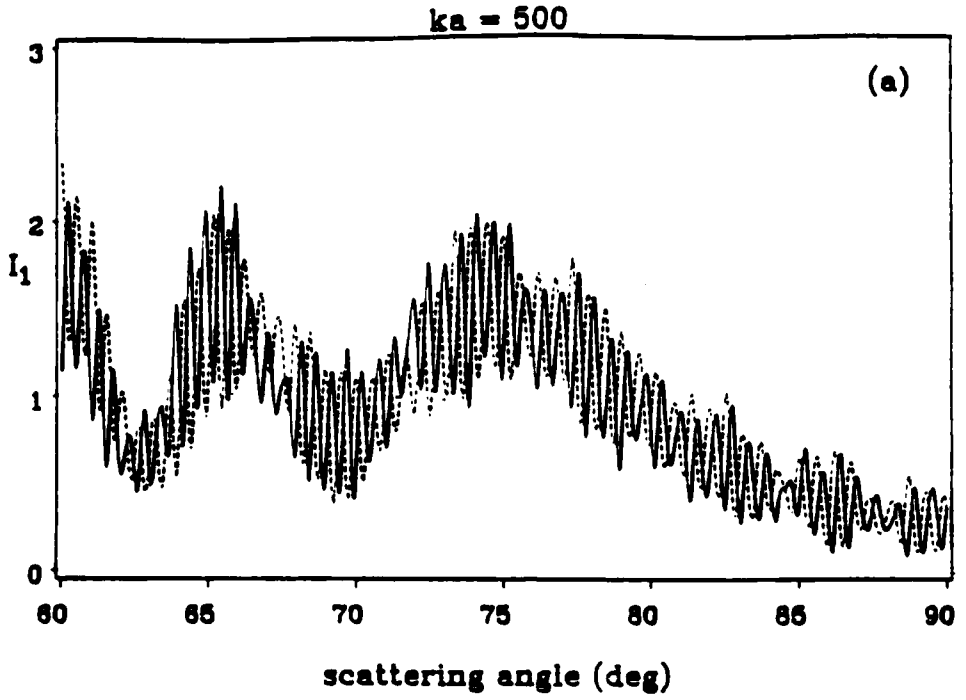
ka = 500
(a)
I_1
3
2
1
0
60
65
70
75
80
85
90
scattering angle (deg)

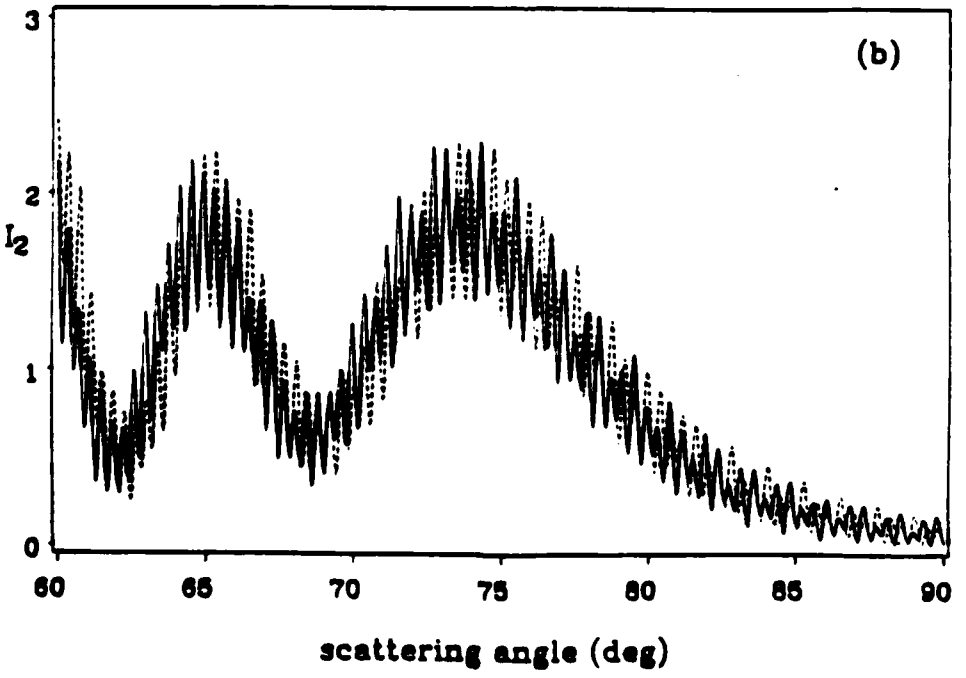
(b)
I_2
3
2
1
0
60
65
70
75
80
85
90
scattering angle (deg)

Fig. C.2 (a) and (b)

Figure C.3. Comparison of irradiance profiles for $n_w = 4/3$ (long-dashed curve) versus $n_w = 1.332$ (solid curve) and $n_w = 1.338$ (short-dashed curve) for noncoated air bubble in water. Note the excellent agreement between the three curves in the $\theta = 60°$ to $\theta = 85°$ range.

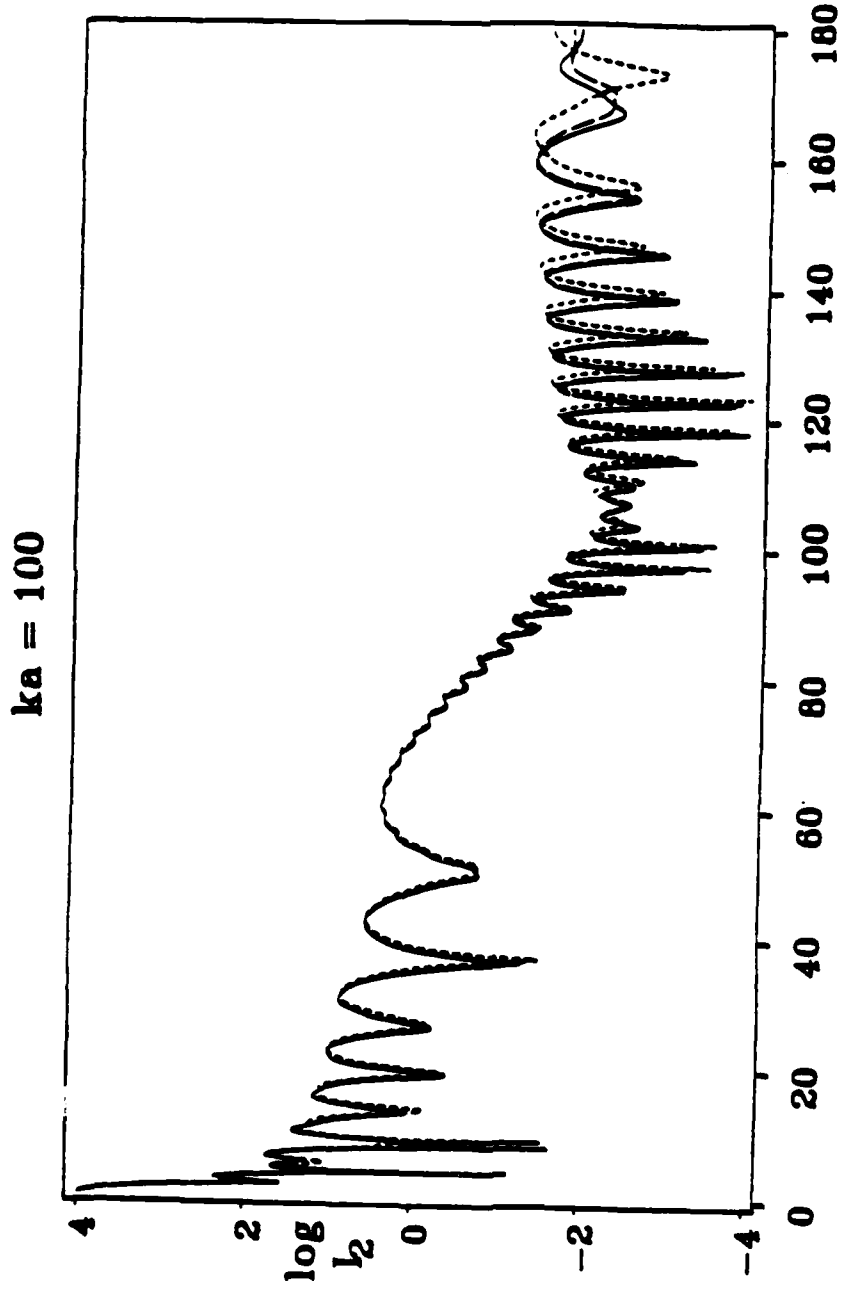
ka = 100
log I_2
4
2
0
−2
−4
0
20
40
60
80
100
120
140
160
180
scattering angle (deg)

Fig. C.3.

SUPPLEMENT TO BILLETTE'S THESIS

Professor Philip L. Marston
Department of Physics
Washington State University
Pullman, WA 99164-2814

(Principal Investigator, ONR Contracts N00014-85-C-0141 and N00014-86-K-0242)

Following the completion of Stuart Billette's thesis (which constitutes the bulk of the present report) an error was discovered in the computer program used to evaluate the physical-optics approximation of Marston and Kingsbury. This error (which could be traced to a previous student) is only concerned with the physical-optics approximation for the scattering from an uncoated bubble. Hence all of the new results of this thesis, which concern the scattering from coated bubbles, were not affected by this error. Furthermore, the Mie theory results (which are exact for an uncoated spherical bubble) were not affected by this error. Indeed, the effect of the programming error on the computed physical-optics approximation (POA) to the normalized irradiances I_j is typically only a few percent of the corrected POA values if $ka \geq 500$.

For completeness, the next few pages show the corrected (solid curve) and erroneous (dashed curve) POA predictions for $ka = 100$, 500, 1000, and 2500. The first set of four plots give I_2. The solid curves of the plots supersede the appropriate POA curves in Fig. 2.5 and 2.8 - 2.13. The second set of four plots give I_1. The solid curves of these plots supersede the appropriate POA curves in Fig. B.1 - B.4. Except for $ka = 100$ the differences resulting from this correction would probably not be noticeable. These corrections do not affect any of the conclusions of this thesis.

The programming error in the POA algorithm (FILE: ESCAT) is on page 101. To correct the error change:

CALL FRES(W, FC, FS)

to read:

CALL FRES(W, FS, FC).

This error was not present in computer programs used in the original development of the POA [Marston and Kingsbury, J. Opt. Soc. Am. 71, 192-196 (1981); Kingsbury and Marston, *ibid* 71, 358-361 (1981).] Consequently the POA predictions there are correctly plotted [see, however, J. Opt. Soc. Am. 71, 917 (1981).]

It is appropriate to comment on an additional aspect of Billette's thesis. Recent tests were performed which give additional support to the correctness of the algorithm (FILE: COATSPHR) used to evaluate the exact partial-wave series for scattering from a spherical bubble. The procedure was to consider the case of a shell with $n_o = 4/3$, $n_c = 1.5$, and $n_i = 1$ in the limit $a/b \rightarrow 0$ so that the radius a of the bubble was negligible in comparison to both the wavelength and the coating radius b. In this case the scattered irradiance went over to that of a uniform sphere (of relative refractive index n_c/n_o) as predicted from Mie theory.

KA = 100

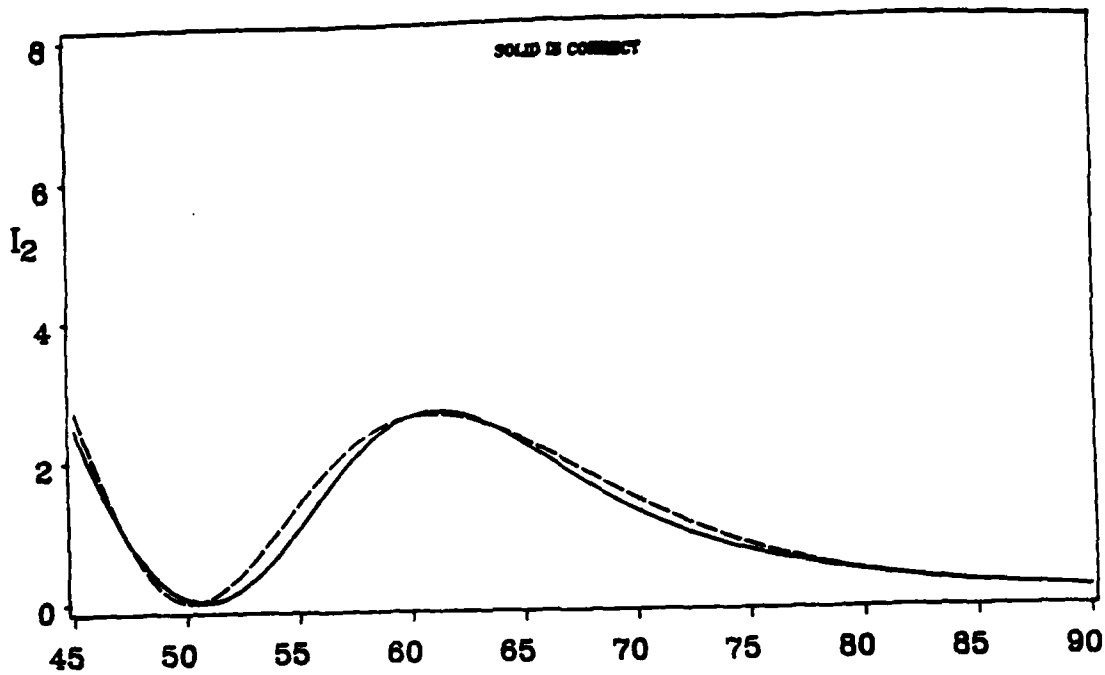

scattering angle (deg)

KA = 500

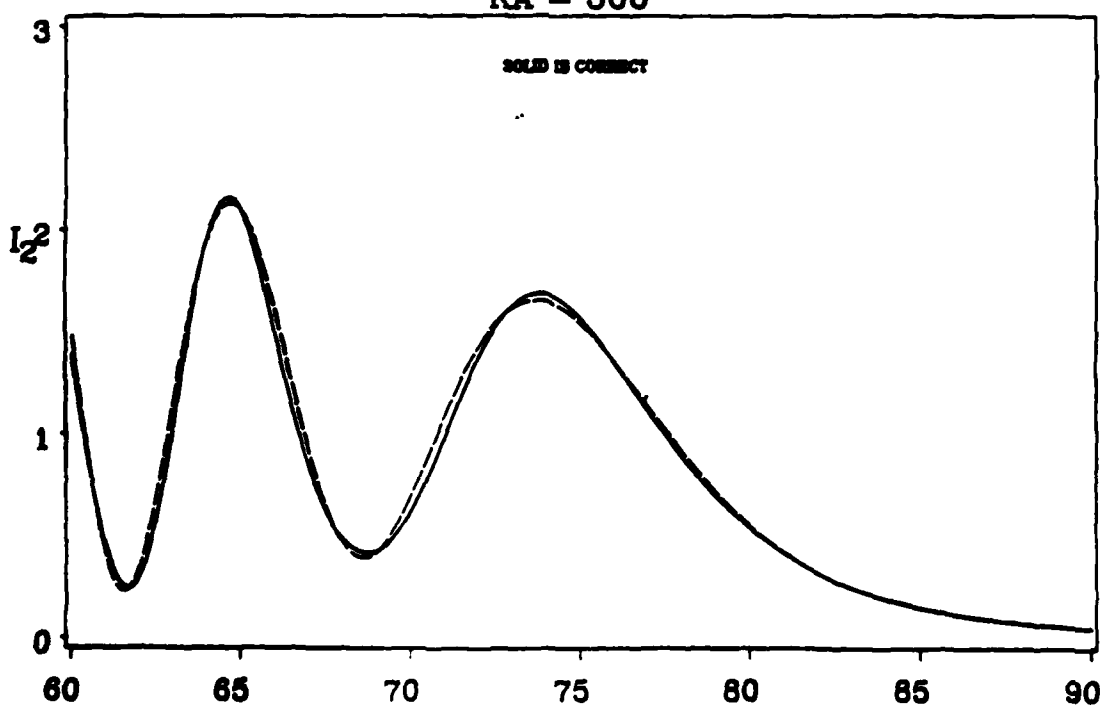

scattering angle (deg)

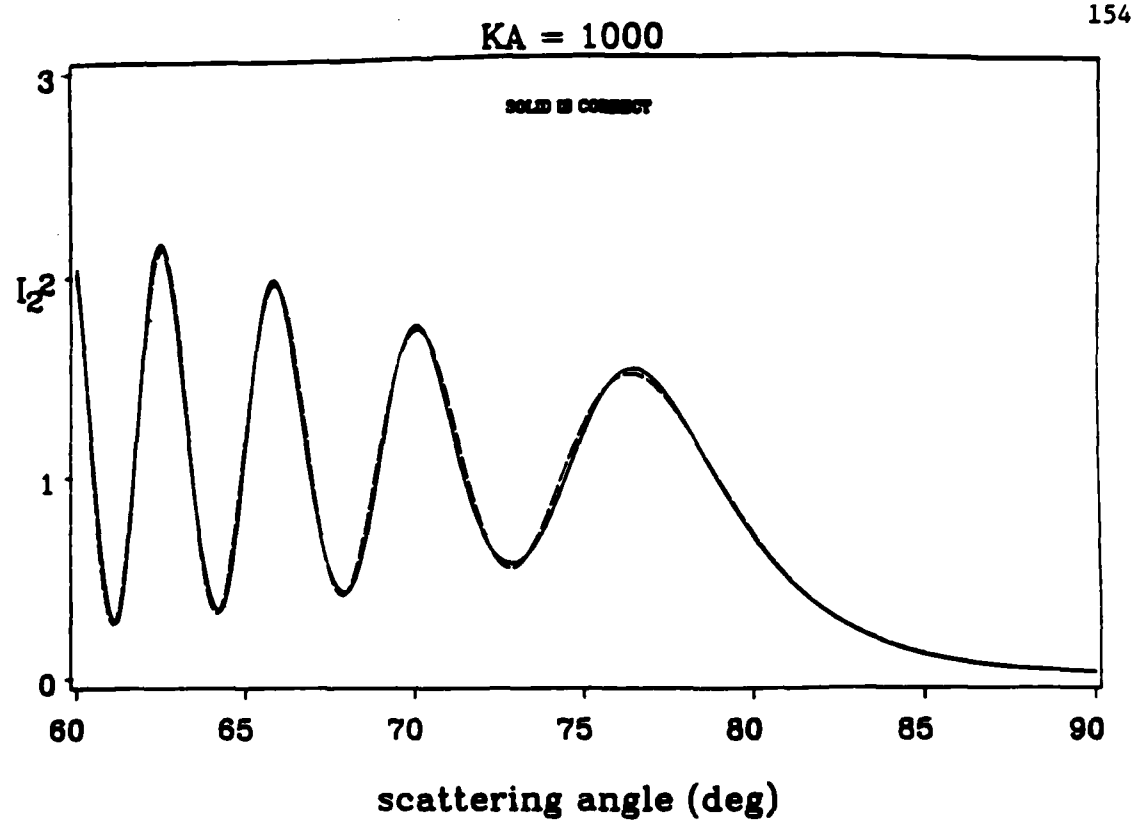
KA = 1000
SOLID IS CORRECT
I_2^2
3
1
0
60
65
70
75
80
85
90
scattering angle (deg)

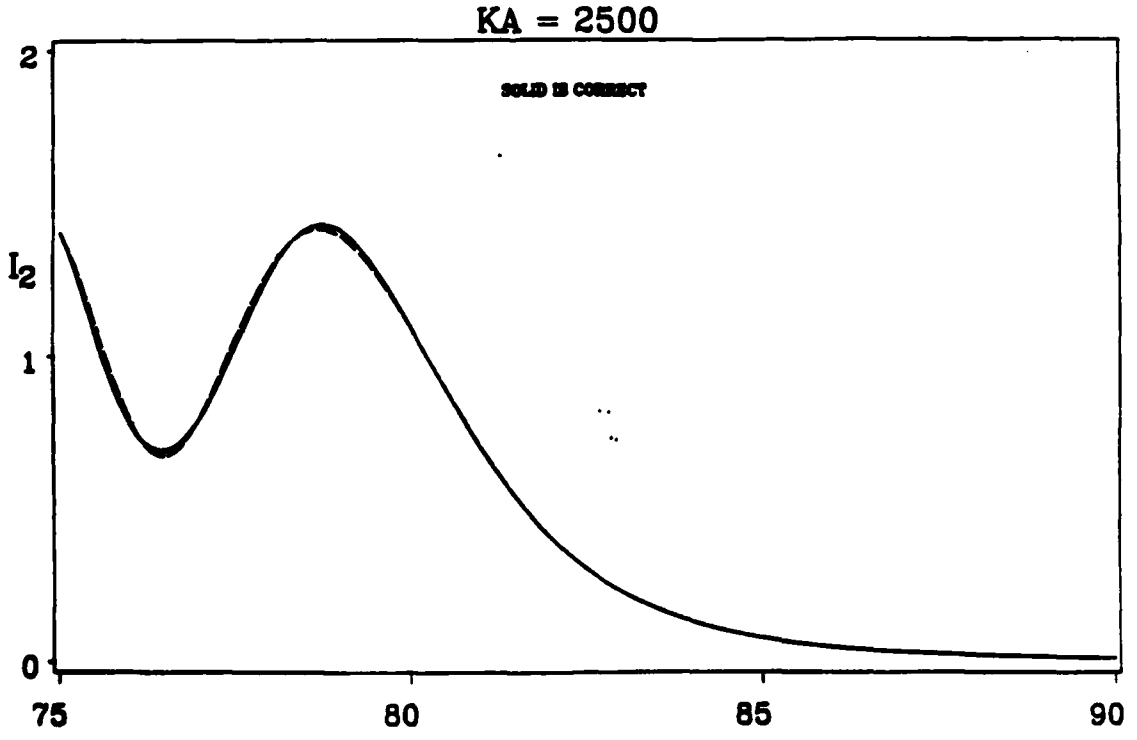
KA = 2500
SOLID IS CORRECT
I_2
2
1
0
75
80
85
90
scattering angle (deg)

KA = 100

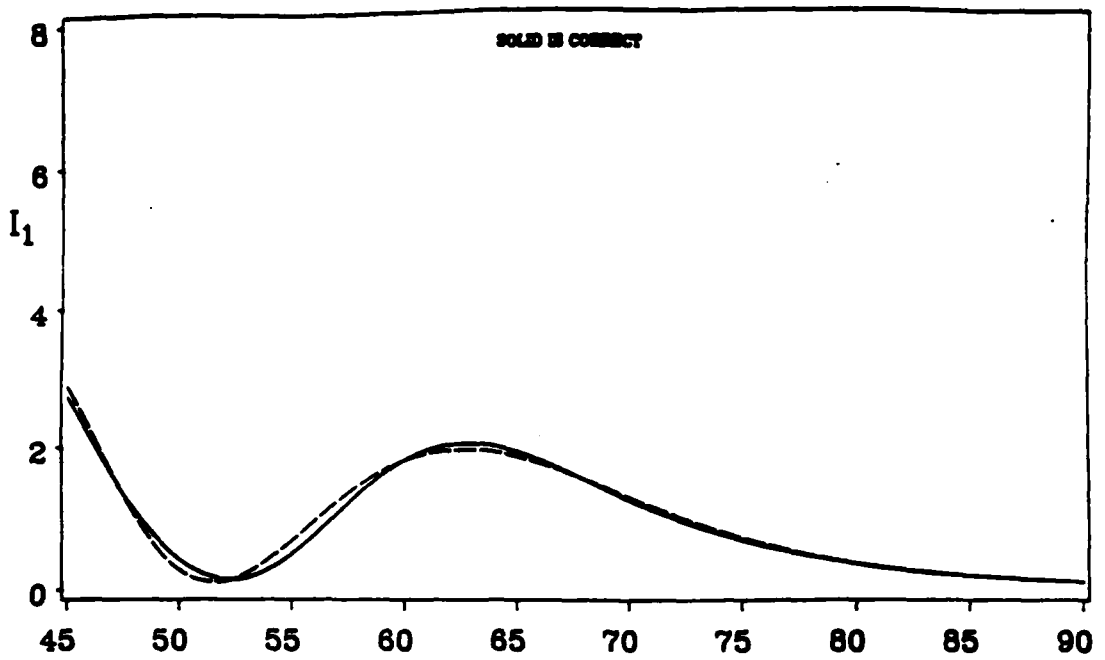

scattering angle (deg)

KA = 500

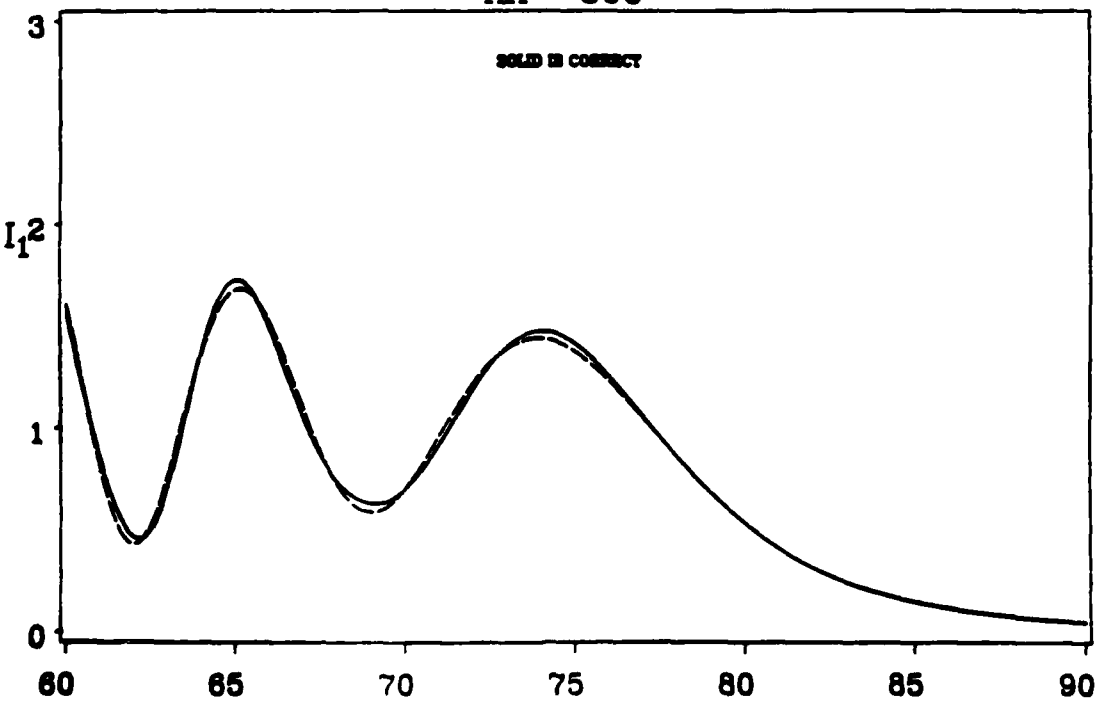

scattering angle (deg)

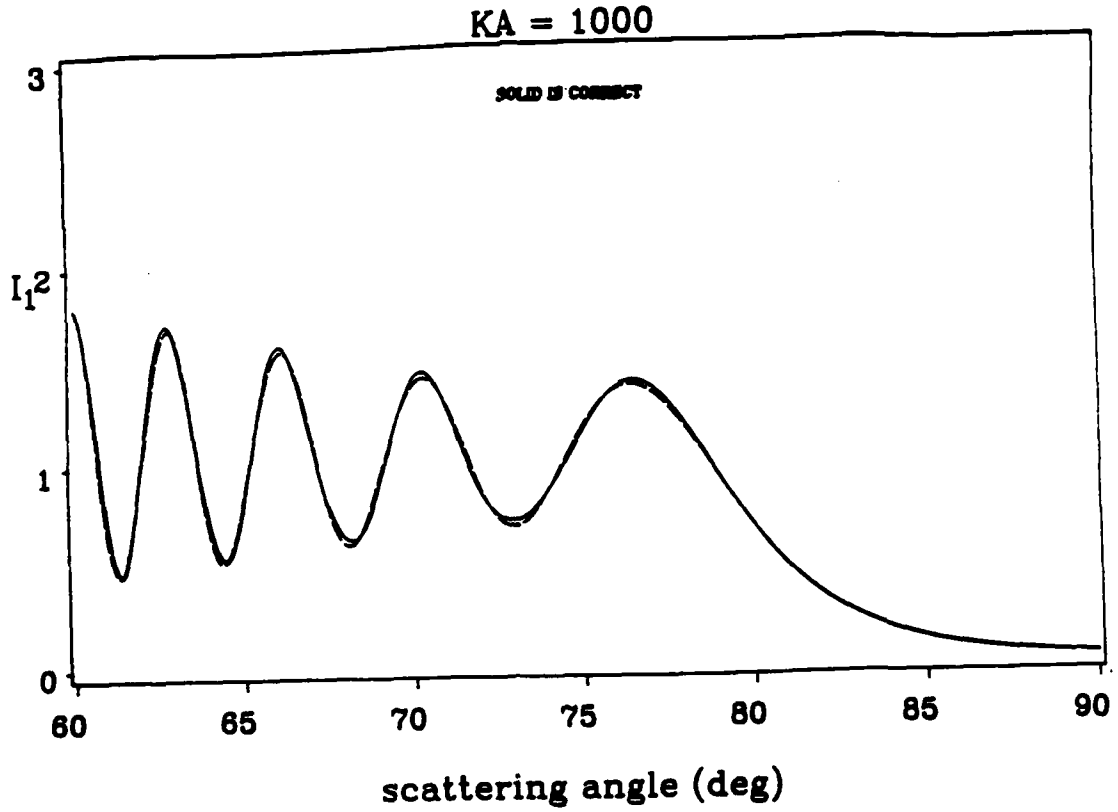
KA = 1000
SOLID IS CORRECT
3
I_1^2
1
0
60
65
70
75
80
85
90
scattering angle (deg)

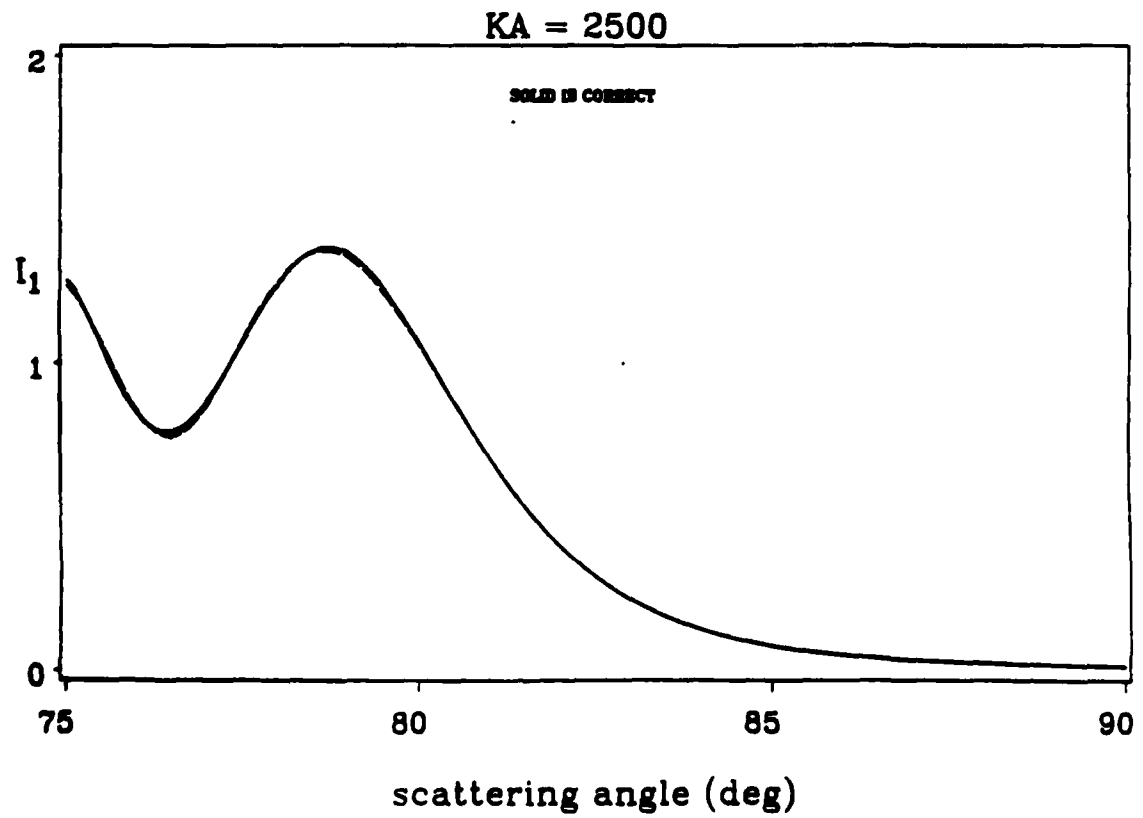
KA = 2500
SOLID IS CORRECT
2
I_1
1
0
75
80
85
90
scattering angle (deg)

Billette Report
Distribution List

R. Hollman
Code 331
Naval Ocean Research and Development Activity
NSTL Station, MS 39529-5004

Ming-Yang Su
Code 331
Naval Ocean Research and Development Activity
NSTL Station, MS 39529-5004

Dr. Logan Hargrove
Physics Division, Code 1112
Office of Naval Research
800 N. Quincy Street
Arlington, VA 22217-5000

ONR, Resident Representative
University of Washington
315 University District Bldg.
1107 N.E. 45th St.
Seattle, WA 98105-4631

Defense Technical
Information Center,
Bldg. 5, Cameron Station
Alexandria, VA 22314

Director, Naval Research
Laboratory, ATTN: Code 2627
Washington, D.C. 20375

Kevin L. Williams
Code 4120
Naval Coastal Systems Center
Panama City, FL 32407-5000

Stuart C. Billette
Bldg. E1, M/S F187
Hughes Aircraft Co.
El Segundo, CA 90245

Prof. L. A. Crum
Dept. of Physics and Astronomy
University of Mississippi
Oxford, MS 38677

Phil Wyatt
Wyatt Technologies
P.O. Box 3003
Santa Barbara, CA 93130

Thomas T. Huang
David W. Taylor Naval Ship R & D Center
Bethesda, MD 20084-5000

END

12-86

DTIC